Doctoral theses at NTNU, 2016:247

Sigrid Lædre

Bipolar Plates for PEM Systems

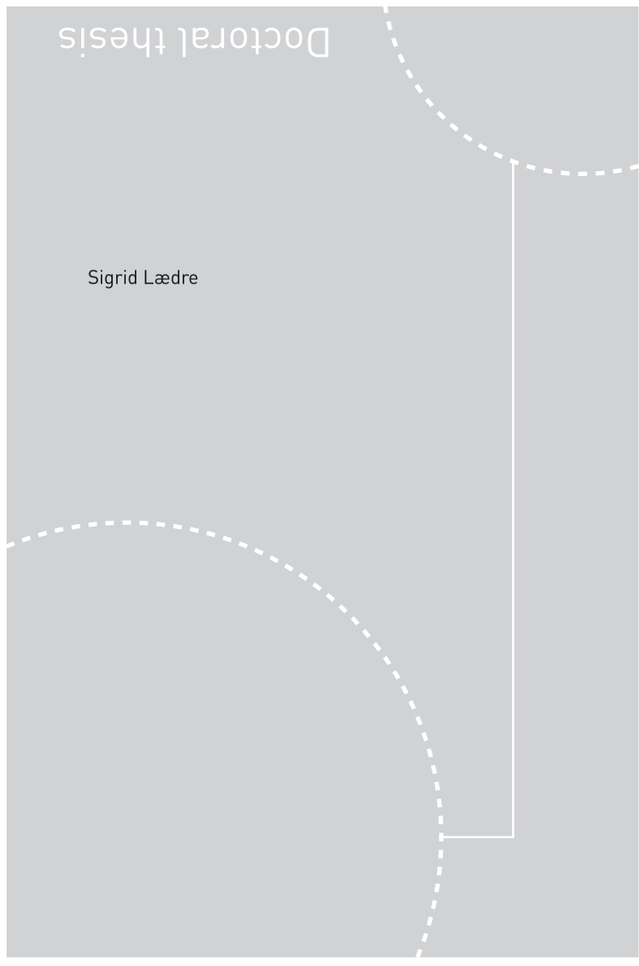

ISBN 978-82-326-1832-3 (printed ver.)
ISBN 978-82-326-1833-0 (electronic ver.)
ISSN 1503-8181

NTNU
Norwegian University of
Science and Technology

NTNU
Norwegian University of
Science and Technology
Thesis for the Degree of
Philosophiae Doctor
Faculty of Natural Sciences and Technology
Department of Materials
Science and Engineering

Doctoral theses at NTNU, 2016:247

NTNU
Norwegian University of
Science and Technology

Sigrid Lædre

Bipolar Plates for PEM Systems

Thesis for the Degree of Philosophiae Doctor

Trondheim, September 2016

Norwegian University of Science and Technology
Faculty of Natural Sciences and Technology
Department of Materials Science and Engineering

NTNU
Norwegian University of
Science and Technology

NTNU
Norwegian University of Science and Technology

Thesis for the Degree of Philosophiae Doctor

Faculty of Natural Sciences and Technology
Department of Materials Science and Engineering

ISBN 978-82-326-1832-3 (printed ver.)
ISBN 978-82-326-1833-0 (electronic ver.)
ISSN 1503-8181

Doctoral theses at NTNU, 2016:247

Printed by NTNU Grafisk senter

This thesis has been submitted to

Department of Materials Science and Engineering
Norwegian University of Science and Technology

In partial fulfillment of the requirements For
the academic degree

Philosophiae Doctor

June 2016

This thesis is dedicated to my dear daughter Astrid.

“Life is what happens to you while you're busy making other plans.”
- Allen Saunders

Acknowledgements

There is only one name on the front page of this thesis, and I would like to take this opportunity to thank all the people who both directly and indirectly helped me finish this PhD.

I have been blessed with four supervisors over the course of my PhD. I would like to start off by thanking associate professor Dr. Håvard Karoliussen for believing in me, even when I didn't. You have been there for me all the way, and I am so grateful for your support. I also wish to thank Dr. Ole Edvard Kongstein in SINTEF, for teaching and supporting me in the laboratories. You have taught me so much about materials and corrosion, and I don't think this PhD would have been possible without you. Thank you to associate professor Dr. Frode Seland for getting me through this PhD. I appreciate all your feedback and help throughout the process. Your guidance has been crucial for the finalization of this thesis. And finally, I wish to thank Dr. Anders Ødegård in SINTEF. Your positivity and encouragement have helped me so many times. To all my supervisors; thank you for all the discussions and honest opinions.

In addition to my supervisors, there are quite a few colleagues that have been there for me throughout my PhD. I want to start off by thanking all my co-workers at the Department of Chemistry and Materials Science at Kalvskinnet. The joyful lunches in "Kjelhuset" have been my escapes from the stressful PhD life. You are such a great group of people, and I am so grateful to have gotten to work with all of you. I would also like to thank all my other colleagues at the Faculty of Technology at NTNU, and in particular the people I have gotten to know through the ENERSENSE project.

I have been so fortunate to work closely with several people from the SINTEF New Energy Solutions group, and my gratitude goes out to all of you. I also wish to thank all my co-workers in K1 and K2. I have enjoyed the institute parties, seminars and "Thursday lunch buffets" with all of you. A special thank you goes out to the master students and St. Andrews exchange students I have been so privileged to work with in the lab. Having you around has made lab work a joy, and there are days I would not have made it to the lab if I didn't know you would be there.

Thank you to John Walmsley and Erik Folven for great help with AES analysis, and to Dr. Ingeborg-Helene Svenum for the XPS analysis. I would also like to thank Dr. Julian Tolchard and Yingda Yu for SEM training.

To my dearest friends, colleagues and partners in crime: Camilla, Karen and Margrethe. Without you, I would probably not be writing this thesis right now. There are few people who know me as well as you do, and your support and friendships have made PhD life livable. Thank you!

In addition to all my great collegues, I have a great family and so many great friends. Thank you so much for supporting and encouraging me, even though most of you don't really know what work with. Thank you to my parents-in-law, who are there for us whenever we need anything.

I wish to thank my parents for always being there for me. I could not have asked for a more supporting mom and dad, and your encouragement has made me believe that anything is possible. I can tell you now that even the highest educational degree is nothing compared to everything you both have though me. A special thank you to all of my siblings, Torstein, Mona, Rune, Børre and Trond. My life would not have been the same without you, and even though you are not always close by, I always carry you in my heart.

I have the most wonderful daughter, Astrid, who has though me that there are things more important in life than a PhD. The thought of being able to come home to you every day has kept me positive. I hope me finishing this PhD shows you that you can do anything you put your mind to.

And finally, I wish to thank my husband, Espen. You are the most loving, selfless and caring person I know. You make me believe in myself and I am so grateful for all your support and love. Elske deg.

Preface

This thesis is a result of work performed between august 2011 and June 2016, where the author spent 16 months teaching and nine months on maternity leave. The author was employed at the department of Chemical Engineering and Materials Technology at Norwegian University of Science and Technology (NTNU), and the work was performed in cooperation with both the electrochemistry group at the Department of Material Science and Engineering at NTNU, and with SINTEF Materials and Chemistry. Håvard Karoliussen and Frode Seland were supervisors from NTNU, while Ole Edvard Kongstein and Anders Ødegård contributed as supervisors from SINTEF Materials and Chemistry.

The majority of the work described in this thesis was performed by Sigrid Lædre at the Department of Materials Science and Engineering at NTNU. The Ta-ITO coatings (chapter 5) were applied to the titanium substrates by Lucia Mendizabal at IK4-Tekniker in Bilbao, Spain. The AES analysis were conducted in cooperation with Erik Folven from the Department of Electronics and Telecommunication at NTNU and John Walmsley at SINTEF Materials and Chemistry. The XRF analysis was conducted together with Ingeborg-Helene Svenum at SINTEF Materials and Chemistry.

The work described in this thesis was funded by:

- The Department of Chemical Engineering and Material Science at NTNU.
- The Department of Electrical Engineering and Renewable Energy at NTNU.
- The Department of Material Science and Engineering at NTNU.
- SINTEF Materials and Energy through the following projects:
    - NORCOAT (Nordic Energy Research, 09051)
    - STAMPEM (Fuel Cells and Hydrogen joint Undertaking, 303449)
    - COATELY (m-Eranet, The Research Council of Norway)

Parts of this work has been published in the following articles:

1. Lædre S, Kongstein OE, Oedegaard A, Seland F, Karoliussen H. *The effect of pH and halides on the corrosion process of stainless steel bipolar plates for proton exchange membrane fuel cells.* International Journal of Hydrogen Energy. 2012;37:18537-46.

2. Ladre S, Kongstein OE, Oedegaard A, Seland F, Karoliussen H. *In Situ and Ex Situ Contact Resistance Measurements of Stainless Steel Bipolar Plates for PEM Fuel Cells.* ECS Transactions. 2013;50:829-39.

The following manuscripts have been prepared for publication:

1. Lædre S, Kongstein OE, Oedegaard A, Seland F, Karoliussen H. *In situ Interfacial Contact Resistance measurements in a custom made Proton Exchange Membrane Fuel Cell.*

2. Lædre S, Kongstein OE, Oedegaard A, Karoliussen H, Seland F. *Materials for Proton Exchange Membrane Water electrolysis Bipolar Plates.*

3. Lædre S, Mendizabal S, Kongstein OE, Oedegaard A, Karoliussen H, Seland F. *Ta-ITO Coated Titanium Bipolar Plates for Proton Exchange Membrane Electrolysis.*

June 30th 2016

Sigrid Lædre

Summary

The Bipolar Plate (BPP) is an important component in both Proton Exchange Membrane Fuel Cells (PEMFCs) and Proton Exchange Membrane Water Electrolyzers (PEMWEs). Bipolar plate material and processing constitutes for a large fraction of the cost and weight of a PEM cell stack. The main tasks for the bipolar plates in both systems are to separate single cell in a stack, conduct current between single cells and remove heat from active areas. In addition, the BPPs distribute hydrogen and air in PEMFCs, and in PEMWEs they distribute the water. The material selection is challenging in PEM systems, primarily due to the acidic environment introduced by the proton exchange membrane. In PEMWEs, the high potentials experienced at the oxygen evolving electrode limits the range of suitable materials even further. Consequently, carbon based BPPs are most commonly used in PEMFCs, while titanium BPPs are more common in PEMWEs.

Stainless steels are desired materials for use as BPPs in PEMFCs due to their high electrical conductivity, high mechanical strength and low material and processing costs compared to carbon based BPPs. However, the durability of stainless steels in PEMFCs is problematic, thus preventing their expected influential role as bipolar plate materials in such systems. Investigating the development of electrical resistances and corrosion behavior ex situ in simulated environment or in situ in a real operating PEM system and complementing this with surface sensitive measurements are crucial in developing the next generation of cost efficient and durable bipolar plate materials.

Ex situ polarizations of stainless steel (AISI 316L) BPPs were conducted in electrolytes made from various concentrations of H_2SO_4 with and without addition of halides. It was found that polarization of the stainless steel BPPs in electrolytes with a low pH resulted in higher corrosion currents than polarization in electrolytes with higher pH. In addition, the Interfacial contact resistance (ICR) values obtained after polarization were higher for the BPPs that had been polarized in high pH electrolytes. Auger Electron Spectroscopy analysis revealed that the surface oxides formed on the AISI 316L were thinner on the plates that had been polarized in 0.1 M and 1 M H_2SO_4 compared to the ones that had been polarized in 0.1 mM and 1.0 mM H_2SO_4. Polarization over longer periods of time in 1 mM H_2SO_4 did not cause as low ICR and high corrosion currents as polarization in 0.1 M and 1 M H_2SO_4. Using very low pH to accelerate the corrosion rate of stainless steel is thus probably not the best solution, as this seems to initiate a thinning of the oxide that would not take place in

an operating fuel cell at all. As opposed to what was frequently described in the literature, addition of F^- and Cl^- to the electrolyte in the amounts expected in an operating PEMFC, did not cause any significant changes in ICR or corrosion current. However, addition of Cl^- in amounts 10 times larger than what can be expected in a PEMFC, caused pitting on the AISI 316L surface during polarization.

ICR measurements can be used to investigate the electrical conductivity between the Gas Diffusion Layer and the BPP in PEMFCs. Ex situ ICR measurements can be done very easily both before and after polarization, and provides a god idea of how promising a BPP material and/or coating is. However, ex situ measurements do not provide continuous study of how the ICR develops over time. In addition, such tests are usually not conducted under real fuel cell conditions. In situ ICR measurements makes it possible to study the ICR during cell operation, but there are not many examples of such methods in the literature. In this work, the main objective was to develop such a method in cells that had been custom made for a previous research project. Thin gold wires were placed at three different locations in the operating fuel cell, making it possible to measure the ICR between the BPP and GDL directly. Using the average ICR from the three measuring points on the BPP surface was found to be far more accurate than just one measuring point, as the average ICR values were found to be in the same range as the ICR values obtained ex situ after operation. Measuring the local ICR by use of a point measuring setup ex situ, confirmed that the variation in ICR between the three in situ measuring points was caused by uneven current distribution.

BPPs for PEMWEs have to withstand the harsh environment caused by high operational potential and acidity from the electrolyte, and they are currently made of titanium. Although it is well-known that titanium easily forms a low conductive oxide, there are surprisingly few studies focusing on testing of substrate materials and coatings for bipolar plate materials for PEMWEs. In this thesis work, a study where several substrate materials were polarized under conditions similar to the ones experienced by BPPs in PEMWE was conducted. Molybdenum, tungsten, Titanium gr. 2, niobium, tantalum, Inconel 625, 254 SMO, AISI 316L and AISI 304L were polarized up to 2.0 V_{SHE}. Weight loss measurements, ICR measurements and scanning electron microscopy imaging were performed before and after polarization. Titanium, niobium and tantalum experienced little or no change in weight during polarization. Tantalum and niobium instead encompassed a substantial increase in ICR. The measured weight loss for AISI 316L, AISI 304L and tungsten showed that only approximately 20 % of the current produced could be attributed to corrosion or dissolution processes. ICR measurements performed after

polarization of titanium up to 122 h at 2.0 V_{SHE} Showed that the ICR kept increasing continuously, even though the current stabilized at a more or less constant value.

A novel bi-layer coating made from a tantalum base layer with a Tin doped Indium Oxide (ITO) layer on top was investigated for use on titanium BPPs for PEMWE. Several Ta-ITO coated plates were polarized in a parameter study, where pH, potential and temperature of the electrolyte was altered, as well as the duration of the polarization. Before polarization, the Ta-ITO coated samples showed an ICR of 10 mΩ cm^2. The ICR measured after polarization at baseline conditions increased for the first 24 hours, and then stabilized at about 30 mΩ cm^2. Polarization of the Ta-ITO coated titanium at 1.4 V_{RHE} and 2.0 V_{RHE} resulted in small increases (both at 15 mΩ cm^2) in the ICR compared to the unpolarized sample (10 mΩ cm^2), but after polarization at 2.5 $_{RHE}$ and 2.6 V_{RHE}, the ICR increased to 102 mΩ cm^2 and 503 mΩ cm^2, respectively. X-ray photoelectron spectroscopy analysis of the surface showed that the significant increase in ICR is related to a lower concentration of oxygen vacancies, an increase in oxygen to metal ratio and a decrease in metallic character of indium compared to the non-coated and baseline sample. However, neither of the components in a PEMWE will experience potentials significantly above 2.0 V_{RHE} under normal operation. The results obtained in this study showed that Ta-ITO coating is promising for use in PEMWEs.

Abbreviations

AES	Auger Electron Spectroscopy
AFC	Alkaline Fuel Cell
AISI	American Iron and Steel Insitute
BPP	BiPolar Plate
COP 21	Paris Climate Conference 2015
DoE	Department of Energy
EIS	Electrochemical Impedance Spectrocsopy
EN	Electrochemical Noise
FEGSEM	Field Emission Gun Scanning Electron Microscopy
GDL	Gas Diffusion Layer
GHG	Green House Gas
HHV	Higher Heating Value
HPPMS	High Power Pulsed Magnetron Sputtering
ICR	Interfacial Contact Resistance
ITO	Tin doped Indium Oxide
LHV	Lower Heating Value
MCFC	Molten Carbonate Fuel Cell
MEA	Membrane Electrode Assembly
NASA	National Aeronautics and Space Administration
OER	Oxygen Evolution Reaction
OCV	Open Circuit Voltage
PAFC	Phosphoric Acid Fuel Cell
PEM	Proton Exchange Membrane

PEMFC	Proton Exchange Membrane Fuel Cell
PEMWE	Proton Exchange Membrane Water Electrolyzer
PMS	Pulsed Magnetron Sputtering
PTFE	PolyTetraFluoroEthylene
RHE	Reversible Hydrogen Electrode
SCCM	Standard Cubic Centimeters per Minute
SEM	Scanning Electron Microscopy
SHE	Standard Hydrogen Electrode
SMO	Stainless steel with high amounts of Molybdenum
SOFC	Solid Oxide Fuel Cell
XPS	X-Ray Photoelectron Spectroscopy

Contents

1 Introduction

1.1 Background

In today's society, we depend on natural oil and gas for the production of various products, one of them being the production of fuels to keep our transportation sector up and running. But the world's reserve of natural oil and gas will not last forever, and the use of fossil fuels (in e.g. cars) result in Greenhouse Gas (GHG) emissions causing irreparable damage to the earth. At the Paris Climate Conference (COP 21) in December 2015, 195 countries worldwide agreed to aim to limit the global temperature increase to 1.5 ^{o}C [1]. In order to make this happen, a reduction in GHG emmisions is very important. The transformation from fossil fuels to renewable energy sources, such as hydro power, wind power, solar cells, osmosis and wave power, is detrimental for the COP 21 goals to be achieved.

Hydrogen is predicted to play a key role in our future renewable energy society as an energy carrier [2, 3]. It can be used as fuel in a variety of applications, and can increase the build-out of renewable energy as an intermittent storage-medium. Reforming of natural gas or other fossil fuels are the most common methods for producing hydrogen today, but the hydrogen produced from such methods has a low purity and there are far more environmentally friendly ways to obtain hydrogen [4]. Electrolysis of water, using electricity from renewable energy sources to split the water molecule, produces close to 100% pure hydrogen without any fossil fuel needed at all. This hydrogen can further be used in fuel cells to create electrical energy.

Fuel cells convert the chemical energy in hydrogen into electrical energy through reaction with for example oxygen. Such devises can be used for stationary (e.g. private households), portable (e.g. cell phones, laptops), and mobile applications (e.g. cars, ferries, buses) [5, 6]. Several of the world's largest car-manufactures have made car prototypes using fuel cells powered with hydrogen and air. Toyota released their first commercial hydrogen car, the Mirai, in 2015. They claim that it can drive 700 km on one tank of hydrogen [7], which is in the same range as Tesla's model S [8]. However, the refueling time is much shorter with hydrogen compared to batteries. Fuel Cells Bulletin [9] just reported that the Mirai will be launched in Norway and Sweden this summer (2016). In Norway, there are currently several ongoing and planned projects where fuel cells are replacing the traditional energy conversion devices in buses and ferries [10-12].

1.2 Theory

1.2.1 Proton Exchange Membrane

Proton exchange membranes (PEM) are used as the main component in both fuel cells and electrolyzers. In both cases the membrane functions as a separator between anode and cathode, where only protons are allowed to pass through the membrane (Figure 1.1). As the membrane is constructed of polymers and functions as a solid electrolyte, it is sometimes also confusingly referred to as a polymer electrolyte membrane, even though not all polymer electrolyte membranes are proton conductors. Dupont™ is a well-known producer of polymer membranes for PEM systems, and has been producing Nafion membranes since its development in early 1960s. Common for all producers of PEM is that sulfonated fluoropolymers are used in the production. The sulfonic acid groups ensure high proton conductivity as long as the membrane is satisfactorily wetted with water, and results in a slightly acidic environment inside an operating PEM system. The acidic nature of the membrane can block the use of certain metals. Furthermore, the use of PTFE in these membranes results in the presence of fluorides in PEM systems, which poses a risk when using certain materials in affiliation to the membrane and electrodes. For example, the presence of fluoride is known for causing pitting corrosion on many metals [13]. [5]

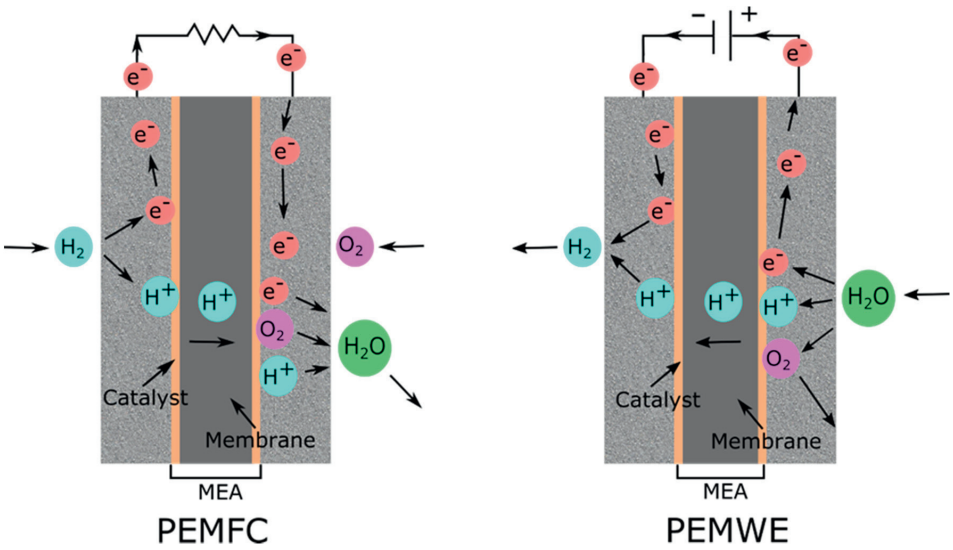

Figure 1.1: Schematic of how the Proton Exchange Membrane works in fuel cells and electrolyzers.

Catalysts are very important in PEM systems, as they lower the activation energy for the electrochemical reactions on both cathode and anode side in the fuel cell or electrolyzer. As the electrochemical reactions differ between anode and cathode and between fuel cells and electrolyzers, different catalysts can be used for each reaction. However, in PEMFCs, platinum is the most common catalyst used for both the oxidation and reduction reaction [5]. Noble metals are most commonly used as catalysts in both fuel cells and electrolyzers, but they are expensive and some are prone to catalyst poisoning by e.g. CO [14-16], an inevitable byproduct in reforming of fossil fuels.

A membrane with porous and supported electrocatalytic layers on each side is called a Membrane Electrode Assembly (MEA) [5]. This is the heart of a PEM fuel cell where chemical energy is converted to electrical energy and pure water, through oxidation of fuel (hydrogen) at the anode and reducing oxygen at the cathode. Conversely, a PEM electrolyzer is used to produce hydrogen and oxygen from water by applying electricity. When working with both PEMWE and PEMFC systems, it is important to be aware that the oxygen electrode operates at a higher potential and is thus more susceptible to degradation and corrosion.

1.2.2 Proton Exchange Membrane Fuel Cells

Even though the first fuel cell was made by William Grove in 1839, the PEM fuel cell was not developed until the 1960s, by General Electric in the United States. The early versions of this fuel cell where used by NASA in their space vehicles, but it was not until a few decades later that the fuel cell was commercialized for stationary applications to produce electricity in e.g. households. Today PEM fuel cells are also used in boats, buses and cars all over the world. Toyota launched its first commercial fuel cell vehicle for the European marked in 2015, and the electrical energy used to operate this car is supplied by a PEM fuel cell [17]. [5]

On the anode side of a PEM fuel cell, hydrogen gas is oxidized into protons and electrons. As the membrane only allows protons to go through, the electrons are forced into an outer circuit (Figure 1.1). This is how one can extract electrical energy from the reactions occurring in a fuel cell. On the cathode side these electrons combine with the protons that have travelled through the membrane and oxygen being supplied to form water in a reduction reaction. The overall reaction is shown in Equation 1. The combination of oxygen and hydrogen to form water is a spontaneous, exothermic reaction. The process operates at constant temperature and pressure and is thus not limited by the Carnot's theorem applicable for cyclically processes (e.g. internal combustion engines). The maximum electrical efficiency of

a fuel cell is rather based on the change in Gibbs free energy divided on the change in enthalpy of the reaction and depends on the physical condition of reactants and products. For liquid water (Higher Heating Value, HHV), the thermodynamic efficiency is 83 %, while it is 98% for gaseous water (Lower Heating value, LHV) [18]. However, in a real operating fuel cell the actual efficiency depends directly on the operating voltage at a given load, and is significantly lower due to various losses related to electron transfer, ohmic resistances and mass transfer. The thermodynamic voltage at standard conditions and at 25 °C is 1.229 V, and should ideally be measured when no current flows through the cell (open circuit). However, this voltage is never obtained primarily due to the poor reaction kinetics of the oxygen electrode. In fact, the open circuit voltage (OCV) in a hydrogen/oxygen fuel cell is typically around 0.9 V.

$$H_2\,(g) + \frac{1}{2}\,O_2(g) \rightarrow H_2O(l) \tag{1}$$

In order to produce a useful voltage, several single fuel cells are connected in series and built into a stack. The overall current is typically tuned with the geometric area of the electrodes. A schematic of a PEMFC stack is shown in Figure 1.2, with MEAs, bipolar plates and Gas Diffusion Layers (GDL). The GDL forms an electrical connection between MEA and the bipolar plate, in addition to allow for transport and even distribution of reactant gas and water to and from the active interface. It is often integrated into the MEA [5].

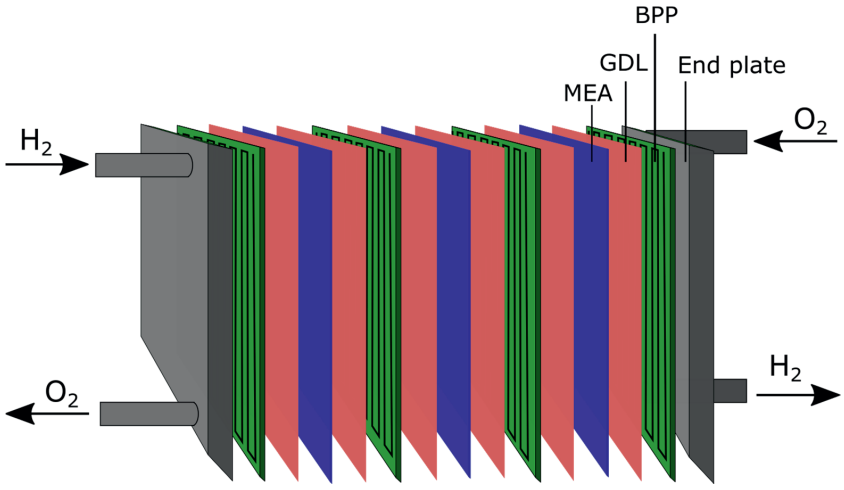

Figure 1.2: PEM fuel cell stack assembly showing how single cells are combined to a stack.

Water management is very important in a PEMFC, and the water balance inside the fuel cell is crucial for the operation. Water is produced at the cathode, and is proportional to the proton conductivity in the membrane. On the other side, too much water can cause flooding, which can lead to blocking of the pores in the electrodes. Another problem with PEMFCs is the degradation of the MEA. Carbon corrosion, catalyst dissolution and corrosion as well as catalyst poisoning are issues which shorten the lifetime of a fuel cell. In addition to water management and MEA degradation, the other components comprising a PEMFC are prone to corrosion and degradation as well. The search for new materials and catalysts is thus important in order to meet these challenges. [5, 16]

In addition to the PEMFC, there are several other types of fuel cells. The main difference between them is the type of electrolyte used dictating the operating temperature and fuel requirements. The Phosphoric Acid Fuel Cell (PAFC) relies on phosphoric acid for proton conductivity and was the first type of fuel cell to be commercially produced. It operates at a medium temperature window around 200 °C, and is reliable and easy to maintain. The Direct Methanol Fuel Cell (DMFC) is a PEM based fuel cell that uses methanol instead of pure hydrogen as a fuel, which eliminates the hydrogen production step. It operates at low temperatures and suffers with poor electrode kinetics resulting in low power densities during operation. These units are best suited for smaller devices where the power density demand is limited, such as portable electronics. The alkaline fuel cell (AFC) operates at low temperatures and has an aqueous alkaline electrolyte allowing for transport of hydroxide ions to complete the circuit. One major setback with the alkaline fuel cell is its sensitivity towards CO_2 poisoning, putting forth very high demands to the purity of the fuel used. Solid Oxide Fuel Cells (SOFC) and Molten Carbonate Fuel Cells (MCFC) are so-called high temperature fuel cells operating at about 650 and 800-1000 °C, respectively. Higher temperatures increase the reaction kinetics for the electrochemical reactions inside the fuel cells, but operation at high temperature sets very high demands for the fuel cell components. Compared to the other types of fuel cells, the PEMFC is simple, with a thin membrane and few components, flexible design and operation allowing for a rather wide temperature window of operation, depending on the choice of membrane material. This makes them ideal for smaller to medium power ranges, for use in portable devices as well as in the transportation sector. [5]

1.2.3 Proton Exchange Membrane Water Electrolysis

William Nicholson and Anthony Carlisle were the first people to liberate hydrogen from water by use of electrolysis in the year 1800 [19], and the laws of electrolysis were reported by Faraday in 1834. The alkaline water electrolyzer has been dominating the marked for many years, mainly due to its relatively low price, long life time and low maintenance cost. However, the alkaline water electrolyzer exhibits a low partial load range, limited current density and has to be operated under low pressures. Compared to the alkaline electrolyzer, the PEM electrolyzer provides a simpler system due to the absence of aqueous KOH or NaOH, higher power densities and efficiencies, a compact stack design allowing for high pressure operation, excellent partial load range and rapid response to fluctuation in power inputs. The latter is very important, as it allows for more flexible operation of the electrolyzer. When used for storing of renewable energy from intermittent sources like wind, solar or wave power, it is crucial that the system can adapt to the fluctuations in the power production. The PEMWE can reach much higher currents than the alkaline electrolyzer and has a lower gas crossover rate. However, the acidic environment sets forth rigid requirements for the components in the PEMWE, resulting in higher costs and shorter lifetime compared to the alkaline electrolyzer. In addition, the acidic environment results in a large anodic overpotential, due to poor kinetics for the oxygen evolution reaction (OER) operating on noble metal oxide electrocatalysts. [4] [20]

$$H_2O\ (l) \rightarrow H_2\ (g) + \frac{1}{2}\ O_2(g) \tag{2}$$

The overall reaction taking place in a PEM electrolyzer is shown in Equation 2. On the anode side of the electrolyzer water is split into oxygen, protons and electrons in an oxidation reaction. By applying a voltage to the system, these electrons are forced in an outer circuit, while the protons travel through the membrane. On the cathode side, protons combine with electrons to form hydrogen gas in a reduction reaction. The electrochemical overall reaction in a PEMWE is the reverse reaction of the one shown in Equation 1. The thermodynamic potential is the same, 1.23 V, but the reaction requires energy to go. PEM electrolyzers typically operate between 1.6 V and 2.0 V depending on production rates. The actual cell voltage is related to the thermodynamic cell voltage and depends on the various overpotential losses related to kinetic, ohmic and mass transfer losses (Equation 3).

$$U_{Cell} = E_{reversible} + \eta_A^a + \eta_T^a + \eta_A^c + \eta_T^c + \sum iR \tag{3}$$

, where *a* represents the anode, *c* represent the cathode, *A* represents activation losses and *T*represents mass transport losses. The activation overpotential is caused by the kinetics of the electron transfer reactions and the transport overpotential is from the diffusion of reactants and product to and from the electrode surface. Of these losses, the activation overpotential at the anode (OER) is dominant. [18-20]

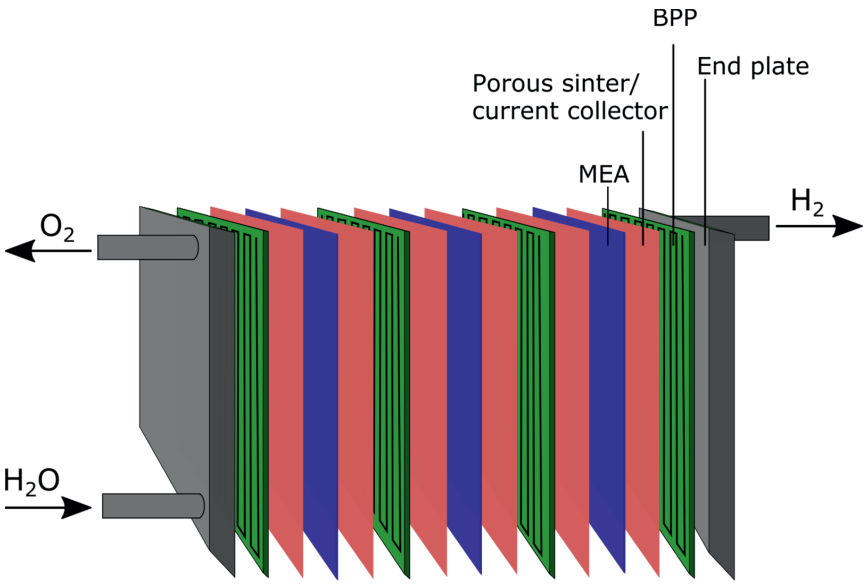

Figure 1.3: PEM water electrolyzer stack assembly showing how single cells are combined to a stack.

As with PEMFC, several cells are combined to form stacks, and the schematic of such a stack is presented in Figure 1.3. The schematic is very similar to the PEMFC, with MEA and bipolar plates. However, carbon materials cannot be used on the oxygen side of the electrolyzer due to corrosion. Carbon support, porous electrode structures made from carbon and carbon based bipolar plates are thus replaced with metals in PEM electrolyzers. [4, 20]

1.2.4 The Bipolar Plate

The bipolar plate is a vital part of PEM systems, as it makes stack building possible. In both fuel cells and electrolyzers its main tasks are to separate individual cells within a stack, manage the gases and water within the stack, conduct electricity between the single cells and remove heat from active areas [5, 21]. It is in contact with the anode side of one cell unit and the cathode side in the next cell unit, hence the name bipolar. The placement of the bipolar plates in PEMFC stacks and PEMWE stacks are displayed in Figure 1.2 and Figure 1.3, respectively. For gases and water to be homogeneously distributed and removed across the active area of each single cell, a flow field is machined or stamped directly on the BPP surface. Various flow field patterns have been used in the past, and some of them are displayed in Figure 1.4. Figure 1.5 shows the bipolar plates used for the PEM fuel cells in this study, and they have a parallel flow field.

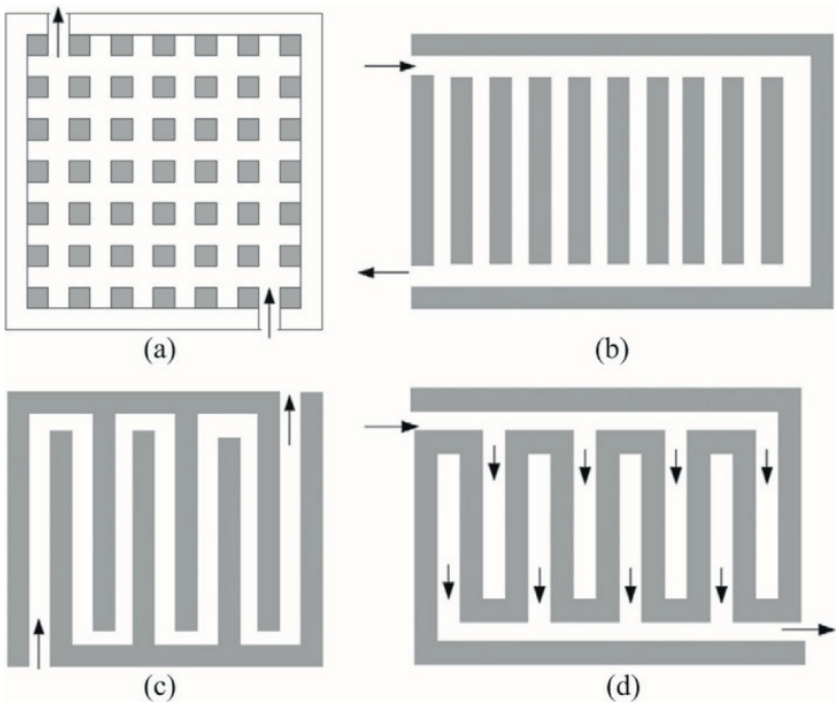

Figure 1.4: Typical flow field designs: a) pin-type, b) series-parallel, c) serpentine and d) interdigitated [22].

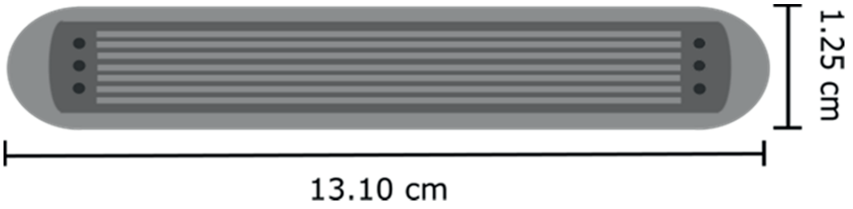

Figure 1.5: The bipolar plate used in this thesis, with a parallel flow field.

The environments inside both PEMFCs and PEMWEs are demanding, due to the proton exchange membrane, electrolyte, temperatures and high electrode potentials. This results in quite strict requirements for the BPPs. The BPP should have a high bulk electrical conductivity, including low surface and contact resistivity, high gas permeability and be resistant to degradation in the given environment [20, 23, 24]. As the potential on the anode side of a PEM electrolyzer can surpass 2.0 V, the requirements for BPPs in PEM electrolyzers are even more rigid than for PEM fuel cells. These requirements makes it difficult to find materials that can withstand the operating conditions inside PEM systems, and it has led to the use of expensive materials. Tsuchiya and Kobayashi [6] reported the BPP to stand for approx. 45 % of the total cost in a PEM fuel cell system in 2000. By their estimates, this cost will be reduced to 37.4 % in 2020, assuming 5 million Fuel Cell Vehicles. In the same paper, the BPP was said to stand for 80 % of the weight in a PEMFC stack. Aalto et al. [25] estimated the cost of the BPP to be approx. 25 % of the total cost in 2009. Ayers et al. [26] reported the cost of flow fields and separator plates in PEM electrolyzers to constitute for 48% of the total cost. These numbers depends on various factors, but regardless of the exact numbers, there are strong incentives to reduce both cost and weight of the BPPs.

In commercial PEM fuel cells, carbon based materials are most commonly used as BPPs, but they have to be individually processed, and the production of such plates is thus time-consuming [23]. This, in addition to the cost and rather porous and fragile nature of the carbon material, results in high prizes for the BPPs. In PEM electrolyzers, carbon based materials are not well suited, as they will corrode due to the high potentials at the oxygen side of the MEA [20]. For both PEMWE and PEMFC systems, metal BPPs might thus be the solution. As opposed to carbon materials, metals can be stamped, which reduces the production cost. In addition they are usually good electrical- and thermal conductors, possess high strength and high chemical stability [27]. Metals that are not noble tend to degrade over time, due to both corrosion and the formation of a passive layer on the metal surface. In addition,

several metals retain rather high thermal expansion coefficients, which can be an issue in compact PEM systems.

In order to avoid several of the issues with non-noble metal BPPs, coating of the surface is considered an alternative solution [4, 5]. Coatings made from noble metals could easily eliminate the problems with degrading of the BPP, but even as a coating, the addition of noble metals increases the cost significantly. As the conditions inside a PEMFC differs from the conditions inside a PEMWE, both substrate material and coating have to be chosen for the specific system it will be used in. For BPPs in PEMFC systems, several coatings have been investigated and tested extensively [28-30]. When it comes to BPPs in PEMWEs, there are fewer studies of coatings on metals. However, some studies have been done on the coating of titanium as BPP material for regenerative fuel cells and electrolyzers [4, 31-37].

1.2.5 Corrosion and Oxide Formation

When working with metals and alloys, it is important to have an understanding of both corrosion and oxide formation. The processes taking place on metal surfaces in various environments have been the topic of numerous books and published articles. When a metal corrodes, oxides can be formed on the material surface. The composition and properties of these oxides differ from metal to metal, and are also affected by the environment. Several oxides possess semiconductor characteristics with for example limited electrical conductivity. Such oxides typically passivates the surface and can protect the metal from further corrosion. How well the oxide adhere to the substrate is detrimental when corrosion is to be avoided. Metals which form insulating surface oxides are often used as structural components in e.g. buildings, where passivation of the metal surface is usually an advantage. However, when metals are used in electrochemical devises such as BPPs in fuel cell- and electrolyzer stacks, electrical conductivity is needed for the device to transport the current in the circuit.

Many metals can form more than one type of oxide, as the metal can have more than one oxidation state. Titanium can e.g. form both TiO and TiO_2 [38], depending on the environment it is in. In alloys, the oxide can be composed of one or several metals, and sometimes in multiple layers of different oxides. The oxide layer formed on AISI 316L has been reported to consist of several metal oxides, organized in multiple layers [39]. Some metals form porous oxides, and the thickness of the oxides also vary from metal to metal. Electrical potential, pH and temperature are some of the factors that can affect the formation and stability of metal oxides. By doping a

semiconductor oxide, the electrical properties can be tailored, and in e.g. Indium Tin Oxide, the addition of tin lowers the resistivity of the indium oxide [40].

Several theories have been put forth in an attempt to explain the general mechanisms of the oxidation of metals. The Tammann-Pilling-Bedworth parabolic law and the Wagner theory are examples of early diffusion theories [41]. Cabrera and Mott published their “Theory of the oxidation of metals” in 1949 [42]. In their theory they suggest that a strong field set up in thin oxide films at low temperatures, due to a potential difference between metal and adsorbed oxygen, enabling ions to move through the oxide. In their theory oxygen atoms absorb to the oxide/atmosphere interface, and as the oxide is very thin, electrons from the metal can pass through [13].

1.3 Motivation and aim of Work

As with all technologies, there are challenges with PEM systems. Lifetime and cost are two major issues with both fuel cells and electrolyzers today. The Proton Exchange Membrane can be used for both fuel cells and water electrolyzers, and this membrane causes an acidic environment in the device. This, in addition to several other factors sets a high standard for the properties of the components inside both PEMFCs and PEMWEs. One of these components is the Bipolar Plate, which is usually made of metals or carbon-based materials. Although the requirements for BPPs are not the same for PEMWEs and PEFCs, the BPP is prone to corrosion under the operating conditions found in both devices. The BPP stand for a major share of the cost and weight in both PEMFC and PEMWE stacks [6, 25], and there is thus a great incentive for further research on BPPs.

Table 1.1: DoEs targets for PEMFC bipolar plates [43].

Properties	Units	2011 status[a]	2020 targets
Cost[b]	$ kW^{-1}	5-10	3
Corrosion, anode[c]	$\mu A\ cm^{-2}$	<1	<1
Corrosion, cathode[d]	$\mu A\ cm^{-2}$	<1	<1
Electrical conductivity	$S\ cm^{-1}$	<100	<100
Areal specific resistance[e]	$\Omega\ cm^2$	0.03	0.01

[a] Status is based on information found in 2010 & 2011 Annual Progress Reports – project description write ups of TreadStone Technologies, Inc. and Oak Ridge National Laboratory.

[b] Costs projected to high volume production (500,000 stacks per year), assuming MEA meets performance target of 1 $W\ cm^{-2}$.

[c] pH 3 0.1 ppm HF, 80°C, peak active current $<1x10^{-6}$ A cm^{-2} (potentiodynamic test at 0.1 mV/s, -0.4V to +0.6V (Ag/AgCl)), de-aerated with Ar purge.

[d] pH 3 0.1 ppm HF, 80°C, passive current $<5x10^{-8}$ A cm^{-2} (potentiostatic test at +0.6V (Ag/AgCl) for >24h, aerated solution.

[e] Includes interfacial contact resistance (on as received and after potentiostatic test) measured both sides per Wang, et al. J. Power Sources 115 (2003) 243-251 at 200 psi (138 N cm^{-2}).

In 2005 the United States Department of Energy (DoE) set fort targets for bipolar plates in PEM fuel cells, which were updated in 2012 [43]. The latter shows the status in 2011 as well as new targets for 2020, and the ones that have been important targets for the work in this thesis are shown in Table 1.1. The complete tables of targets from 2005 and 2012 are presented in Chapters 2 and 3, respectively. Both the corrosion

and resistance targets have been important for the work on BPPs for PEMFCs described in this thesis, and they were used when specific goals were set for this project. Even though there does not exist similar goals for bipolar plates in PEMWE, the targets in Table 1.1 have been used to some extent in this part of the project as well.

The overarching objective with the work described in this thesis, is to contribute to reducing the cost and increasing the lifetime of PEM systems through investigation and improvement of the bipolar plate. The primary goal is to establish good and reliable testing procedures for both in situ and ex situ measurements, as the procedures described in the literature have not been satisfactory. For instance, the pH values used for ex-situ polarization of BPPs for PEMFCs are generally very low, and there has been a lack of studies describing in situ ICR measurements in operating PEM systems. The secondary goal of this PhD work, is to investigate various BPP materials and coatings that can contribute to increasing the lifetime and minimizing the cost of PEM water electrolyzers. No previous studies have extensively tested and compared various materials as potential BPP substrates at high voltage operation. Tin doped Indium Oxide (ITO) has previously been used for various applications, including coating for solar cells, camera lenses and automobile windows. With its good electrical conductivity, it could be a promising coating for BPPs in PEM electrolysis. Literature describing testing of ITO coated BPP for PEMWE has yet to be found.

1.4 Outline of Thesis

This thesis is built up around the four articles/manuscripts presented in Chapter 2-5. In Chapter 2 and 3, work with BPPs for PEMFCs are described, while Chapter 4 and 5 present work related to BPPs for PEMWEs. In order to better understand the overall scope of the thesis, an overall introduction and an overall conclusion are included. Descriptions of the materials and methods used are described in each of the articles/manuscripts. The introduction was written as a supplement to the introductions included in each of the articles/manuscripts, and the in depth literature reviews are thus included in Chapter 2-5.

Chapter 2 describes ex situ polarization and ICR measurements performed on stainless steel bipolar plates for PEMFC, with the objective of testing what effect the pH and halides in the electrolyte has on the corrosion processes taking place on the stainless steel (AISI 316L) surface. Sulfuric acid was used to alter the pH in the electrolytes, and chlorides and fluorides were added in different amounts. In

addition to ICR measurements before and after polarization, SEM and AES analysis were used to analyze the steel surfaces.

The setup used for measuring ICR in Chapter 2 was the early version, where the BPPs tested were limited in size to the cell housing. A new and improved setup for ICR measurements was thus built, which could handle various sized samples and was easier to use.

In Chapter 3, a method for in situ ICR measurements is presented. It was inspired by the few similar methods described in the literature, but was customized for the fuel cells used in this work. By incorporating thin gold wires in-between the layers of BPPs, gasket and GDL in the fuel cell, measurements were performed during operation without interfering with the processes in the fuel cell. The objective was to create a method for ICR measurements under real conditions, that would prove to be as reliable as the ex situ ICR measurements already used in Chapter 2.

Chapter 4 is a material study, where nine different materials (both pure metals and alloys) were investigated for use as BPP in PEMWEs. The incentive behind this study was the lack of studies in the literature with focus on substrate materials for BPPs in PEMWE at high voltage operation. In addition, there was an objective of comparing the corrosion currents and ICR values of these substrate materials against each other.

The choice of reference electrode differed in the various chapters. The Hg/Hg_2SO_4 reference was used for the work described in Chapters 2-4, carefully selected to avoid any aggressive ions in the electrolyte. However, the setup using this electrode was complex, as it was connected to the electrolyte via a salt bridge. The Hg/Hg_2SO_4 reference was thus replaced with a reversible hydrogen electrode, with an integrated battery producing hydrogen gas. This electrode was situated directly into the working electrode electrolyte.

Chapter 5 presents a bi-layer coating consisting of a tantalum baselayer deposited by High Power Pulsed Magnetron Sputtering (HPPMS) and an Indium Tin Oxide top layer deposited by pulsed dc Magnetron Sputtering (PMS). The bi-layer coating was applied to titanium plates and polarized in an ex situ setup. Potential, temperature and pH of the electrolyte was altered, in addition to duration of polarization, with the objective of studying how the ICR after polarization differed from test to test.

A summarizing concluding chapter (Chapter 6) and a chapter (Chapter 7) describing suggestions for further work are also included as the final chapters of this thesis.

1.5 Literature

1. *United Nations Framework on Climate Change (UNFCCC), Annual Conference of Parties, COP21, Paris, France, 7–8 December 2015. Adoption of the Paris Agreement*. 2015.
2. Barbir, F., *PEM electrolysis for production of hydrogen from renewable energy sources.* Solar Energy, 2005. **78**(5): p. 661-669.
3. Holladay, J.D., et al., *An overview of hydrogen production technologies.* Catalysis Today, 2009. **139**(4): p. 244-260.
4. Carmo, M., et al., *A comprehensive review on PEM water electrolysis.* International Journal of Hydrogen Energy, 2013. **38**(12): p. 4901-4934.
5. Larminie, J. and A. Dicks, *Fuel cell systems explained*, ed. Wiley. 2003.
6. Tsuchiya, H. and O. Kobayashi, *Mass production cost of PEM fuel cell by learning curve.* International Journal of Hydrogen Energy, 2004. **29**(10): p. 985-990.
7. Wind, J., *1 - Hydrogen-fueled road automobiles – Passenger cars and buses A2 - Ball, Michael*, in *Compendium of Hydrogen Energy*, A. Basile and T.N. Veziroğlu, Editors. 2016, Woodhead Publishing: Oxford. p. 3-21.
8. Tesla. *Model S*. 2016; Available from: https://www.teslamotors.com/sites/default/files/tesla-model-s.pdf.
9. *Fuel Cells Bulletin, Toyota to launch Mirai in Sweden, Norway to boost European fleet.* Fuel Cells Bulletin, 2016. **2016**(4): p. 2-3.
10. Hua, T., et al., *Status of hydrogen fuel cell electric buses worldwide.* Journal of Power Sources, 2014. **269**: p. 975-993.
11. Vogler, F. and G. Sattler, *3 - Hydrogen-fueled marine transportation A2 - Ball, Michael*, in *Compendium of Hydrogen Energy*, A. Basile and T.N. Veziroğlu, Editors. 2016, Woodhead Publishing: Oxford. p. 35-65.
12. Kendall, K. and B.G. Pollet, *4.12 - Hydrogen and Fuel Cells in Transport A2 - Sayigh, Ali*, in *Comprehensive Renewable Energy*. 2012, Elsevier: Oxford. p. 301-313.
13. Talbot, E.J. and D.R. Talbot, *Corrosion Science and Technology*. 2007: CRC Press.
14. Chu, H.S., et al., *Transient behavior of CO poisoning of the anode catalyst layer of a PEM fuel cell.* Journal of Power Sources, 2006. **159**(2): p. 1071-1077.
15. Zhang, J. and R. Datta, *Sustained Potential Oscillations in Proton Exchange Membrane Fuel Cells with PtRu as Anode Catalyst*. Journal of The Electrochemical Society, 2002. **149**(11): p. A1423-A1431.
16. Shao, Y., G. Yin, and Y. Gao, *Understanding and approaches for the durability issues of Pt-based catalysts for PEM fuel cell.* Journal of Power Sources, 2007. **171**(2): p. 558-566.
17. Yoshida, T. and K. Kojima, *Toyota MIRAI Fuel Cell Vehicle and Progress Toward a Future Hydrogen Society.* The Electrochemical Society Interface, 2015. **24**(2): p. 45-49.
18. Harrison, K.W., *Hydrogen production, fundamentals and case study summaries preprint*. 2010, National Renewable Energy Laboratory: Golden, CO :.
19. Millet, P., *Water Electrolysis for Hydrogen Generation*, in *Electrochemical Technologies for Energy Storage and Conversion*. 2011, Wiley-VCH Verlag GmbH & Co. KGaA. p. 383-423.
20. Smolinka, T., S. Rau, and C. Hebling, *Polymer Electrolyte Membrane (PEM) Water Electrolysis*, in *Hydrogen and fuel cells*, D. Stolten, Editor. 2010. p. 269-289.
21. Hermann, A., T. Chaudhuri, and P. Spagnol, *Bipolar plates for PEM fuel cells: A review.* International Journal of Hydrogen Energy, 2005. **30**(12): p. 1297-1302.
22. Peng, L., P. Yi, and X. Lai, *Design and manufacturing of stainless steel bipolar plates for proton exchange membrane fuel cells.* International Journal of Hydrogen Energy, 2014. **39**(36): p. 21127-21153.

23. Wang, H.L., M.A. Sweikart, and J.A. Turner, *Stainless steel as bipolar plate material for polymer electrolyte membrane fuel cells.* Journal of Power Sources, 2003. **115**(2): p. 243-251.
24. Chang, Y.-Y., et al., *Antibacterial properties and cytocompatibility of tantalum oxide coatings.* Surface and Coatings Technology, 2014. **259, Part B**: p. 193-198.
25. Aalto, S., et al., *Bipolar plate, method for producing bipolar plate and PEM fuel cell*. 2009, Google Patents.
26. Ayers, K.E., et al., *Research Advances towards Low Cost, High Efficiency PEM Electrolysis.* ECS Transactions, 2010. **33**(1): p. 3-15.
27. Wang, H. and J.A. Turner, *Reviewing Metallic PEMFC Bipolar Plates.* Fuel Cells, 2010. **10**(4): p. 510-519.
28. Tawfik, H., Y. Hung, and D. Mahajan, *Metal bipolar plates for PEM fuel cell - A review.* Journal of Power Sources, 2007. **163**(2): p. 755-767.
29. Taherian, R., *A review of composite and metallic bipolar plates in proton exchange membrane fuel cell: Materials, fabrication, and material selection.* Journal of Power Sources, 2014. **265**: p. 370-390.
30. Antunes, R.A., et al., *Corrosion of metal bipolar plates for PEM fuel cells: A review.* International Journal of Hydrogen Energy, 2010. **35**(8): p. 3632-3647.
31. Jung, H.-Y., et al., *Performance of gold-coated titanium bipolar plates in unitized regenerative fuel cell operation.* Journal of Power Sources, 2009. **194**(2): p. 972-975.
32. Jung, H.-Y., S.-Y. Huang, and B.N. Popov, *High-durability titanium bipolar plate modified by electrochemical deposition of platinum for unitized regenerative fuel cell (URFC).* Journal of Power Sources. **195**(7): p. 1950-1956.
33. Lin, M.-T., C.-H. Wan, and W. Wu, *Comparison of corrosion behaviors between SS304 and Ti substrate coated with (Ti,Zr)N thin films as Metal bipolar plate for unitized regenerative fuel cell.* Thin Solid Films, 2013. **544**(0): p. 162-169.
34. Nikiforov, A.V., et al., *Corrosion behaviour of construction materials for high temperature steam electrolysers.* International Journal of Hydrogen Energy, 2011. **36**(1): p. 111-119.
35. Zhang, H., et al., *Performance of Ti–Ag-deposited titanium bipolar plates in simulated unitized regenerative fuel cell (URFC) environment.* International Journal of Hydrogen Energy, 2011. **36**(9): p. 5695-5701.
36. Zhang, M., et al., *Honeycomb-like nanocomposite Ti-Ag-N films prepared by pulsed bias arc ion plating on titanium as bipolar plates for unitized regenerative fuel cells.* Journal of Power Sources, 2012. **198**(0): p. 196-202.
37. Wang, J.-T., et al., *Corrosion behavior of three bipolar plate materials in simulated SPE water electrolysis environment.* International Journal of Hydrogen Energy, 2012. **37**(17): p. 12069-12073.
38. Pourbaix, M., *Atlas of electrochemical equilibria in aqueous solutions*. 1966, Oxford; New York: Pergamon Press.
39. da Cunha Belo, M., et al., *Composition, structure and properties of the oxide films formed on the stainless steel 316L in a primary type PWR environment.* Corrosion Science, 1998. **40**(2): p. 447-463.
40. Kim, H., et al., *Electrical, optical, and structural properties of indium–tin–oxide thin films for organic light-emitting devices.* Journal of Applied Physics, 1999. **86**(11): p. 6451-6461.
41. Fromhold, A.T., *Theory of metal oxidation.* 1976.
42. Cabrera, N. and N.F. Mott, *Theory of the oxidation of metals.* Reports on Progress in Physics, 1949. **12**(1): p. 163.
43. *U.S. Department of Energy, Fuel Cell Technologies Office Multi-Year Research, Development, and Demonstration Plan*. 2012. p. 29.

2 The Effect of pH and Halides on the Corrosion Process of Stainless Steel Bipolar Plates for Proton Exchange Membrane Fuel Cells

Authors: Sigrid Lædre[a,c], Ole Edvard Kongstein[b] Anders Oedegaard[b] Frode Seland[c] and Håvard Karoliussen[a]

a Sør-Trøndelag University College (HIST), Norway

b SINTEF Materials and Chemistry, Norway

c Norwegian University of Science and Technology (NTNU), Norway

This article was published in The International Journal of Hydrogen Energy in October 2012 [1]. The layout of the article has been altered to fit this thesis, but the content has not been changed.

2.1 Abstract

Stainless steel is attractive as material for Bipolar Plates (BPPs) in PEM fuel cells, due to its high electrical conductivity, high mechanical strength and relatively low material and processing cost. Potentiostatic and potentiodynamic tests were performed in H_2SO_4 solutions on AISI 316L stainless steel bipolar plates with etched flow fields. The effect of pH and presence of small amounts of fluoride and chloride on the corrosion rate and Interfacial Contact Resistance (ICR) of the stainless steel BPPs were investigated. The tests performed in electrolytes with various pH values revealed that the oxide layer was thinner and more prone to corrosion at pH values significantly lower than the pH one expects the bipolar plate to experience in an operating PEMFC. The use of solutions with very low pH in such measurements is thus probably not the best way of accelerating the corrosion rate of stainless steel bipolar plates. By use of strongly acidic solutions the composition and thickness of the oxide layer on the stainless steel is probably altered in a way that might never have happened in an operating PEM fuel cell. Additions of fluoride and chloride in the amounts expected in an operating fuel cell (2 ppm F^- and 10 ppm Cl^-) did not cause significant changes for neither the polarization- nor the contact resistance measurements, as opposed to what is frequently described in the literature. However, by increasing the amount of Cl^- to 100 ppm, pitting was initiated on the stainless steel surface.

2.2 Introduction

The Bipolar Plate (BPP) accounts for about 80% of the total cell-weight and about 25% of the total cell cost in a Proton Exchange Membrane Fuel Cell (PEMFC) [2, 3]. The principle tasks for a bipolar plate is to distribute the gas in the cell, manage the water in the cell, remove heat from active areas, prevent leakage and to conduct the current away from each single cell in a stack [4]. Furthermore, a bipolar plate needs to be electrically conducting, corrosion resistant, easy to produce, relatively cheap and both chemically and mechanically stable [5]. Most commercialized bipolar plates made today are carbon based, but they are expensive and time consuming to manufacture. Metal bipolar plates, on the other hand, are cheaper and easier to produce, and they are in general very good electrical- and thermal conductors. However, metal plates tend to degrade over time, mainly due to corrosion or electronic passivation of the surface layer due to oxide formation. Furthermore, common metals possess rather high thermal expansion coefficients, which is undesirable. A bipolar plate needs to have a low electrical resistivity in order to conduct the current between individual Membrane Electrode Assemblies (MEAs) in a stack. Passivity, which protects the metal from corrosion by formation of a thin surface film under oxidizing conditions at high anodic polarization, can result in high contact resistance between the metal and the Gas Diffusion Layer (GDL) in a PEMFC.

Table 2.1: DoEs targets for PEMFC bipolar plates [6].

Properties	Units	2005 status	2010	2015
Cost[a]	\$ kW^{-1}	10[b]	5	3
Weight	kg kW^{-1}	0.36	<0.4	<0.4
H_2 permeation flux	cm^3 s^{-1} cm^{-2} @ 80 °C, 3 atm	$<2{\cdot}10^{-6}$	$<2{\cdot}10^{-6}$	$<2{\cdot}10^{-6}$
Corrosion	μA cm^{-2}	<1[c]	<1[c]	<1[c]
Electrical conductivity	S cm^{-1}	<600	<100	<100
Resistivity[d]	Ω cm^2	<0.02	<0.01	<0.01
Flexural strength	MPa	<34	<25	<25
Flexibility	% deflection at midspan	1.5-3.5	3-5	3-5

[a] Based on 2002 dollars and costs projected to high volume production (500,000 stacks per year)

[b] Status is from 2005 TIAX study.

[c] May have to be as low as 1 nA cm^{-2} if all corrosion product ions remain in ionomer.

[d] includes contact resistance.

Several studies have investigated the possibility of using stainless steel as bipolar plate material [2, 5, 7-11]. Stainless steel has a relatively high strength, low gas permeability, high chemical stability, a wide range of alloy choices and it is relatively cheap to produce into desired shape and size [4]. The U.S. Department of Energy (DoE) [6] has established some development targets for various properties of bipolar plates for PEM fuel cells. These are given in Table 2.1 for the years 2005, 2010 and 2015.

Previous studies on the corrosion resistance of stainless steel bipolar plates have been conducted, both in situ and ex-situ [5, 12-15], and various electrolytes have been used for the polarization of these plates. Feng et al. [12] carried out potentiodynamic, potentiostatic and Electrochemical Impedance Spectroscopy (EIS) measurements of AISI 316L under both simulated fuel cell conditions (pH from 3 to 6) and accelerated conditions (0.5 M and 1 M H_2SO_4). $1{\cdot}10^{-4}$ M F^-, $2{\cdot}10^{-6}$ M SO_4^{2-} and $2{\cdot}10^{-6}$ M Cl^- was also added to some of the electrolytes. It was found that the nature of the passive film depends on both pH and applied potential during polarization. Wang et al. [5] polarized different grades of stainless steel, from Open Circuit Voltage (OCV) in both anodic and cathodic direction, using a 1 M H_2SO_4 with 2 ppm F^- as electrolyte. They also performed potentiostatic measurements at 0.6 V_{SCE} and -0.1 V_{SCE} to simulate the cathode and anode potentials, respectively, in an operating fuel cell. They suggested that the thickness of the passive film formed on stainless steel during potentiostatic polarization remains constant throughout the polarization. Kumagai et al. [14] used a 0.05 M H_2SO_4 electrolyte to study the behavior of various austenitic steels as a function of pH, where the pH was adjusted by addition of 0.5 M Na_2SO_4. It was found that at pH values below 3.3, relatively thin films enriched with chromium oxide was formed, while the films formed at higher pH were thicker and mainly consisted of iron oxide.

Nafion membranes are made from a copolymer of two different fluoride containing compounds [16], and when used in PEM fuel cells, fluoride in the form of HF is susceptible to be released. Agneaux et al. [17] analyzed solutions gathered from both anodic- and cathodic outlets of PEM fuel cells operated with bipolar plates made from different grades of stainless steel, and the fluoride content in the water from the anode and cathode outlets were found to be $5.7{\cdot}10^{-4}$ M and $4.1{\cdot}10^{-4}$ M, respectively. Healy et al.[18] found that the amount of F^- in the fuel cell product water, when operated at temperatures between 75-82 °C and current densities of 0.2-0.8 A cm^{-2}, varies between approximately $1.6{\cdot}10^{-4}$ M and $5.6{\cdot}10^{-6}$ M. Borup et al. [19] suggested that both fluoride and chloride facilitates the initiation of corrosion of bipolar plate materials. Yang et al. [13] performed potentiodynamic and potentiostatic experiments in $1.0{\cdot}10^{-5}$ M H_2SO_4 solutions with addition of different amounts of F^-.

Although all currents measured satisfied DoEs target, these tests indicated that the corrosion current, and also pitting corrosion, increases with F^- concentrations. Rivas et al. [20] characterized the corrosion resistance of AISI 316 coated with molybdenum oxide films by potentidynamic and potentiostatic test in a 0.5 M sulfuric acid solutions with 2 ppm fluoride. They found that the deposited Mo oxides offer a high degree of protection against corrosion on specific areas of the stainless steel. Matsuoka et al. [21] found no effect on MEA performance (voltage degradation and loss of ESA) with additions of small amounts of F^- (3 mM solutions) to the fuel stream during operating conditions (70 °C and 0.3 A cm^{-2}). On the other hand, a significant change was observed with addition of similar amounts of Cl^-, as reported in the same work.

There are several possible resources to the Cl^- found in PEM fuel cells. Hydrogen, produced as a bi-product in the chlorine-alkali industry [22], contains ppm levels of Cl_2. Cl^- can also be found in PEM fuel cells operated in marine environment because they might take up the chloride ions from this environment through the fuel and/or air. Schmidt et al.[23] claimed that high-surface area fuel cell catalysts, which are often synthesized from halide-containing educts, can release halides into the fuel cell. They also suggested that water in the feed streams can contain traces of Cl^-. Previous research has shown that Cl^- can contaminate a PEM fuel cell by adsorbing to the active sites of the catalyst [23], and by accelerating the catalyst dissolution [24]. Ageneaux et al. [17] found the chloride concentrations for anodic and cathodic media in PEM fuel cells to be $9{\cdot}10^{-7}$ M and $1{\cdot}10^{-6}$ M respectively. Li et al. [22] performed in situ experiments by operating a Teldyne single fuel cell where Cl^- was added in various amounts as HCl to the fuel and air. Their aim was to understand the impacts and mechanisms of chlorine contamination on the MEA and they found the severity of contamination to be independent of injection side (fuel vs. air). Ofstad et al. [25] evaluated the stability of different types of platinum surfaces in the presence of chloride. They added 10, 20 and 50 ppm chloride as hydrochloric acid to a 0.5 M H_2SO_4 solution, and found the dissolution rate of the Pt/C catalyst to be up to 170 times larger with the addition of chloride in these amounts.

Abd El Meguid et al. [26] explored the potentiodynamic anodic polarization behavior of AISI 304 in 0.1 M NaCl with addition of several anions. It was found that the sulfate ion increases the pitting potential of AISI 304, which reveals that the competition between Cl^- and SO_4^{2-} to adsorb to the surface may inhibit the pitting attack. Pujar et al. [27] performed Electrochemical Noise (EN) measurements on AISI 316 in deaerated solutions of sodium chloride and sodium sulfate. They reported that the sulfate ions strengthens the passive film by being incorporated into it, as opposed to the chloride ions, which adsorb to the passive film and initiate pitting corrosion.

The oxide layer formed on AISI 316L is a chromium oxide (Cr_2O_3), and can be formed in air, without anodic polarization. This layer is what makes the stainless steel protected against corrosion, but when stainless steel is used as bipolar plate material, the oxide layer also impedes the flow of current between individual cells in a stack. Wang et al. [5] and Lee and Lim [28] tested the interfacial contact resistance (ICR) of stainless steel. Their setups were similar, with carbon paper next to the sample on both top and bottom, and copper plates as an outer structure where the current was sent through. Wang et al. [5] measured the contact resistance of stainless steel bipolar plates after pre-treating them under potentiostatic conditions at 0.6 V_{SCE} for different periods of time. They found the contact resistance after 60 minutes of polarization at 0.6 V_{SCE} to be 250 mΩ cm^2 at 140 N cm^{-2} (14 bar), and the tests performed over different time spans showed similar results. Several studies have been conducted where Auger Electron Spectroscopy (AES) have been used as a method for investigating oxide layers on stainless steel [29, 30]. Davies et al. [31] performed surface analyses of the passive film on AISI 316L by use of AES as part of their investigation of AISI 316L as material for bipolar plates in solid polymer fuel cells. Their research showed that the oxygen content decreases with increasing depth.

Our aim in this study was to investigate AISI 316L bipolar plates when polarized in solutions with different molarities, in order to study the influence of pH on the corrosion rate and contact resistance. There was also an interest to study the effect F^- and Cl^- have on the performance of stainless steel bipolar plates. Previous studies have been performed on bipolar plates with respect to F^- [16-18], where significant effects were reported. However, previous studies on Cl^- additions to PEM fuel cells have primarily been focused on the overall effect on the fuel cell, and/or on the polymer membrane [22, 25]. Sulfate was not added to the electrolyte because previous research has suggested that the ion has a corrosion inhibiting effect [26, 27], which was not desirable during this work. To get a better understanding of how the thickness of the chromium oxide layer changes under different polarization conditions, ICR measurements and Scanning Electron Microscopy (SEM) imaging were also performed.

2.3 Experimental

AISI 316L bipolar plates were used for the tests. The surface area of the plates was 16 cm^2 before the flow field was etched in, and the surface of the non-etched area was 8.059 cm^2. Potentiostatic-, potentiodynamic- and ICR measurements were performed during this study, as well as SEM (Hitachi S-3400N) and AES (JEOL JAMP-9500) analysis.

2.3.1 Electrochemical Measurements of the Bipolar Plates

A three-electrode system was used to perform the potentiostatic and potentiodynamic measurements. Concentrated sulfuric acid (Merck, 95-97 %) was mixed with Millipore water (18.2 MΩ) till the desired acid concentration and used as electrolyte. A potentiostat (IM6 Zahner electric) was used to polarize the stainless steel bipolar plate acting as the working electrode vs. a Mercury/mercury sulfate (Hg/Hg_2SO_4) reference electrode. The reference electrode was placed in a separate compartment containing a solution of saturated K_2SO_4, which was connected to the electrolyte via a salt bridge made of sulfuric acid of the same molarity as used in the electrode compartment. The counter electrode, a platinum foil, was placed in the electrolyte along with the working electrode and a temperature gauge, which was connected to a heating plate controlling the temperature in the test cell. The temperature in the cell was set to 75 ^oC, and nitrogen gas (5.0 N_2, Yara) was continuously bubbled into the electrolyte during the experiments. Two predesigned experiments, a potentiodynamic scan and the other a potentiostatic test, were used to measure the corrosion rate. They are both described in Table 2.2.

Table 2.2: The predesigned potentiodynamic and potentiostatic experiments designed to measure corrosion currents.

Test	Potentials [V_{SHE}]	Duration/speed	Description
Potentiodynamic	-0.25 to 1.05	2 mV s^{-1}	A potential scan covering the potentials of both anode and cathode reactions in a PEMFC.
Potentiostatic	0.951	60 min	Potential close to the cathode potential in a PEMFC.

pH Variations and Addition of Fluoride and Chloride

Both potentiostatic- and potentiodynamic measurements (Table 2.2) were performed in solutions with molarities of 0.1 mM, 1 mM, 0.1 M and 1 M of sulfuric acid. The same measurements were also performed in electrolytes made from 1 mM H_2SO_4 with 2 ppm fluoride, 1 mM H_2SO_4 with 10 ppm chloride and 1 mM H_2SO_4 with 100 ppm. The fluoride was added as NaF (Merck, 99 %) and the chloride was added as NaCl (Merck, 99.5 %). AES analyses were performed on the plates that had been polarized in solutions with various pH values in order to estimate the effect pH has on the thickness of the oxide layer.

2.3.2 Interfacial Contact Resistance Measurements

The ICR of the AISI 316L bipolar plates was measured before and after each corrosion test, and the setup of the contact resistance equipment is shown in Figure 2.1. The setup was designed in such way as to enforce the bipolar plates for similar conditions as in a real fuel cell. A gold coated bipolar plate was used as standard, and the contact resistance was measured between this plate, the backing and the bipolar test plate.

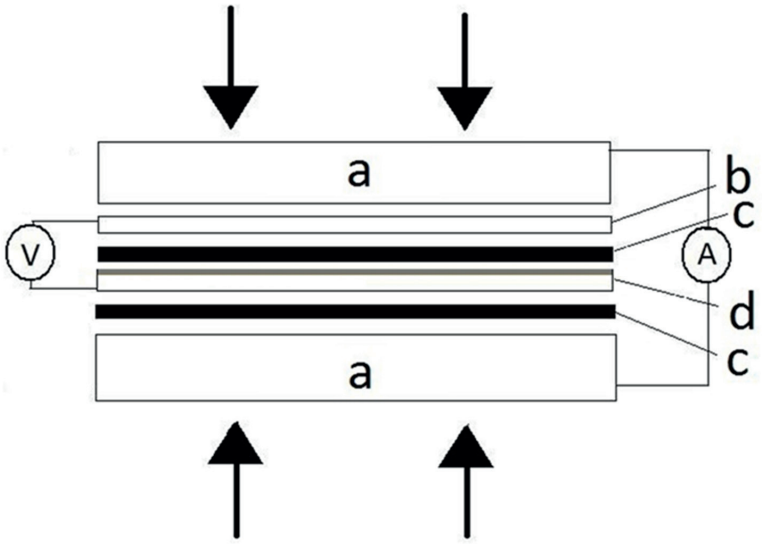

Figure 2.1: Setup for measuring ICR with a) copper plates, b) bipolar test plate, c) carbon backing and d) gold coated stainless steel plate (standard).

A XDL 56-4 DC power supply (Xantex) was connected to the copper plates in order to send current through the whole setup, and the resulting voltage was measured with a multimeter (Fluke 76 True RMS) between the two bipolar plates. A current of 2.0 A was used in the experiments, and the compaction pressure was controlled by a pneumatic cylinder (Camozzi, QP2A080A010).

2.4 Results and Discussion

The potentiostatic- and potentiodynamic tests were chosen to match relevant potentials in an operating PEM fuel cell to study the effect of acidity (pH) an additives (Cl^- and F^-). The first test was a linear polarization, where the potential was set to run from -0.25 V_{SHE} to 1.05 V_{SHE} at 2.00 mV s^{-1}. 1.05 V_{SHE} was chosen because in an operating fuel cell, even with maximum overpotential, the voltage is rarely higher than 1 V_{SHE}. The lowest potential was set to -0.25 V_{SHE} to cover the anode potential in an operating PEM fuel cell. The potential used in the second corrosion test was chosen to simulate the open circuit voltage in a PEM fuel cell, which is typically slightly below 1.00 V.

2.4.1 Variation of pH

In order to study the effect of acid concentration and evaluate whether or not it is possible to accelerate ex-situ tests by simply increasing the acidity, tests were performed in electrolytes with different molarities. The molarities and corresponding pH values are presented in Table 2.3. The local pH variations inside an operating fuel cell is hard to measure, but measurements done (Figure 2.2) on the water leaving the fuel cell, shows that the pH is always higher than 3.75. Healy et al.[18] found the minimum pH in the PEM fuel cell product water to be around 3.80. The pH close to the bipolar plate is probably slightly lower than in the water leaving the fuel cell. Among the four acid concentrations tested during this study, the 1 mM solution was assumed to be the one that lies closest to the actual pH experienced by the bipolar plate. Several previous studies have been conducted in 1 M or 0.50 M H_2SO_4 electrolytes [5, 28, 32]. Some authors used electrolytes with low pH values to accelerate the degrading rate of the plates, but this introduces the possibility of altering the kinetics of the existing surface processes. Furthermore, a too high pH might initiate processes that are unlikely to occur in an operating fuel cell with only moderate pH values.

Table 2.3: Acid concentrations and the corresponding pH values used in this work.

Concentration H_2SO_4	0.0001 M	0.001 M	0.1 M	1 M
pH	3.72	2.87	1.01	0.51

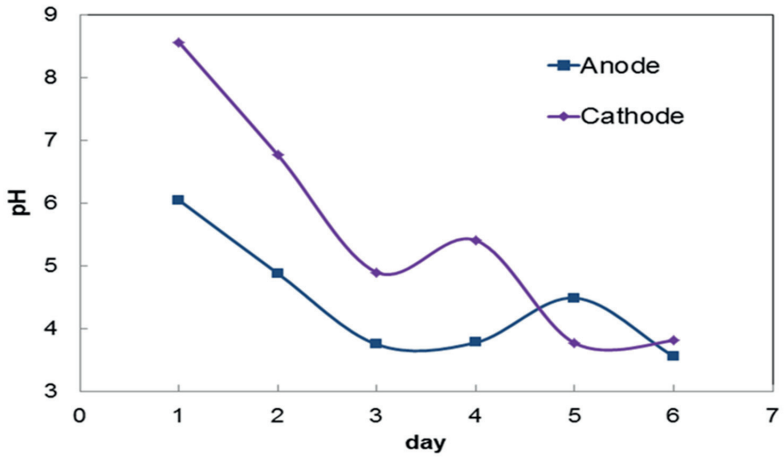

Figure 2.2: pH values measured in the effluent of a fuel cell operating at 75 °C for several days.

The majority of the polarization tests, both potentiostatic and potentiodynamic, produced small currents, sometimes not much larger than the general noise. Figure 2.3 and Figure 2.4 show the potentiostatic and potentiodynamic results, respectively, for the various acidities used in this work. The polarizations performed in 1M solutions show the highest corrosion currents in both figures.

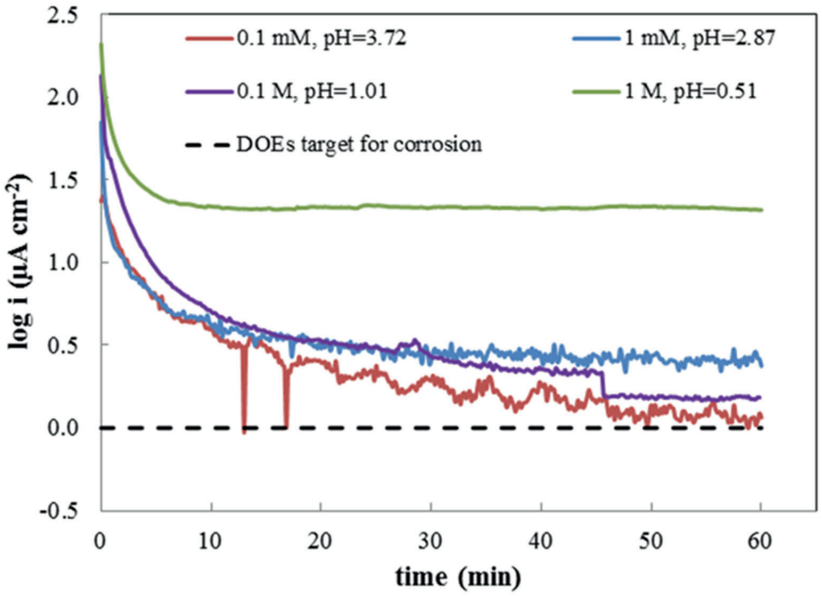

Figure 2.3: Potentiostatic measurements at 0.951 V_{SHE} for 1 hour, variation in pH.

When a strong acidic solution is used, the passivated oxide layer is susceptible to be destabilized, especially at the lower potential. If this happens, the oxide layer could start to reduce, or even dissolve, and the bare stainless steel surface might come in direct contact with the electrolyte. This could in turn initiate corrosion processes at the stainless steel surface that would not have taken place in an electrolyte with lower acidity. From the potentiostatic measurements in Figure 2.3 performed at 0.951 V_{SHE}, a significant steady corrosion current, just below 22 µA cm^{-2}, can be observed for the curve representing the 1 M electrolyte about 5 minutes into the test. The other current transients slowly decay to low values depending on acidity. This effect is also visualized in the potentiodynamic measurements in Figure 2.4. Once again the "passive" region observed between about 0.3 and 0.9 V depends again on acidity, where the 1 M solution obtains a markedly increased current compared to the other three acid concentrations. The corrosion current observed for lower potentials, about 0 to 0.2 V_{SHE} increased with acidity as expected, although a negligible difference was observed for the lowest acid concentrations. Nevertheless, the trend is that a higher acid concentration induces higher corrosion current densities at all relevant potentials, but only small variations are observed when the acid concentration becomes low enough.

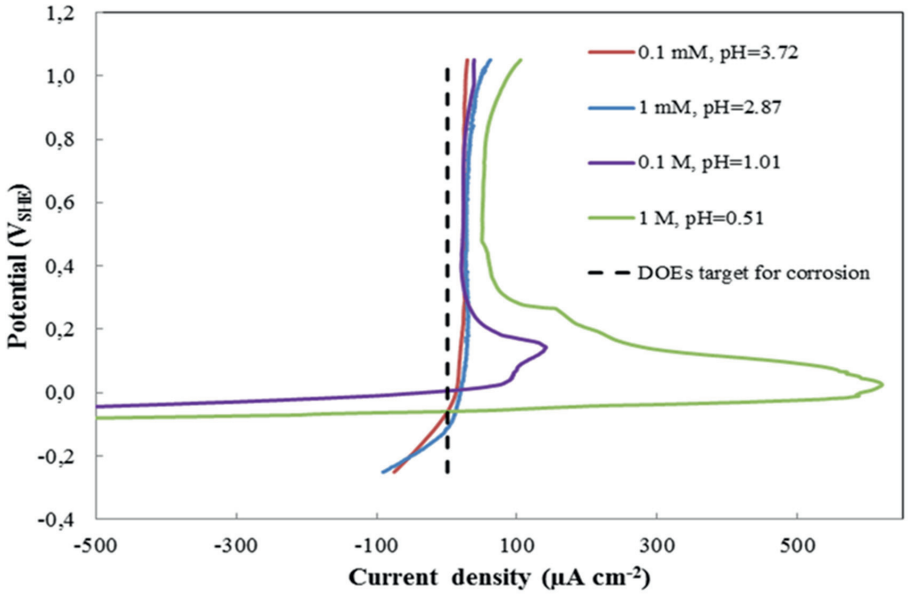

Figure 2.4: Current - potential relation during the potentiodynamic measurements from -0.25 V to 1.05 V_{SHE}, at 2 mVs^{-1}, variation in pH.

DoEs target for corrosion current for bipolar plates in PEM fuel cells is set to less than 1 μA cm^{-2} [33]. Non-coated stainless steel in 0.1 mM, 1 mM and 0.1 M solutions (Figure 2.3) showed current densities close to this value in the potentiostatic tests. These low values are most likely a result of the passivated oxide layer formed on the surface of the plates. It is worth pointing out that an increased passivity, hence lower corrosion current, by lowering the acidity could possibly increase the contact resistance beyond the target put forward by DoE for bipolar plates.

The contact resistance measurements performed after the potentiostatic and potentiodynamic tests for various acid concentrations are presented in Figure 2.5 and 2.6, respectively. From both these figures it becomes obvious that the bipolar plates that had been polarized in solutions with mild pH conditions produced higher contact resistances than the plates polarized in solutions with low pH (very acidic). The low contact resistances measured on the plates used in the 0.1 M and the 1 M tests indicates that there is a difference in oxide layer thickness between the plates polarized in high acidity solutions compared to the ones that had been polarized in lower acidity solutions.

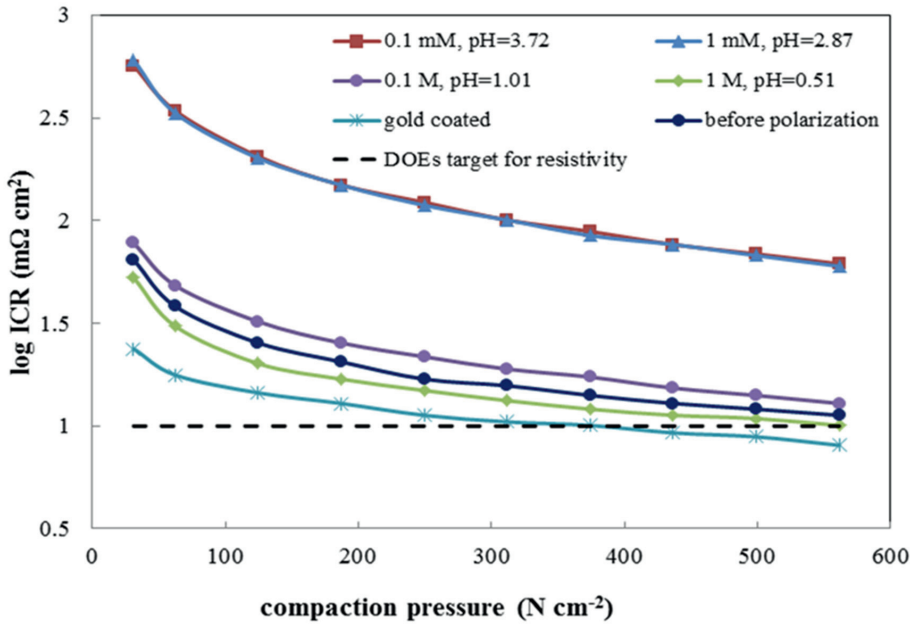

Figure 2.5: ICR results after the potentiostatic measurements at 0.951 V_{SHE}, variation in pH.

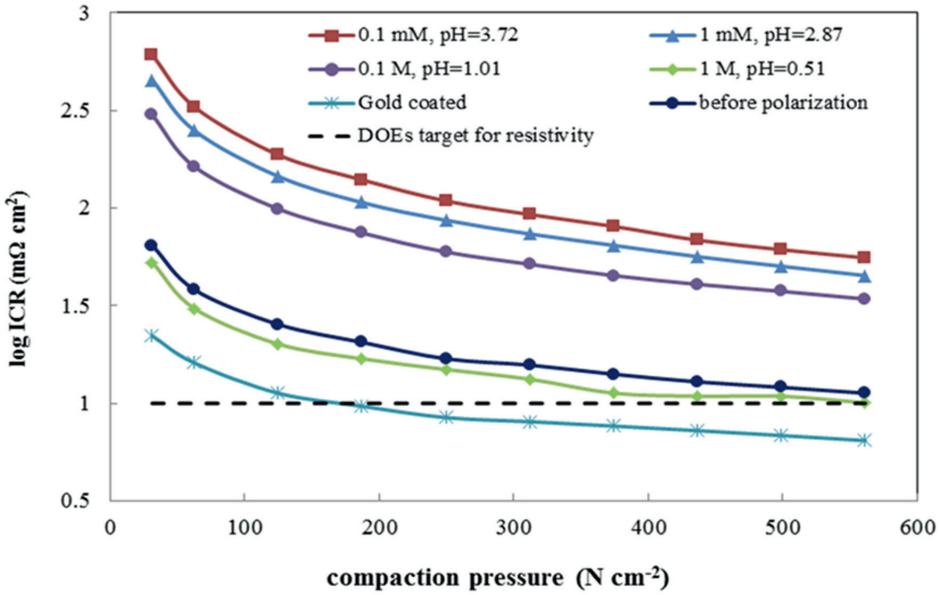

Figure 2.6: ICR results after the potentiodynamic measurements from -0.25 V to 1.05 V_{SHE}, variation in pH.

To confirm this relationship, AES analysis were performed to measure the relative oxide layer thickness on the stainless steel plates. The results are presented in the graphs a, b, c and d in Figure 2.7. The sputtering was performed at a constant rate, and the sputtering time is thus equivalent to the thickness of the oxide layer. Note that the oxygen intensity does not reach zero because of oxygen present in the SEM chamber. All four graphs show a decrease in oxygen content and a corresponding increase in iron content with oxide layer thickness. The AES results from the stainless steel plates that had been polarized in 1 M and 0.1 M sulfuric acid solutions both show a faster decrease in oxygen intensity and a corresponding faster increase in iron intensity than any of the other plates. This shows that the polarization of stainless steel plates in highly acidic solutions produce thinner oxide layers on the plates than if they were polarized in solutions with lower acidities. The thickness of the oxide layer on the stainless steel bipolar plates is thus amongst other characteristics controlled by the acidity of the sulfuric acid electrolyte the plates are tested in. At higher acidities the oxide layer becomes thinner than at lower acidities, which would in turn support the ICR values obtained.

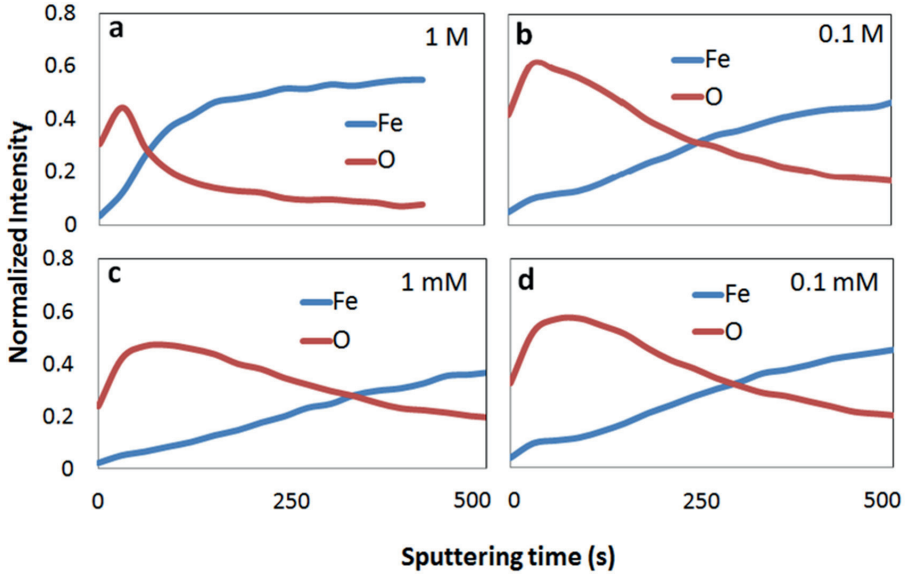

Figure 2.7: AES results showing the change in oxygen and Iron intensity as a function of sputtering time into the oxide layers on the stainless steel samples that had been polarized in solutions with molarities of a) 1M, b) 0.1 M, c) 1 mM and d) 0.1 mM.

By using Ohm's Law in its simplest form, $U = R_{contact} \cdot I$, high contact resistance value have a potentially huge impact on the overall losses in an operating fuel cell. For example, a 100 mΩ cm^2 contact resistance corresponds to a 100 mV voltage loss if the current drawn from the fuel cell is set to 1 A cm^{-2}. At high currents, the voltage loss can be significant even for rather low ICR values.

ICR measurements were performed on gold coated stainless steel bipolar plates that had experienced the same test history as the ordinary stainless steel samples, i.e. they had gone through the potentiostatic- and potentiosdynamic tests in a 1 mM H_2SO_4 electrolyte. The corresponding current-potential values are displayed together with the stainless steel curves in Figure 2.5 and 2.6. These plates produced very low contact resistances, as is to be expected for gold plated surfaces. This pattern coincides with the high current densities produced during the potentiostatic- and potentiodynamic tests. The absolute values of the contact resistances (Table 2.4) are all higher than DoEs requirements (Table 2.1). Both gold coated steel and steel tested in 1 M H_2SO_4 showed ICR results in the same order of magnitude as DoEs target. The bipolar plates tested in 1 mM H_2SO_4 showed ICR results between 134.5 and 183 mΩ cm^2 after the polarization tests, which is almost 20 times higher than DoEs target for contact resistance (< 10 mΩ cm^2). In fact,

contact resistance measurements itself rules out regular stainless steel as bipolar plate material, when assuming that the pH experienced by the bipolar plate is around 2.87 (1 mM H_2SO_4).

Table 2.4: Contact resistance results at 140 N cm^{-2} (14 bar) after all the polarization tests. All the contact resistances values are given in mΩ cm^2.

What was tested	Test 1: -0.25 V to 1.05 V_{SHE}	Test 2: 0.951 V_{SHE}
Gold coated stainless steel	10.65	14.00
0.1mM/pH=3.72	170.5	186.5
1mM/pH=2.87	134.2	183.0
0.1M/pH=1.01	90.60	29.80
1M/pH=0.51	18.80	18.80
Addition of 2 ppm fluoride	157.5	171.9
Addition of 10 ppm chloride	185.0	201.3
Addition of 100 ppm chloride	194.5	268.0

What is evident from the polarization tests performed at different acidities and the ICR measurements done before and after each electrochemical test is that the acidity of the electrolyte in which the tests are performed in, is crucial. There are great differences in contact resistance measurements and the current densities produced in the solutions with different acidities. From the results obtained during this work it is suggested to choose a pH value that lies close to the real pH in an operating PEM fuel cell, which is typically milder than what is chosen for accelerated degradation/corrosion tests. Lowering of the pH might not only speed up the reactions that normally takes place on a stainless steel surface in an operating fuel cell. It may also alter the relative rate of the reactions as well as introducing new processes on the plates (e.g. severe pitting at high electrode potentials), which is perhaps insignificant, or of low impact in a real PEM fuel cell operated under normal conditions.

2.4.2 Fluoride and Chloride Additions to the Electrolyte

Previous research performed in electrolytes containing chloride [22, 25] were not focused on the degrading of the bipolar plate, but rather on degradation of the expensive electrocatalyst (typically platinum) and the polymer membrane. The low amounts of fluoride (2 ppm) and of chloride (10 ppm) added to the electrolyte in this work, were chosen in accordance with the amounts discussed in relevant literature [5, 18, 25]. The 100 ppm addition of Cl^- was done to investigate the effect that high

amounts of chloride could have on the bipolar plate. A piece of gold coated glass was put through the potentiodynamic measurement to find the corrosion current of pure gold, and the results are included in Figure 2.9 as a reference. In this study, the addition of 2 ppm fluoride and 10 ppm chloride to the 1 mM H_2SO_4 electrolyte did not result in substantial changes for neither the polarization tests (Figures 2.8 and 2.10) nor the ICR measurements (Figures 2.11 and 2.12) compared to the tests done in electrolytes without these ions. Addition of 2 ppm fluoride or 10 ppm chloride to the electrolyte seems to produce corrosion currents in the same range as similar electrochemical tests performed without additions. This indicates that such low amounts of fluoride and chloride, which can be expected to be found in an operating PEM fuel cell, does not seem to promote corrosion processes. The resulting current-potential behavior for a gold coated glass piece functioning as the working electrode during potentiodynamic test is also given in Figure 2.10. The current is found to be essentially zero in the relevant potential window, as expected. Even though the absolute values of the current density is apparently low for the stainless steel bipolar plates, they are substantial compared to the current produced during the gold coated glass polarization.

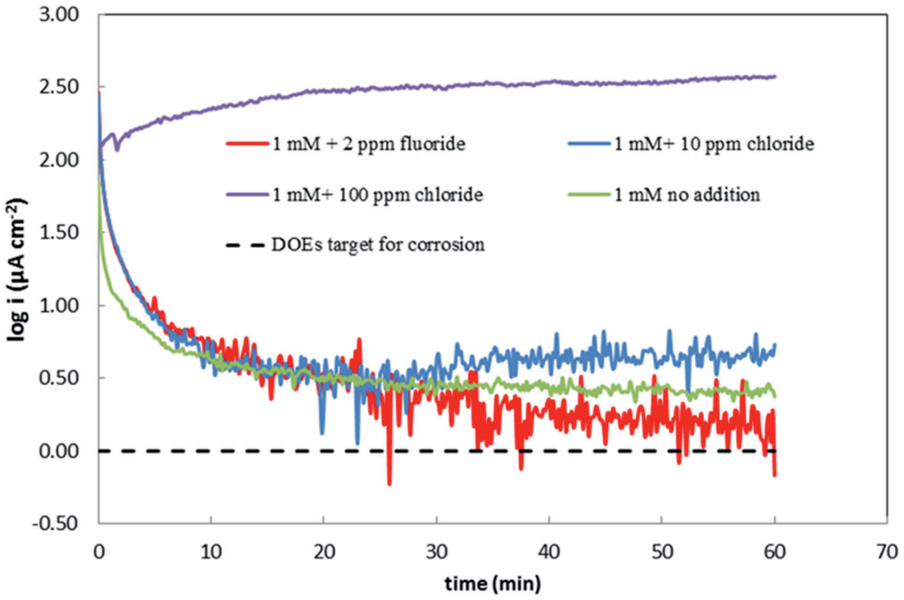

Figure 2.8: Potentiostatic measurements at 0.951 V_{SHE} for 1 hour, addition of F^- and Cl^-.

From Figure 2.8 (1 hour at 0.951 V_{SHE}) it is clear that the 100 ppm chloride addition to the electrolyte influences the current density in the potentiostatic measurements,

and the current produced is much higher than similar tests without this addition. The current density towards the end of the test was close to 300 times the current density produced in any of the other tests presented in Figure 2.8. SEM imaging revealed obvious signs of pitting corrosion on the plate used for this test (Figure 2.9), and it proves how fatal pitting corrosion can be for a material. This could explain the high currents produced during the potentiostatic tests, because pitting corrosion usually accelerates rapidly when first initiated [34]. However, 100 ppm is too high a concentration likely to occur in a PEM fuel cell under normal operation.

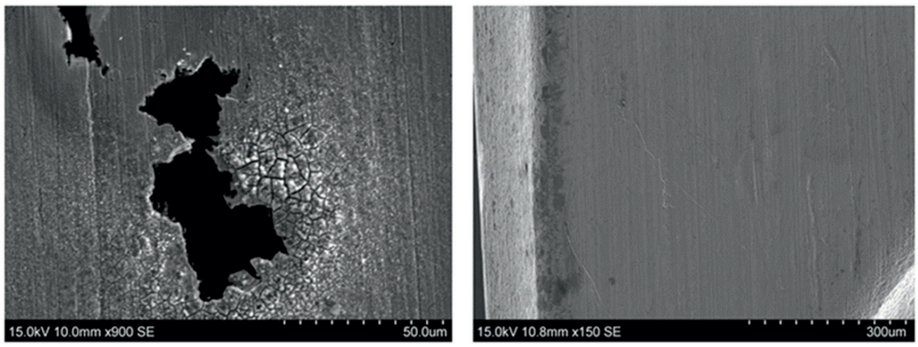

Figure 2.9: SEM imaging performed with an accelerating voltage of 15 kV a) A new, pristine, stainless steel plate. b) Pitting corrosion on the stainless steel surface after the polarization test performed at -0.951 V_{SHE} for 1 hour with 100 ppm Cl^- added to the electrolyte.

Figure 2.10 shows the potentiodynamic measurements performed in 1 mM H_2SO_4 containing either fluoride or chloride, along with measurements performed in a 1 mM H_2SO_4 electrolyte without additions. The shape of the 2 ppm fluoride and 10 ppm chloride curves are almost identical to the curves obtained from tests performed in 1 mM H_2SO_4 electrolyte without additions. The 100 ppm chloride curve is a little different, with a more emphasized current peak at around 0.1 V. This peak indicates a higher corrosion current, and confirms that 100 ppm chloride affects the corrosion rate of the steel.

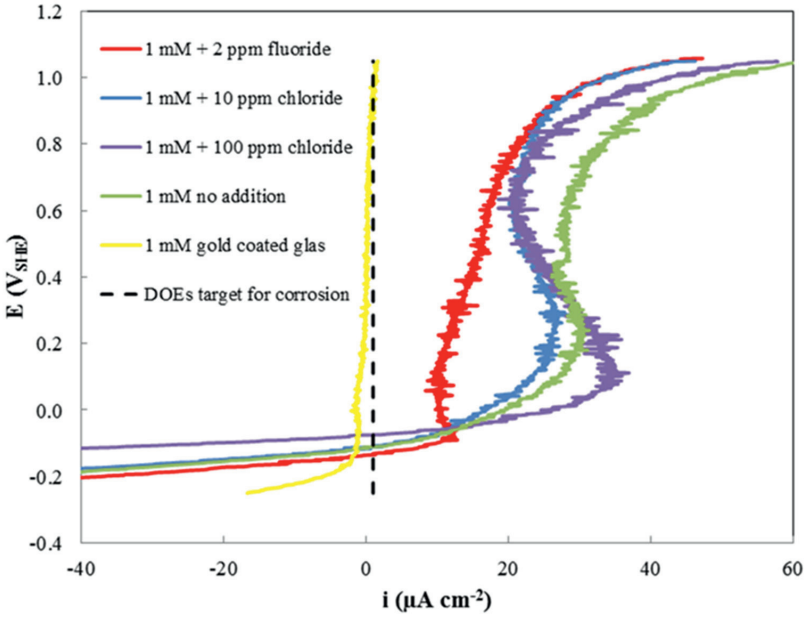

Figure 2.10: Potentiodynamic measurements from -0.25 V to 1.05 V_{SHE}, addition of F^- and Cl^-.

The ICR measurements (Figure 2.11 and 2.12) seem to agree with the polarization test results since the 2 ppm fluoride and 10 ppm chloride. ICR values are in the same order of magnitude as the values obtained after polarization of SS316L in 1 mM sulfuric acid solutions without additions. This indicates that the amounts of chloride and fluoride found in a fuel cell do not affect the surface reactions taking place on the stainless steel bipolar plate. The ICR results obtained after the potentiostatic and potentiodynamic tests where 100 ppm of F^- was added to the electrolyte do not show a change in contact resistance compared to the other test presented in Figures 2.11 and 2.12. The general thickness of the oxide layer on the stainless steel surface does not necessarily change when pitting occurs, because pitting attacks the oxide layer in very small fractions of the surface area [34]. This could in turn explain why the contact resistance measurements of the 100 ppm Cl^- test do not seem all that different from the other tests presented in Figures 2.11 and 2.12.

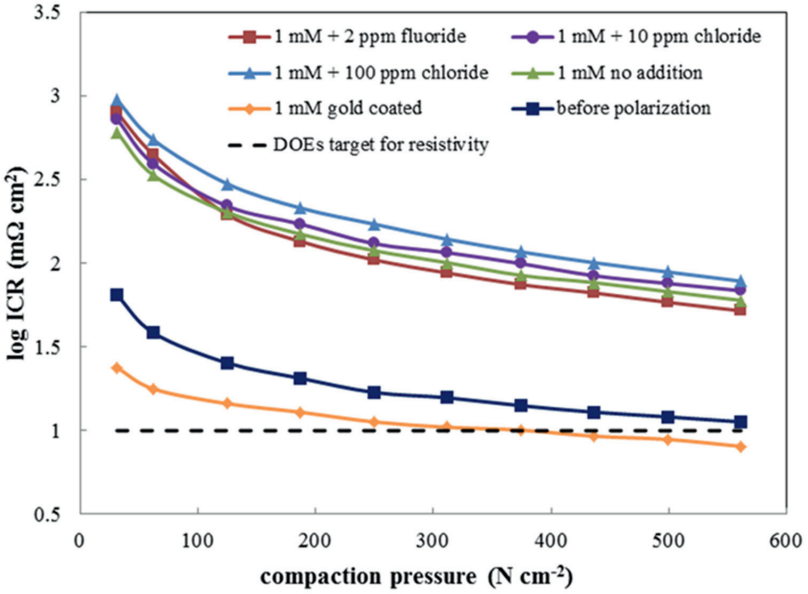

Figure 2.11: ICR results after the potentiostatic measurements at 0.951 V_{SHE}, addition of F^- and Cl^-.

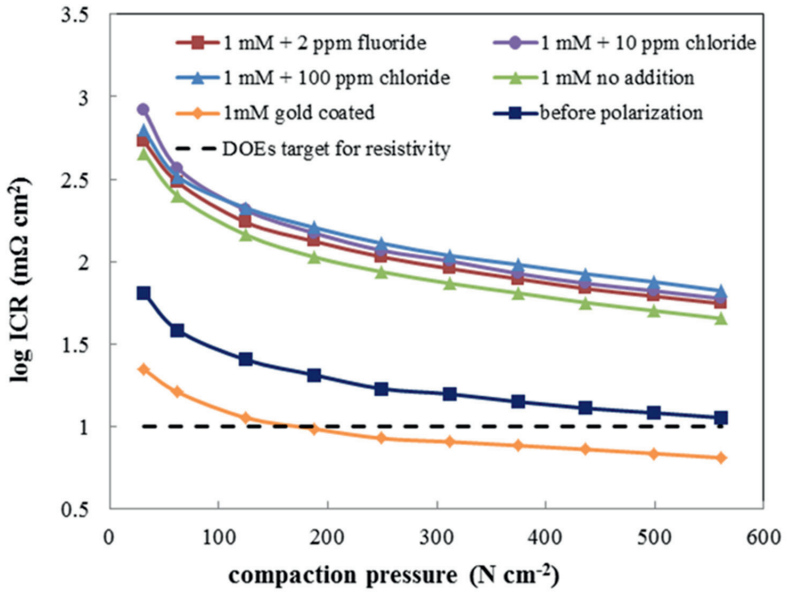

Figure 2.12: ICR results after the potentiostatic measurements from -0.25 V_{SHE} to 1.05 V_{SHE} addition of F^- and Cl^-.

2.5 Conclusions

Both electrochemical- and ICR measurements were performed to study the effect pH and halide additions have on the corrosion of AISI 316L bipolar plates for PEM fuel cells. Highest corrosion currents where measured when the steel was tested in electrolytes with the lowest pH (0.51), and the corresponding contact resistances were low enough to satisfy DoEs targets. DoE's requirements for corrosion current is less than 1 $\mu A\ cm^{-2}$, which were obtained in the high voltage tests performed in 0.1 mM and 1 mM solutions. This indicates that the passivated oxide layer created during the polarization test was disintegrated at higher molarities, which was also expected as the formation of chromium oxides depends on the pH in the electrolyte. If the oxide layer got thin enough or was completely removed, the surface of the stainless steel could easily have reacted with the electrolyte and corrosion reactions could have taken place which would be unlikely to take place in an operating fuel cell. Use of electrolytes with lower pH than what is found in an operating PEM fuel cell, with the aim of accelerating the reactions on the bipolar plates, might not produce the desired results. Other factors may also be altered if the objective is to accelerate reactions taking place in an operating fuel cell.

The polarization tests performed in the 1 mM solutions containing either 2 ppm F^- or 10 ppm Cl^- did not produce higher corrosion currents than the tests performed without these additions, and the contact resistances measured after the polarizations were also in the same order of magnitude. The stainless steel plates polarized in the electrolytes containing 100 ppm chloride revealed clear signs of pitting corrosion after the 1 hour polarization at 0.951 V_{SHE}. This confirms that high amounts of Cl^- does initiate pitting, but the amounts experienced by the bipolar plates in a PEM fuel cell, at least up to 10 ppm, does not seem to cause any more corrosion than what was detected in the similar test without Cl^-.

Out of all the ICR measurements performed during this study, very few of the contact resistance measurements were satisfying according to DoE's requirements of less than 10 $m\Omega\ cm^2$. Gold coated stainless steel showed the best results, with values right above 10 $m\Omega\ cm^2$, but the price of gold makes it unattractive as coating for stainless steel bipolar plates. The general trend is that the bipolar plates used for the polarizations resulting in low current densities, are the same plates showing high ICR. Avoiding formation of such a layer through e.g. complete coverage of the surface with a highly conductive, and corrosion resistive material, is highly desired before making stainless steel bipolar plates a viable alternative for large-scale production.

2.6 Acknowledgements

This work was financially supported by Sør-Trøndelag University College (HIST), Norwegian University of Science and Technology (NTNU), SINTEF and Nordic Innovation. Nordic innovation is greatly acknowledged for funding the NORCOAT project (09051). S.L. thanks HIST for the award of a PhD-scholarship.

2.7 Literature

1. Lædre, S., et al., *The effect of pH and halides on the corrosion process of stainless steel bipolar plates for proton exchange membrane fuel cells.* International Journal of Hydrogen Energy, 2012. **37**(23): p. 18537-18546.
2. Antunes, R.A., et al., *Corrosion of metal bipolar plates for PEM fuel cells: A review.* International Journal of Hydrogen Energy, 2010. **35**(8): p. 3632-3647.
3. Wang, H. and J.A. Turner, *Reviewing Metallic PEMFC Bipolar Plates.* Fuel Cells, 2010. **10**(4): p. 510-519.
4. Hermann, A., T. Chaudhuri, and P. Spagnol, *Bipolar plates for PEM fuel cells: A review.* International Journal of Hydrogen Energy, 2005. **30**(12): p. 1297-1302.
5. Wang, H.L., M.A. Sweikart, and J.A. Turner, *Stainless steel as bipolar plate material for polymer electrolyte membrane fuel cells.* Journal of Power Sources, 2003. **115**(2): p. 243-251.
6. *U.S. Department of Energy, Hydrogen, Fuel Cells & Technologies Program. Multi-year Research, development and Demonstration Plan*, D.o. energy, Editor. 2005: http://www1.eere.energy.gov/hydrogenandfuelcells/mypp/. p. 26.
7. Heras, N.D.L., et al., *A review of metal separator plate materials suitable for automotive PEM fuel cells.* Energy & Environmental Science, 2009. **2**(2): p. 206-214.
8. Tawfik, H., Y. Hung, and D. Mahajan, *Metal bipolar plates for PEM fuel cell - A review.* Journal of Power Sources, 2007. **163**(2): p. 755-767.
9. Wang, Y. and D.O. Northwood, *Effects of O2 and H2 on the corrosion of SS316L metallic bipolar plate materials in simulated anode and cathode environments of PEM fuel cells.* Electrochimica Acta, 2007. **52**(24): p. 6793-6798.
10. Lafront, A.M., E. Ghali, and A.T. Morales, *Corrosion behavior of two bipolar plate materials in simulated PEMFC environment by electrochemical noise technique.* Electrochimica Acta, 2007. **52**(15): p. 5076-5085.
11. Yang, Y., L.-j. Guo, and H. Liu, *Corrosion characteristics of SS316L as bipolar plate material in PEMFC cathode environments with different acidities.* International Journal of Hydrogen Energy, 2011. **36**(2): p. 1654-1663.
12. Feng, K., et al., *Corrosion behavior of SS316L in simulated and accelerated PEMFC environments.* International Journal of Hydrogen Energy, 2011. **36**(20): p. 13032-13042.
13. Yang, Y., L.J. Guo, and H.T. Liu, *Effect of fluoride ions on corrosion behavior of SS316L in simulated proton exchange membrane fuel cell (PEMFC) cathode environments.* Journal of Power Sources, 2010. **195**(17): p. 5651-5659.
14. Kumagai, M., et al., *Corrosion behavior of austenitic stainless steels as a function of pH for use as bipolar plates in polymer electrolyte membrane fuel cells.* Electrochimica Acta, 2008. **53**(12): p. 4205-4212.
15. Yang, Y., L. Guo, and H. Liu, *Influence of fluoride ions on corrosion performance of 316L stainless steel as bipolar plate material in simulated PEMFC anode environments.* International Journal of Hydrogen Energy, 2012. **37**(2): p. 1875-1883.

16. Curtin, D.E., et al., *Advanced materials for improved PEMFC performance and life.* Journal of Power Sources, 2004. **131**(1-2): p. 41-48.
17. Agneaux, A., et al., *Corrosion behaviour of stainless steel plates in PEMFC working conditions.* Fuel Cells, 2006. **6**(1): p. 47-53.
18. Healy, J., et al., *Aspects of the Chemical Degradation of PFSA Ionomers used in PEM Fuel Cells.* Fuel Cells, 2005. **5**(2): p. 302-308.
19. Borup, R.L. and N.E. Vanderborgh, *Design and testing criteria for bipolar plate materials for pem fuel cell application.* MRS Proceedings, 1995. **393**: p. 151-155.
20. Rivas, S.V., et al., *Evaluation of Materials for Bipolar Plates in Simulated PEM Fuel-cell Cathodic environments.* J. New Mater. Electrochem. Syst., 2008. **11**: p. 81-85.
21. Matsuoka, K., et al., *Degradation of polymer electrolyte fuel cells under the existence of anion species.* Journal of Power Sources, 2008. **179**(2): p. 560-565.
22. Li, H., et al., *Chloride contamination effects on proton exchange membrane fuel cell performance and durability.* Journal of Power Sources, 2011. **196**(15): p. 6249-6255.
23. Schmidt, T.J., et al., *The oxygen reduction reaction on a Pt/carbon fuel cell catalyst in the presence of chloride anions.* J. Electroanal. Chem, 2001. **508**(1–2): p. 41-47.
24. Yadav, A.P., A. Nishikata, and T. Tsuru, *Effect of halogen ions on platinum dissolution under potential cycling in 0.5 M H2SO4 solution.* Electrochimica Acta, 2007. **52**(26): p. 7444-7452.
25. Ofstad, A.B., et al., *Assesment of Platinum Dissolution from Pt/Cfuel cell catalyst: An electrochemical Quartz Crystal Microbalance study.* J. Electrochem. Soc., 2010. **157**: p. B621-B627.
26. Abd El Meguid, E.A., N.A. Mahmoud, and S.S. Abd El Rehim, *The effect of some sulphur compounds on the pitting corrosion of type 304 stainless steel.* Mater. Chem. Phys., 2000. **63**(1): p. 67-74.
27. Pujar, M.G., et al., *Use of electrochemical noise (EN) technique to study the effect of sulfate and chloride ions on passivation and pitting corrosion behavior of 316 stainless steel.* Journal of Materials Engineering and Performance, 2007. **16**(4): p. 494-499.
28. Lee, Y.B. and D.S. Lim, *Electrical and corrosion properties of stainless steel bipolar plates coated with a conduction polymer composite.* Current Applied Physics, 2010. **10**: p. S18-S21.
29. Vesel, A., et al., *AES investigation of the stainless steel surface oxidized in plasma.* Vacuum, 2007. **82**(2): p. 228-231.
30. Mandrino, D. and Č. Donik, *Chemical-state information obtained by AES and XPS from thin oxide layers on duplex stainless steel surfaces.* Vacuum, 2011. **86**(1): p. 18-22.
31. Davies, D.P., et al., *Bipolar plate materials for solid polymer fuel cells.* Journal of Applied Electrochemistry, 2000. **30**(1): p. 101-105.
32. Dur, E., O.N. Cora, and M. Koc, *Experimental investigations on the corrosion resistance characteristics of coated metallic bipolar plates for PEMFC.* International Journal of Hydrogen Energy, 2011. **36**(12): p. 7162-7173.
33. Hamilton, P.J. and B.G. Pollet, *Polymer Electrolyte Membrane Fuel Cell (PEMFC) Flow Field Plate: Design, Materials and Characterisation.* Fuel Cells, 2010. **10**(4): p. 489-509.
34. Talbot, E.J. and D.R. Talbot, *Corrosion science and technology*. 2007: CRC Press Taylor and Francis group.

3 In situ Interfacial Contact Resistance Measurements in a custom made Proton Exchange Membrane Fuel Cell

Authors: Sigrid Lædre[a], Ole Edvard Kongstein[b] Anders Oedegaard[b] Frode Seland[a] and Håvard Karoliussen[a]

a Norwegian University of Science and Technology (NTNU)

b SINTEF Materials and Chemistry

This manuscript has been prepared for publication. It is a continuation of the work described by Ladre et al. in an ECS transactions article from 2012 [1]. However, none of the work described in this manuscript has been published previously.

3.1 Abstract

Interfacial Contact Resistance (ICR) measurements have been used extensively to study the resistance between the Bipolar Plate (BPP) and the Gas Diffusion Layer (GDL) in Proton Exchange Membrane Fuel Cell (PEMFC) in the past. The majority of ICR measurements in the literature were performed ex situ, which can be quick and easy, but there are several drawbacks with the ex situ method. One cannot study the ICR development continuously, and such tests are usually not performed at real conditions. In situ ICR measurements makes it possible to obtain measurements in an operating PEM fuel cell. In situ ICR measurements are not as easy to perform as ex situ measurements, and there are few previous studies focusing on measuring in situ ICR. The main objective of this study was to develop a reliable method for in situ ICR measurements in a PEMFC test cell. By using thin gold wires, the ICR was measured between the BPP and the GDL in an operating fuel cell. Due to uneven current distribution, it was found that the average ICR values from three measuring points inside the operating fuel cell was by far more accurate than the values obtained from one measuring point. The uneven current distribution was confirmed by measuring the local ICR ex situ on smaller areas of the plate. The average ICR values were in the same range as the ICR values measured ex situ after fuel cell operation.

3.2 Introduction

Proton exchange membrane fuel cells (PEMFCs) coverts chemical energy to electrical energy, and is predicted to play an important role in the future sustainable society [2]. Even though the first mass produced fuel cell vehicles have entered the marked, there are still several durability and economic issues with fuel cells. The main component in a PEM fuel cell is the Membrane Electrode Assembly (MEA), but the Bipolar Plates (BPPs) are essential when connecting several single cells into a stack. In addition to serve as physical separator plates between each individual cell in a stack, these plates assist with water management, cooling, current collection and distribution of fuel and air [2, 3]. In order to serve these functions over the lifetime of a fuel cell stack, the BPP needs to be electrically conducting, corrosion resistant, relatively cheap, easy to produce and both mechanically and chemically stable [4].

Table 3.1: DoEs targets for PEMFC bipolar plates [5].

Properties	Units	2011 status[a]	2020 targets
Cost[b]	\$ kW^{-1}	5-10	3
Plate H_2 permeation coefficient[c]	Std $cm^3/(sec\ cm^2\ Pa)$ @ 80°C, 2 atm 100% RH	N/A	$<1.3 \cdot 10^{-14}$ [d]
Corrosion, anode[e]	μA cm^{-2}	<1	<1
Corrosion, cathode[f]	μA cm^{-2}	<1	<1
Electrical conductivity	S cm^{-1}	<100	>100
Areal specific resistance[g]	Ω cm^2	0.03	0.01
Flexural strength[h]	MPa	<34 (carbon plate)	>25
Forming elongation[i]	%	20-40	40

[a] *Status is based on information found in 2010 & 2011 Annual Progress Reports – project description write ups of TreadStone Technologies, Inc. and Oak Ridge National Laboratory.*
[b] *Costs projected to high volume production (500,000 stacks per year), assuming MEA meets performance target of 1000 mW* cm^{-2}.
[c] *Per the standard gas transport test (ASTM D1434).*
[d] *Blunk, et al, J. Power Sources 159 (2006) 533-542.*
[e] *pH 3 0.1 ppm HF, 80°C, peak active current* $<1x10^{-6}$ A cm^{-2} (potentiodynamic test at 0.1 mV s^{-1}, -0.4V to +0.6V (Ag/AgCl)), de-aerated with Ar purge.
[f] *pH 3 0.1 ppm HF, 80°C, passive current* $<5x10^{-8}$ Acm^{-2} (potentiostatic test at +0.6V (Ag/AgCl) for >24h, aerated solution.
[g] *Includes interfacial contact resistance (on as received and after potentiostatic test) measured both sides per Wang, et al. J. Power Sources 115 (2003) 243-251 at 200 psi (138 N* cm^{-2}*).*
[h] *ASTM-D 790-10 Standard Test method for flexural properties of unreinforced and reinforced plastics and electrical insulating materials.*
[i] *Per ASTM E8M-01 Standard Test Methods for Tension Testing of Metallic Materials.*
[j] *Details in this table are being revised to match recent changes in the high level cost target.*

Various sources in the literature have estimated the cost and weight of the BPP in a PEMFC stack [3, 6, 7], and even though the numbers vary to some extent, it is obvious that the BPP stands for a relatively large part of the total weight and cost. In 2012, the U.S. Department of energy (DoE) [5] updated their targets for bipolar plates in PEM fuel cells (Table 3.1). As can be seen from these targets, the near future aim (2020) of the ICR is set to be less than 10 mΩ cm^2 [5].

Carbon-based BPPs are most common in commercially available fuel cells today [8], due to their stability and performance in the acidic environment created by the Nafion membrane in PEMFCs. There are, however, incentives to move away from carbon BPPs, as the production of such plates is time-consuming and relatively expensive. Metal bipolar plates are generally cheaper and easier to produce, as they can be stamped instead of formed. Metals possess high electrical- and thermal conductivities, but non-noble metals are prone to degradation in the harsh environment inside a PEMFCs stack [9]. When metals corrode, ions are released into the fuel cell, which can be detrimental for both catalyst activity and membrane conductivity. Some metals will also form passive oxides when polarized to more positive potentials, which tends to increase the ICR between the BPP and Gas diffusion layer (GDL) in a PEMFC. The high thermal expansion coefficients of common metals can be an issue in PEMFC systems, where variations in temperature can occur. Various grades of Stainless steel has previously been investigated for use as bipolar plate materials [3, 4, 10-18]. Stainless steel exhibits high mechanical strength, high chemical stability, low gas permeability and is easy to produce into various designs shapes and sizes [2, 4]. In addition, there are a number of different stainless steel alloys with various properties.

Even though stainless steel possess several qualities that make it a good candidate for use as BPP material, the poorly conductive oxide formed in contact with oxygen and water on the steel surface is a drawback for use in its non-coated form. The poor electrical conductivity of this oxide causes an increase in contact resistance between the BPP and the GDL in a PEMFC. There are several studies described in the literature where interfacial contact resistance of stainless steel has been measured ex situ [4, 19-21]. Both Lee and Lim [19] and Wang et al. [4] used a configuration where a stainless steel plate was put in-between two carbon papers with copper plates in an outer structure. Wang et al. [4] measured an ICR of 50 mΩ cm^2 at 140 N cm^{-2} after polarization at 0.6 V_{SCE} for 60 minutes. Similar results were found when the polarization test duration was altered. Lee and Lim [19] coated the stainless steel with a polymer-based coating containing various amounts of carbon black filler. They measured ICR values between 25 mΩ cm^2 and 850 mΩ cm^2, where high carbon black content resulted in the lowest ICR values. Wang et al. [20] performed ICR

measurements on both coated and non-coated stainless steel. For bare steel, the ICR was reported to be 66.4 mΩ cm^2 at a compaction pressure of 274.4 N cm^{-2}.

Ex situ measurements of ICR between the bipolar plate and other components in the fuel cell have been thoroughly explored in the literature [4, 9, 16, 19-28]. The literature also describes various models for estimation of ICR in operating fuel cells [29-34]. Even though several attempts have been made to estimate the ICR inside an operating PEM fuel cell, very few studies have been focused on actually measuring this resistance in situ [24, 35-37]. There are several advantages with in situ ICR measurements compared to ex situ ICR measurements. By measuring the ICR during fuel cell operation, one can obtain continuously measurements, showing how the ICR develops over time. ICR measurements performed ex situ are usually conducted without any external humidification and gas flow. When measuring the ICR during fuel cell operation, the water produced in the electrochemical process as well as from humidification of the gases, is present inside the fuel cell, along with reactant gases under pressure. In situ ICR measurements also provide the opportunity to study parameter variations, and one can measure how the ICR varies with e.g. humidity.

Makkus et al. [37] studied the ICR between the flow plate and the backing at different compaction pressures for Solid Polymer Fuel cell (SPFC) applications, by introducing a thin gold wire between the E-TEK backing plus electrode and the membrane during MEA assembly. They measured the voltage drop between the gold wire and the flow plate. They found the ICR to be higher at lower compaction pressures. Ihonen et al. [36] developed a setup for in situ ICR measurements, where potential probes were connected to both gas backing and current collectors. The cell they developed provided reproducible measurements, and they also found that the placement of the probes themselves is crucial for correct ICR measurements.

The literature describes several works which have been focused on both measuring and estimating current distribution in PEM fuel cells [38-43]. Alaefour et al. [38] found variations in the local current distribution in both co-flow and counter-flow arrangements. Noponen et al. [43] studied the relation between current distribution and mass transport in free-breathing a PEMFC. The principle for the current distribution measurements where similar to the one used by Alaefour et al., and similar principles can also be used when measuring the ICR in an operating fuel cell. The literature focusing on current distributions in PEMFCs, can thus be helpful when working with in situ ICR measurements. However, the measurement of ICR is a bit more complicated, as it should be measured between the GDL and BPP directly,

not throughout the entire setup. The setups used for measuring current distribution can thus not be used for accurate ICR measurements.

Even though there are a number of previous studies describing the use of ex situ ICR measurements, there is a lack of literature describing setups for measuring the ICR in situ. Most of the ex situ ICR measurements described in the literature were performed without any gas flow or humidification during testing. These measurements are ok for initial testing and evaluation of materials and coatings, but they do not provide a complete picture of the actual ICR development in an operating fuel cell. The authors believe in situ measurements are crucial for understanding the ICR development and its importance for an operating fuel cell. The main objective of this work has been to develop a reliable method for measuring interfacial contact resistance in situ. This has proven to be very challenging, as there are several extra parameters to consider compared to ex situ testing. Another objective with this work was to compare the absolute values from the ex situ and in situ ICR measurements, and find how much they deviated from one another.

3.3 Materials and Method Development

The base material for all the tests in this study was AISI 316. The surface area of the plates was 16 cm^2 before the flow field was etched in, and the surface of the non-etched area was 8.059 cm^2.

3.3.1 In situ Interfacial Contact Resistance Measurements

A profile view of the in situ setup for measuring of contact resistance is shown in Figure 3.1. The setup was made from a PEM fuel cell, where 0.025 mm thick gold wires (99.95% pure gold, Goodfellow) were used to measure the contact resistance between the bipolar test plate and a GDL (H23C6, Freudenberg). Another GDL (H2315 T10A, Quintech) was put on top of the first to make sure the gold wires were not exposed to the MEA. The plates used were made from AISI 316L, with flow fields as shown in Figure 3.2. The ICR measurements were limited to the cathode side of the fuel cell.

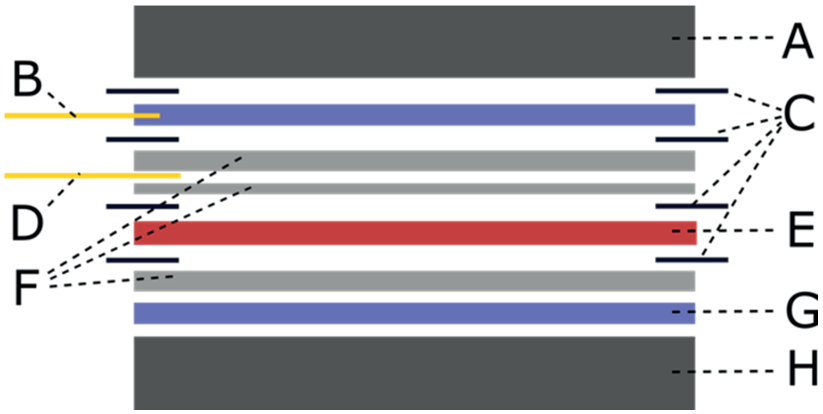

Figure 3.1: Setup for in situ measurements of ICR as seen from the side with A) Cathode housing. B) Gold wires welded to bipolar plate C) Gasket, preventing contact between gold wires and other electrically conducting parts of the fuel cell. D) Gold wires placed in between to sheets of GDL. E) MEA. F) GDL, one on the anode side and two on the cathode side. G) Bipolar plate. H) Anode housing.

One gold wire was welded to each end of the cathode bipolar plate (Figure 3.2), and three gold wires were put in between two GDLs as shown in Figure 3.1. The voltage was thus measured between the gold wires welded to the bipolar plate and the gold wires put in between the two GDLs. This resulted in three measured voltages, one from each side of the setup and one in the middle. Note that when the cell was operating, it was tilted so that the flow channels were vertical with inlet on the top

and outlet in the bottom. This resulted in one measuring point at the top, one in the middle and one at the bottom of the fuel cell. Welding the gold wires to the plate instead of just placing them on top of the plate, makes sure the wires stays where they should throughout the measurements. In addition, the calculated contact resistance only included the oxide on the top of the BPP in addition to the resistance through the GDL.

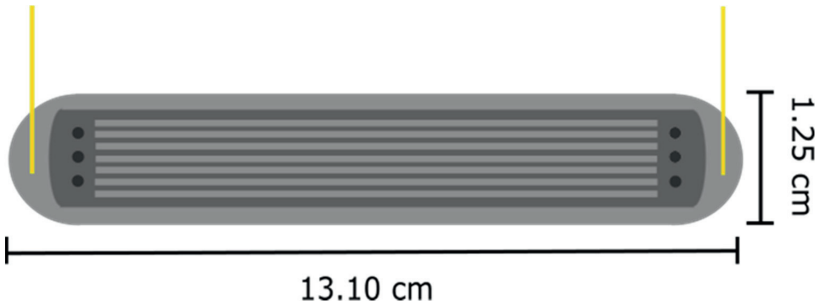

Figure 3.2: The bipolar plate with parallel flow field. Gold wires were welded to the plate for in situ ICR measurements.

Figure 3.3 shows how the fuel cell was assembled with the in situ ICR setup inside. In addition to the bipolar plate and the two GDLs, two layers of gasket were used on the cathode side of the fuel cell to make sure none of the gold wires came into contact with each other or the cell housing. The gold wires were reinforced on the outside of the cell house with conductive tape, and connected to a data acquisitions/switch unit of brand Agilent (34470A). As the ICR was only measured on the cathode side of the fuel cell, only one GDL was needed in addition to the bipolar plate and gaskets on the anode side.

When the fuel cell had been put together, it was mounted into the test station as shown in Figure 3.3 F. Wires, tubes and thermocouples were connected to the cell, in order to control the current, gas pressures, humidity and temperature. Compaction pressure over the active cell area was applied by a pneumatic system, and this pressure was kept stable throughout the entire fuel cell operation. The operational parameters that were applied are shown in Table 3.2. A customized lab view program was used to operate the fuel cell, and a Fuel Cell Technologies Inc humidifier was used to keep a 100 % relative humidity of both hydrogen (anode) and oxygen (syntetic air, cathode) entering the fuel cell. The cell was set to operate under current control for most of the test procedures, and thus the cell voltage varied somewhat throughout the tests.

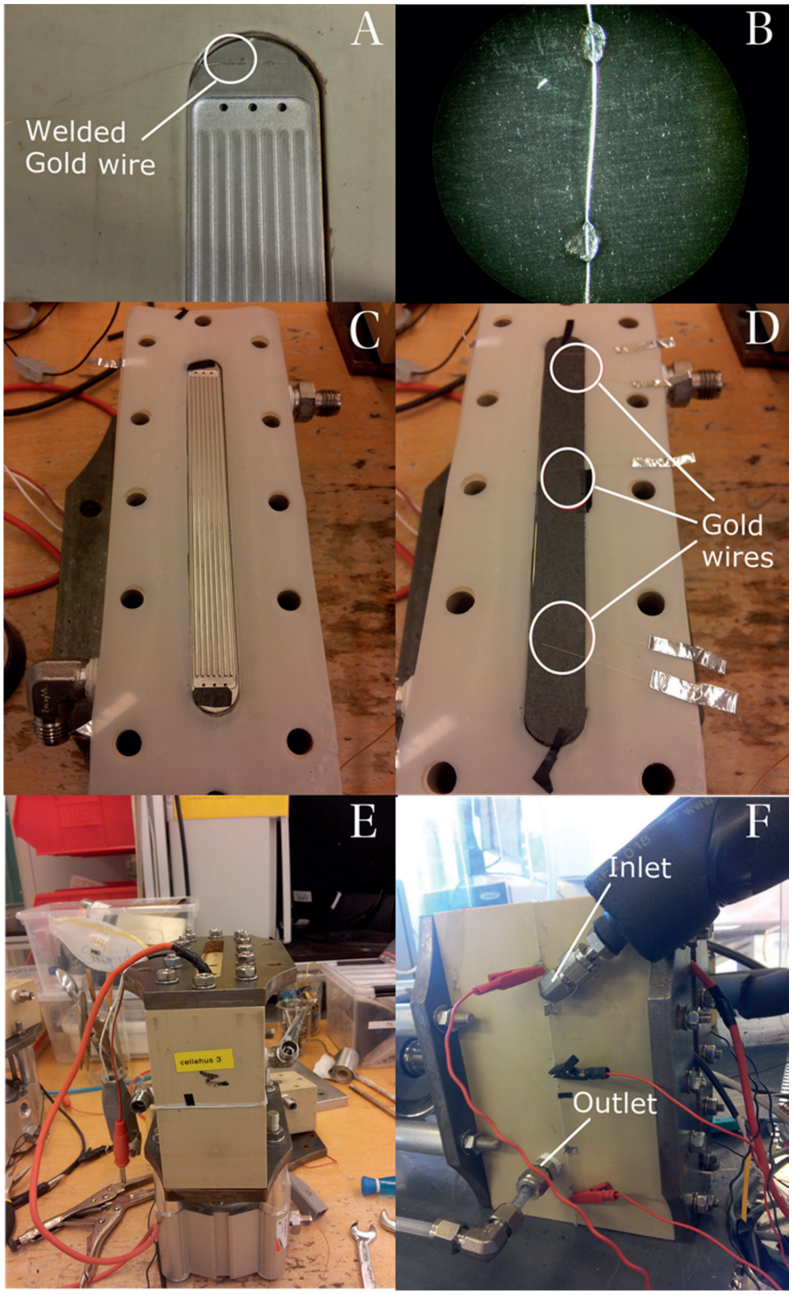

Figure 3.3: A) BPP with gold wires welded to it placed in the cell housing. B) Light microscopy image showing the welded gold wires. C) Gasket used to isolate the wires. D) Gold wires placed in between two GDLs. E) Assembled fuel cell. F) Fuel cell mounted in test station.

Table 3.2: Parameters used to operate the PEM fuel cell.

Parameter	Value	Parameter	Value
Cell temperature [°C]	75	Conversion synthetic air	0.5
Gas pressure anode [bar]	0.2	Conversion hydrogen	0.67
Gas pressure cathode [bar]	0.3	Compaction pressure [N cm^{-2}]	206
Cell current density [A cm^{-2}]	0.3		

Table 3.3 shows the different fuel cell tests performed during this study. The duration of each test in this study was set to 72 hours, and all the tests were performed on Stainless Steel grade 316L (AISI 316L) BPPs. However, the coating and current/voltage were altered. For three of the tests, OCV was applied for various time intervals. Non-coated AISI 316L BPPs were used during these tests. In addition, gold coated- and titanium coated AISI 316L BPPs were put through the 72 hour test at baseline conditions.

Table 3.3: The tests performed during this study, including material, coating and operational conditions.

Name	Coating	Description
Baseline	none	0.3 A cm^{-2} for 72 hours
OCV 4.2 %	none	0.3 A cm^{-2} for 23 hours + 1 hour at OCV*
OCV 16.7 %	none	0.3 A cm^{-2} for 50 min + 10 min at OCV*
OCV 50 %	none	0.3 A cm^{-2} 30 min + 30 min at OCV*
Gold coating	Gold	0.3 A cm^{-2} for 72 hours
Titanium coating	Titanium	0.3 A cm^{-2} for 72 hours

* The test was cycled between 0.3 A cm^{-2} and OCV for 72 hours.

3.3.2 Ex situ Interfacial Contact Resistance Measurements

A picture of the ex situ ICR measurement setup is shown in Figure 3.4 and the schematic of the setup with a BPP inside is shown in Figure 3.5. This setup was designed to simulate the structure of a PEM fuel cell, and at the same time make it time efficient to measure the ICR. The setup was comprised of two gold coated copper plates, a pneumatic cylinder (Camozzi QP2A080A010) to control compaction pressure by moving the bottom plate and an external power supply (XDL 56-5 DC, Xantex). The test specimen with a GDL (H23C6, Freudenberg) on top was placed in between the two gold coated plates, and a current of 2.0 A was applied. The corresponding voltage between the top gold coated plate and an isolated pressure

controlled pin mounted in the center of the bottom gold coated plate was measured with a Fluke 76 true RMS multimeter. The ICR was calculated from this voltage by use of Ohm's law.

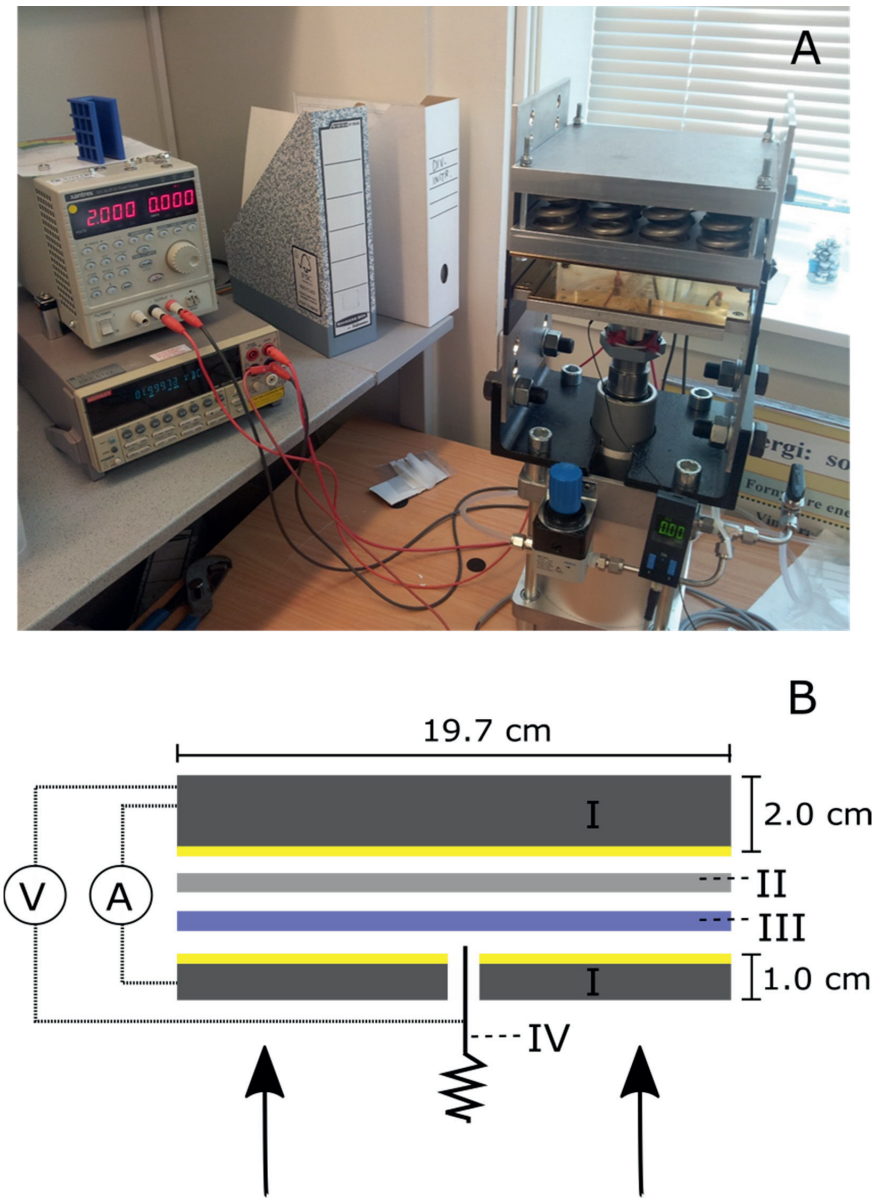

Figure 3.4: A) Picture of ex situ ICR setup used during this study. B) Setup for ex situ ICR measurements with I) Gold coated copper plates, II) GDL, III) Bipolar test plate and IV) spring loaded pin.

As smaller version of the ex situ ICR setup was also used during this study. This was a point measuring setup, were the ICR could be measured on small areas (0.6 cm^2) along the length of the BPP. A picture of this setup is shown in Figure 3.5.

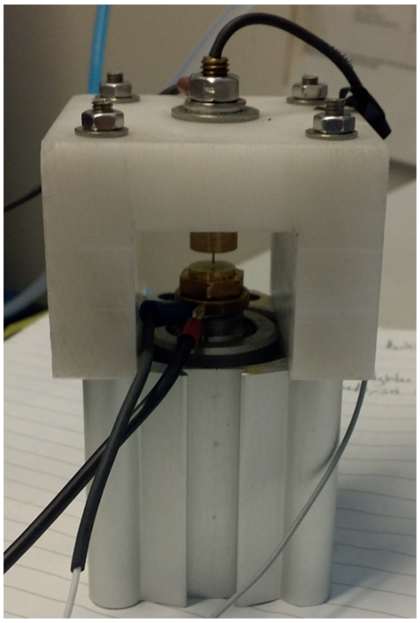

Figure 3.5: Setup for measuring the ICR on small areas along the length of the BPP.

3.4 Results and Discussion

3.4.1 In situ Interfacial Contact Resistance Measurements

Figures 3.6, 3.7, 3.8 and 3.9 displays the results from the in situ fuel cell tests. The cathode side was chosen, as it is expected to experience the highest voltages and temperatures, as well as to compile the highest amounts of water, which could potentially affect the ICR. The cell voltages obtained for each test are shown in Figure 3.6. This figure shows that the voltage responses for the three different materials/coatings at 0.3 A cm^{-2} were similar, and within 30-40 mV of each other. The differences observed can be attributed to the insufficient initial conditioning of the cells. As this work focused on the effect of coatings and time at OCV, it was decided to minimize the start-up procedure. For three of the tests the current was set to 0 (OCV) for various periods of time, which explains the larger variations and the voltages close to 0.9 V in Figure 3.6. For the OCV 4.2 %, OCV 16.7 % and OCV 50 % the currents are spread between approx. 0.6 V and 0.9 V, where the lower values are from the 0.3 A cm^{-2} operation, and the higher ones are from the OCV operation.

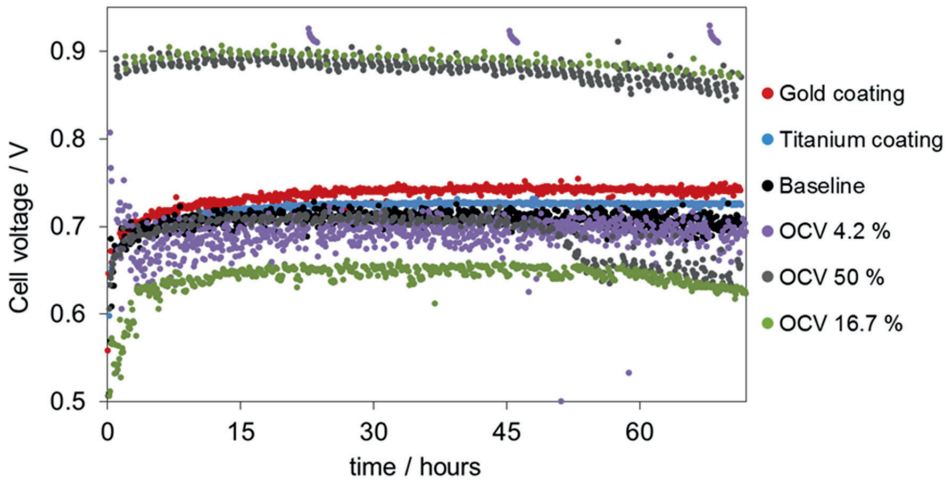

Figure 3.6: Cell voltages with time obtained during fuel cell operation for all of the tests in this study.

Figure 3.7A and B display the interfacial contact resistances for each test (see Table 3.3) in this study, shown as the average ICR calculated from the three measuring points in each cell. The test resulting in highest average ICR values is the one where the cell was operated at OCV 50 % of the time, with ICR values close to 30 mΩ cm^2 throughout the entire test. The gold coated steel BPP showed the lowest average ICR

values, at approximately 4 mΩ cm^2. This test was the only one resulting in ICR values below DoEs target for ICR at 10 mΩ cm^2 [5]. The low ICR value for gold was to be expected, as it does not form a thick non-conducting oxide on its surface. The titanium coated steel BPP showed ICR values between 20 and 25 mΩ cm^2, placing it second highest in Figure 3.7. At the voltages inside an operating PEM fuel cell, titanium is expected to form a stable oxide (TiO_2), with semiconductor properties [44]. This oxide is thus most likely responsible for the relatively high ICR encountered with the titanium coated plates.

The results from the Baseline test showed ICR values similar to the OCV 16.7 % and the OCV 4.2 % tests. Towards the end of the 72 hour operation they were all close to 15 mΩ cm^2 (Figure 3.7 A). This shows that operating the fuel cell between OCV and 0.3 A cm^{-2} causes an increase in ICR when the OCV periods are as long as the 0.3 A cm^2 periods (OCV 50%). Stopping the current flow for small periods of time (OCV 16.7 % and OCV 4.2 %), may not be as harmful as sustaining OCV over a prolonged time period.

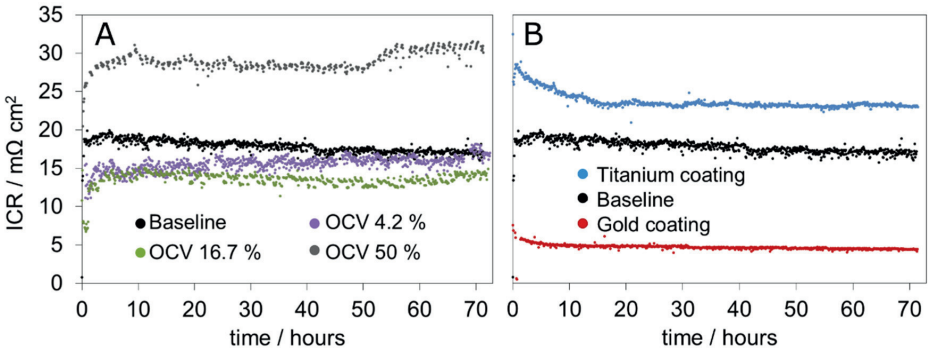

Figure 3.7: In situ ICR measurements from fuel cells operated for 72 hours. A) OCV applied for various durations of time with non-coated AISI 316L BPPs. B) Gold- and titanium coated AISI 316L BPPs.

As can be seen in Figure 3.7, there is not a common trend for how the ICR developed within the first hours of operation. One reason for the changes in ICR at the beginning of any test, can be the build-up and/or stabilization of oxides on the surfaces of the stainless steel. In order to study how the ICR developed from the very beginning of cell operation, gas flow, temperature and humidity was introduced into the cell house at the same time as the current was set. For the same reason, conditioning was skipped at the beginning of cell operation. All of these factors could cause a change in the oxide on the BPP surface, which could explain the instabilities in ICR at the beginning of each test. The pH in the fuel cell will also take some time

to stabilize, and thus possibly effect the stability of already formed oxides. Another important aspect of fuel cell operation is that the overall performance of the cell can differ from test to test, depending on the MEA performance and the symbiotic effects between all the parameters in an operating fuel cell.

Figure 3.8 shows three ICR values for each in situ test after 72 hours of operation, one for each measuring point in the cell. The three measuring points were placed on the top, middle and bottom of the cell, as seen in Figure 3.3. The highest of all the ICR values in this bar chart is the one obtained from the bottom measuring point in the 50% OCV test, resulting in and ICR of 62 mΩ cm^2. The measuring point on top of the cell operated at constant current with gold coated steel plates showed the lowest ICR at 2 mΩ cm^2. As a general trend, the ICR obtained from the BPP at the outlet part is higher than the inlet part. A likely cause for this is that the area close to the outlet is more prone to flooding by the water accumulated from both humidification and the reaction at the cathode, due to the way the cell was placed in the station. For all the tests, the ICR obtained from the measuring point close to the inlet is lower than the ICR obtained from the middle and close to the outlet. The values obtained from the point close to the outlet are higher than the other measuring points for all the tests performed on pure AISI 316L steel, whereas for the titanium and gold coated BPPs, the measuring point in the middle showed the highest ICR value. As there are variations in ICR across the BPP surface, the average ICR is a better way of displaying the actual ICR. Uneven current distribution probably explains some of the variation in ICR values between the measuring points.

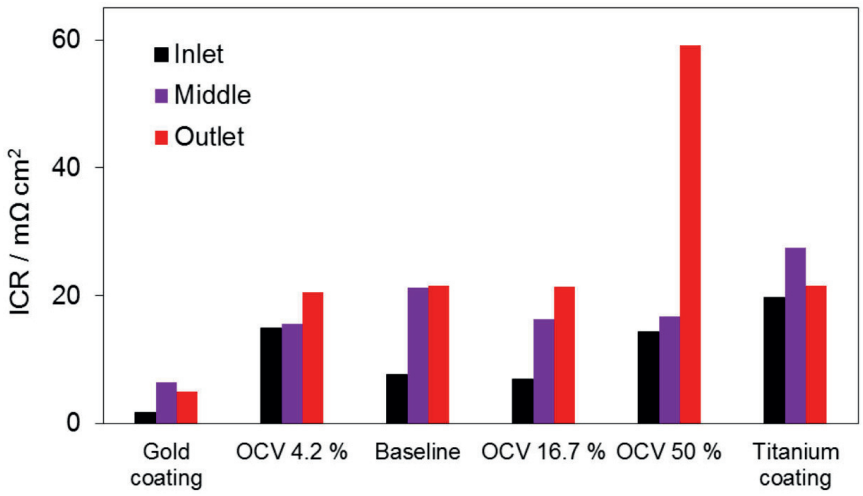

Figure 3.8: In situ ICR values obtained at three measuring points in the cell after 72 hours fuel cell operation.

The ICR values in Figure 3.8 were obtained after 72 hours of operation. Figure 3.9 shows how the ICR varied with time at each measuring point, and for most of the tests, the ICR was stable throughout the operation. Figure 3.9A shows the ICR from the constant current test (non-coated steel at 0.3 A cm^{-2}), and Figure 3.9B shows the ICR from the test where OCV was applied every 24 hour. As can be seen from these graphs, the ICR did vary some during both tests. However, these variations are not important for the main observations in this study, when the average ICR values were used.

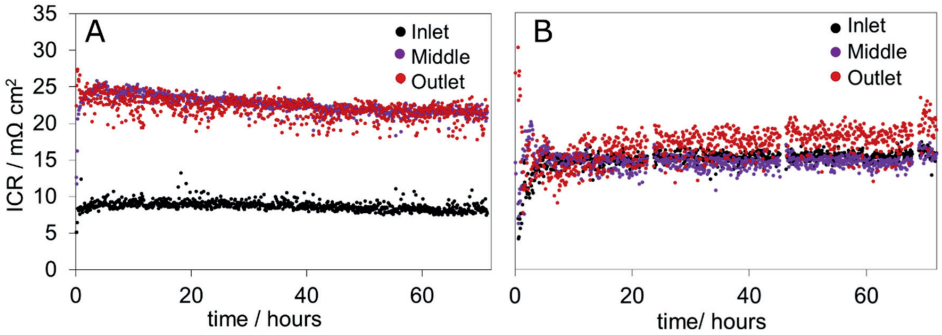

+

Figure 3.9: In situ ICR values obtained during 72 hours fuel cell operation for A) the baseline test, B) the OCV 4.2 % test.

Measuring the interfacial contact resistance between the bipolar plate and the gas diffusion layer during fuel cell operating is challenging, as the effects from various parameters can be difficult to separate from one another. Current distribution, water distribution, heat distribution and pH variations throughout the fuel cell could have an effect on the ICR. The current distribution in an operating fuel cell will mainly depend on the (in)homogenity of fluid flow over the cell area. Depending on how ideal/perfect the cell design and operation conditions are, measuring the ICR at one point on the BPP surface would create a very high uncertainty. The authors believe that increasing from one to three measuring points, greatly increases the accuracy of the measurements. The bipolar plate used in this work resulted in co-flow arrangement of fuel and synthetic air in the fuel cell (Figure 3.2). Alaefour et al. [38] found the current to decrease from inlet to outlet in a co-flow arranged fuel cell. This corresponds well with the generally higher ICR values obtained during this work at the outlet of the fuel cell.

In order to confirm the variation in in situ ICR across the BPP surface, point measurements were performed ex situ on the BPP from the OCV 50 % test (Table 3.4). Five points were used, where points 1, 3 and 5 were in the same area as the three in situ measuring point. The absolute values from Table 3.4 are not comparable to the other measurements presented in this article, as the compaction pressures used in the point measuring setup was much higher than 200 N cm^{-2} (1190 N cm^{-2}). Due to the way this setup was made, it was not possible to get accurate measurements at pressures similar to the ones experienced by the BPP in an operating fuel cell. The OCV 50 % BPP was chosen, as it showed the greatest variation between the various in situ ICR measuring points. As can be seen from Table 3.4, there are some variations between the different measuring points, but they are small compared to the variations between the in situ measurement points. This strengthens the assumption that uneven current distribution during fuel cell operation could be the cause of the variations in the observed in situ measurements.

Table 3.4: Ex situ ICR measurements performed on 5 smaller areas of the bipolar plate used on the cathode side during the OCV 50 % test.

Measuring point	1	2	3 (middle)	4	5
ICR value [mΩ cm^2]	11.0	10.4	10.0	10.1	9.8

3.4.2 Ex situ Interfacial Contact Resistance Measurements

Figures 3.10 and 3.11 show the results obtained from the ex situ ICR measurements. The graph in Figure 3.10 display the ICR values after the in situ tests at various compaction pressures, while Figure 3.11 shows the ICR values obtained before and after the in situ tests at 200 N cm^{-2}.

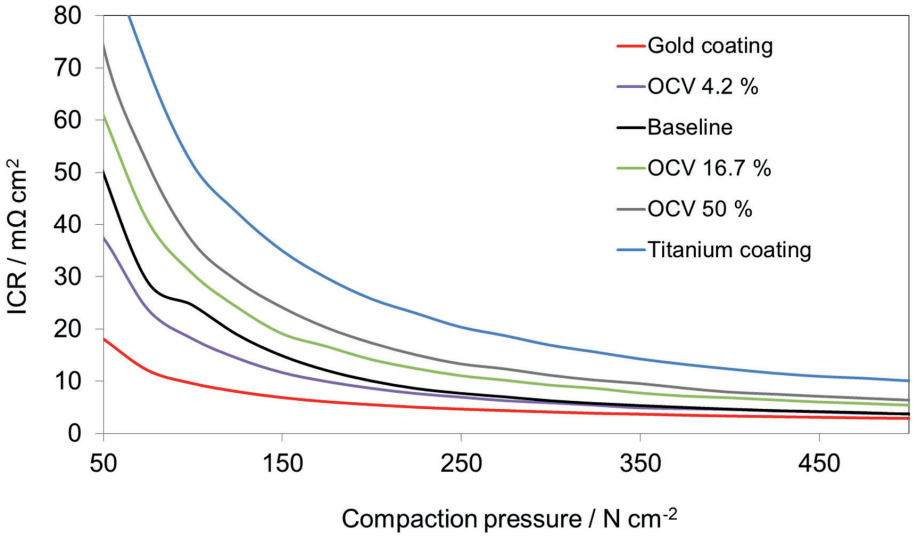

Figure 3.10: Ex situ ICR between GDL and BPP obtained for after 72 hours of in situ fuel cell operation.

The before and after ICR values in Figure 3.11 show that all the materials experienced an increase in ICR during polarization, except for the gold coated stainless steel. This was to be expected, as there should be no oxide formation on the gold surface. The ICR measured for titanium coated stainless steel before the fuel cell test, was close to twice the values of the bare steel. This plate also showed the highest value in Figure 3.11 at 26 mΩ cm^2. The results from both in situ and ex situ measurements show that the ICR was lowest for gold coated steel. The two tests resulting in highest measured ICR values, were the tests performed with titanium coated BPPs and OCV operation 50 % of the time. At high potentials, the BPP is more prone to corrosion and oxide formation, which could result in higher ex situ ICR values for the BPPs that were exposed to OCV over longer periods of time. This could explain why the measured ICR after polarization was higher for the OCV 50 % and OCV 16.7 % BPPs, compared to the baseline and OCV 4.2 % BPPs.

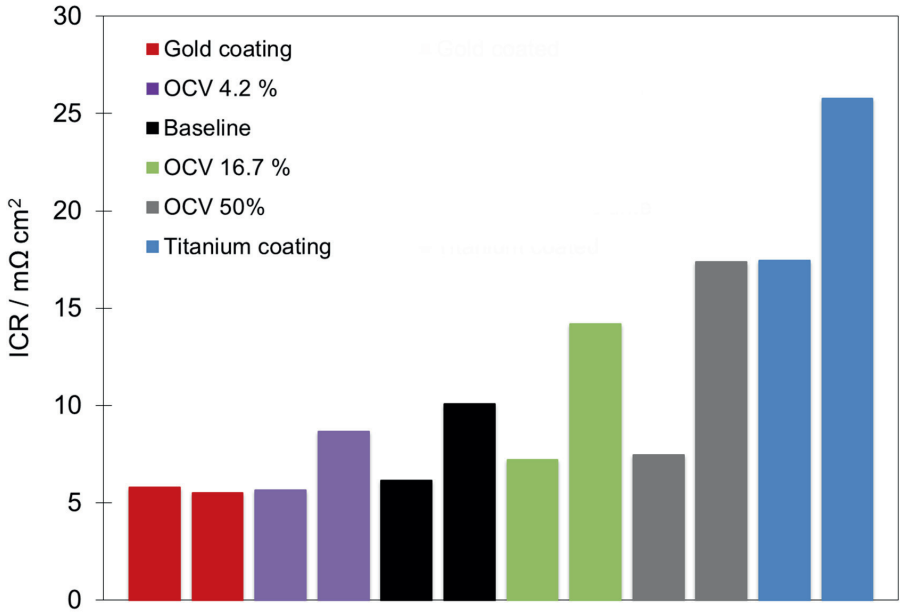

Figure 3.11: Ex situ ICR measurements at 200 N cm^{-2} obtained after 72 hours of operation. The values to the left were obtained before polarization and the values to the right were obtained after.

When comparing the ex situ (Figure 3.10 and Figure 3.11) to the in situ ICR values (Figures 3.7 and 3.8), it becomes evident that the in situ and ex situ ICR values are all in the same range at approximately 200 N cm^{-2}. The lowest ICR values obtained from both in situ and ex situ measurements were the ones with gold coated stainless steel BPPs, and the ICR values were close to 5 mΩ cm^2 (average in situ) and 6 mΩ cm^2 (ex situ). The highest average ICR values from the in situ measurements were close to 30 mΩ cm^2 (OCV 50%), while the highest value from the ex situ measurements were approx. 26 mΩ cm^2 (titanium coated steel). These results show that the ex situ and in situ ICR absolute values are comparable and that most of the trends seen in situ correlate with the ICR values measured ex situ. Continuous, in situ measuring of ICR provides an option for online monitoring and diagnostic tool of the status and performance of BPPs, as well as the interaction between the BPP and the GDL.

Even though most of the ICR values obtained after fuel cell operation in this study were higher the 10 mΩ cm^2 target set by DoE [5], they are all in the same order for magnitude. The compaction pressure in this study was a bit higher than the recommended 138 N cm^{-2} (Table 3.1), but as can be seen from Figure 3.10, the numbers are still in the same range.

3.5 Conclusions

The objective with this work was to develop a method for in situ ICR measurements, and also verify that such a method provides results comparable to the already established ex situ measurements. The principle of the method is simple, using thin gold wires to measure the ICR directly between the BPP and the GDL. From the results presented, it can be seen that the average ICR value obtained from three measuring points in situ was is the same range as the ICR value measured ex situ after fuel cell operation. The gold coated BPP showed in situ ICR values close to 5 mΩ cm^2, while the ex situ ICR obtained after operation was 7 mΩ cm^2. The highest ICR values obtained from both in situ and ex situ measurements were on the OCV 50%, at approx. 30 mΩ cm^2 and 35 mΩ cm^2, respectively. Trends seen in the in situ (online) values were confirmed by the ex situ measured ICR. As expected, longer periods of OCV leads to an increase in ICR, and non-coated stainless steel and titanium-coated steel BPPs experienced a higher increase in ICR compared to the gold coated stainless steel.

Ex situ ICR measurements performed on smaller areas of the plates, with a point measuring setup, showed that the variation between the three in situ measuring points were probably caused by uneven current distribution in the cell. The use of three measuring points was thus more accurate than just one. The method developed during this work will be an important tool when evaluating coatings for BPPs in future projects. The accuracy of the measurements are more than good enough for evaluating whether a coating is promising enough for further research.

3.6 Acknowledgements

The authors would like to thank the Norwegian University of Science and Technology and SINTEF Materials and Chemistry for funding the work described in this article. The STAMPEM and COATELY project are both acknowledged for contributions to this work.

3.7 Literature

1. Ladre, S., et al., *In Situ and Ex Situ Contact Resistance Measurements of Stainless Steel Bipolar Plates for PEM Fuel Cells.* ECS Transactions, 2013. **50**(2): p. 829-839.
2. Hermann, A., T. Chaudhuri, and P. Spagnol, *Bipolar plates for PEM fuel cells: A review.* International Journal of Hydrogen Energy, 2005. **30**(12): p. 1297-1302.
3. Antunes, R.A., et al., *Corrosion of metal bipolar plates for PEM fuel cells: A review.* International Journal of Hydrogen Energy, 2010. **35**(8): p. 3632-3647.
4. Wang, H.L., M.A. Sweikart, and J.A. Turner, *Stainless steel as bipolar plate material for polymer electrolyte membrane fuel cells.* Journal of Power Sources, 2003. **115**(2): p. 243-251.
5. *U.S. Department of Energy, Fuel Cell Technologies Office Multi-Year Research, Development, and Demonstration Plan*. 2012. p. 29.
6. Tsuchiya, H. and O. Kobayashi, *Mass production cost of PEM fuel cell by learning curve.* International Journal of Hydrogen Energy, 2004. **29**(10): p. 985-990.
7. Aalto, S., et al., *Bipolar plate, method for producing bipolar plate and PEM fuel cell*. 2009, Google Patents.
8. Taherian, R., *A review of composite and metallic bipolar plates in proton exchange membrane fuel cell: Materials, fabrication, and material selection.* Journal of Power Sources, 2014. **265**: p. 370-390.
9. Wang, H. and J.A. Turner, *Reviewing Metallic PEMFC Bipolar Plates.* Fuel Cells, 2010. **10**(4): p. 510-519.
10. Heras, N.D.L., et al., *A review of metal separator plate materials suitable for automotive PEM fuel cells.* Energy & Environmental Science, 2009. **2**(2): p. 206-214.
11. Tawfik, H., Y. Hung, and D. Mahajan, *Metal bipolar plates for PEM fuel cell - A review.* Journal of Power Sources, 2007. **163**(2): p. 755-767.
12. Wang, Y. and D.O. Northwood, *Effects of O2 and H2 on the corrosion of SS316L metallic bipolar plate materials in simulated anode and cathode environments of PEM fuel cells.* Electrochimica Acta, 2007. **52**(24): p. 6793-6798.
13. Lafront, A.M., E. Ghali, and A.T. Morales, *Corrosion behavior of two bipolar plate materials in simulated PEMFC environment by electrochemical noise technique.* Electrochimica Acta, 2007. **52**(15): p. 5076-5085.
14. Yang, Y., L.-j. Guo, and H. Liu, *Corrosion characteristics of SS316L as bipolar plate material in PEMFC cathode environments with different acidities.* International Journal of Hydrogen Energy, 2011. **36**(2): p. 1654-1663.
15. Lædre, S., et al., *The effect of pH and halides on the corrosion process of stainless steel bipolar plates for proton exchange membrane fuel cells.* International Journal of Hydrogen Energy, 2012. **37**(23): p. 18537-18546.
16. Turan, C., Ö.N. Cora, and M. Koç, *Investigation of the effects of process sequence on the contact resistance characteristics of coated metallic bipolar plates for polymer electrolyte membrane fuel cells.* Journal of Power Sources, 2013. **243**: p. 925-934.
17. André, J., L. Antoni, and J.-P. Petit, *Corrosion resistance of stainless steel bipolar plates in a PEFC environment: A comprehensive study.* International Journal of Hydrogen Energy, 2010. **35**(8): p. 3684-3697.
18. Jin, C.K., J.Y. Koo, and C.G. Kang, *Fabrication of stainless steel bipolar plates for fuel cells using dynamic loads for the stamping process and performance evaluation of a single cell.* International Journal of Hydrogen Energy, 2014. **39**(36): p. 21461-21469.
19. Lee, Y.B. and D.S. Lim, *Electrical and corrosion properties of stainless steel bipolar plates coated with a conduction polymer composite.* Current Applied Physics, 2010. **10**: p. S18-S21.

20. Wang, L., et al., *Corrosion properties and contact resistance of TiN, TiAlN and CrN coatings in simulated proton exchange membrane fuel cell environments.* Journal of Power Sources, 2010. **195**(12): p. 3814-3821.
21. Papadias, D.D., et al., *Degradation of SS316L bipolar plates in simulated fuel cell environment: Corrosion rate, barrier film formation kinetics and contact resistance.* Journal of Power Sources, 2015. **273**: p. 1237-1249.
22. André, J., et al., *Electrical contact resistance between stainless steel bipolar plate and carbon felt in PEFC: A comprehensive study.* International Journal of Hydrogen Energy, 2009. **34**(7): p. 3125-3133.
23. Turan, C., Ö.N. Cora, and M. Koç, *Contact resistance characteristics of coated metallic bipolar plates for PEM fuel cells – investigations on the effect of manufacturing.* International Journal of Hydrogen Energy, 2012. **37**(23): p. 18187-18204.
24. Oyarce, A., et al., *Operating conditions affecting the contact resistance of bi-polar plates in proton exchange membrane fuel cells.* Journal of Power Sources, 2013. **231**(0): p. 246-255.
25. Feng, K., et al., *Ex situ and in situ evaluation of carbon ion-implanted stainless steel bipolar plates in polymer electrolyte membrane fuel cells.* Journal of Power Sources, 2012. **199**: p. 207-213.
26. Miyazawa, A., T. Himeno, and A. Nishikata, *Electrical properties of bipolar plate and gas diffusion layer in PEFC.* Journal of Power Sources, 2012. **220**: p. 199-204.
27. Ismail, M.S., et al., *The contact resistance between gas diffusion layers and bipolar plates as they are assembled in proton exchange membrane fuel cells.* Renewable Energy, 2013. **52**: p. 40-45.
28. Mishra, V., F. Yang, and R. Pitchumani, *Measurement and Prediction of Electrical Contact Resistance Between Gas Diffusion Layers and Bipolar Plate for Applications to PEM Fuel Cells.* Journal of Fuel Cell Science and Technology, 2004. **1**(1): p. 2-9.
29. Zhou, P., C.W. Wu, and G.J. Ma, *Contact resistance prediction and structure optimization of bipolar plates.* Journal of Power Sources, 2006. **159**(2): p. 1115-1122.
30. Zhou, Y., et al., *A micro-scale model for predicting contact resistance between bipolar plate and gas diffusion layer in PEM fuel cells.* Journal of Power Sources, 2007. **163**(2): p. 777-783.
31. Akbari, M.H. and B. Rismanchi, *Numerical investigation of flow field configuration and contact resistance for PEM fuel cell performance.* Renewable Energy, 2008. **33**(8): p. 1775-1783.
32. Lai, X., et al., *A mechanical–electrical finite element method model for predicting contact resistance between bipolar plate and gas diffusion layer in PEM fuel cells.* Journal of Power Sources, 2008. **182**(1): p. 153-159.
33. Sadeghifar, H., N. Djilali, and M. Bahrami, *A new model for thermal contact resistance between fuel cell gas diffusion layers and bipolar plates.* Journal of Power Sources, 2014. **266**: p. 51-59.
34. Zhang, L., et al., *Estimation of contact resistance in proton exchange membrane fuel cells.* Journal of Power Sources, 2006. **162**(2): p. 1165-1171.
35. Netwall, C.J., et al., *Decreasing contact resistance in proton-exchange membrane fuel cells with metal bipolar plates.* Journal of Power Sources, 2013. **227**: p. 137-144.
36. Ihonen, J., et al., *A novel polymer electrolyte fuel cell for laboratory investigations and in-situ contact resistance measurements.* Electrochimica Acta, 2001. **46**(19): p. 2899-2911.
37. Makkus, R.C., et al., *Use of stainless steel for cost competitive bipolar plates in the SPFC.* Journal of Power Sources, 2000. **86**(1–2): p. 274-282.

38. Alaefour, I., et al., *Measurement of current distribution in a proton exchange membrane fuel cell with various flow arrangements – A parametric study.* Applied Energy, 2012. **93**: p. 80-89.
39. Noponen, M., et al., *Current distribution measurements in a PEFC with net flow geometry.* Journal of Applied Electrochemistry. **34**(3): p. 255-262.
40. Stumper, J., et al., *In-situ methods for the determination of current distributions in PEM fuel cells.* Electrochimica Acta, 1998. **43**(24): p. 3773-3783.
41. Yoon, Y.-G., et al., *Current distribution in a single cell of PEMFC.* Journal of Power Sources, 2003. **118**(1–2): p. 193-199.
42. Mennola, T., et al., *Mass transport in the cathode of a free-breathing polymer electrolyte membrane fuel cell.* Journal of Applied Electrochemistry, 2003. **33**(11): p. 979-987.
43. Noponen, M., et al., *Measurement of current distribution in a free-breathing PEMFC.* Journal of Power Sources, 2002. **106**(1–2): p. 304-312.
44. Pourbaix, M., *Atlas of electrochemical equilibria in aqueous solutions*. 1966, Oxford; New York: Pergamon Press.

4 Materials for Proton Exchange Membrane Water Electrolyzer Bipolar Plates

Authors: Sigrid Lædre[a], Ole Edvard Kongstein[b], Anders Oedegaard[b], Håvard Karoliussen[a] and Frode Seland[a]

a Norwegian University of Science and Technology (NTNU), Norway

b SINTEF Materials and Chemistry, Norway

This manuscript has been prepared been prepared for publication.

4.1 Abstract

Even though titanium based Bipolar Plates (BPPs) are most commonly used in Proton Exchange Membrane Water Electrolyzers (PEMWE) today, there is a lack of studies investigating non-coated materials at conditions as harsh as inside an operating PEM electrolyzer. The requirements for BPPs in electrolyzers are more difficult to achieve compared to BPPs for use in PEM fuel cells because of the higher operation potential. Molybdenum, 254 SMO, tungsten, AISI 316L, AISI 304L, Inconel 625, Titanium gr. 2, niobium and tantalum were all put through pre-designed potentiostatic and potentiodynamic tests at potentials up to 2.0 V_{SHE}. Interfacial contact resistance (ICR) measurements, Scanning Electron Microscopy (SEM) imaging and weight loss measurements were also conducted. To the author's knowledge, there is no literature describing such testing for several of the materials in this study. Titanium, tantalum and niobium experienced little or no weight change during potentiostatic polarization, while for AISI 304L, AISI 316L and tungsten the measured weight loss was much lower than the weight loss calculated from currents produced. When the potentiostatic test was prolonged for titanium, it was found that even though the currents kept stable over time, the ICR increased.

4.2 Introduction

Hydrogen is considered one of the most promising energy carriers for the future [1-3], and is said to play an important role in storing of energy from renewable energy sources [4]. Today, hydrogen is predominantly produced by steam reforming of natural gas or gasification of coal and oil [1]. This method is a cost effective way of producing hydrogen, but simultaneously leads to significant carbon dioxide production impeding the transition to renewable and sustainable energy sources. Only about 4 % of the overall hydrogen production is done with water electrolysis [3]. On the other hand, production of hydrogen by electrolysis of water produces close to 100% pure hydrogen, is not dependent on fossil fuels and emits no carbon dioxide if produced with renewable energy. Alkaline water electrolysis has since its discovery in 1789 become the most common electrolyzer technology commercially available worldwide [1, 5, 6]. It is comprised of rather cheap components, has a very long life time at low maintenance costs and can be built into large units. It is, however, associated with a low partial load range, limited current density and low operating pressure [1].

Proton Exchange Membrane water electrolyzers (PEMWE) represent a zero-gap concept where a solid electrolyte, typically a humidified perfluorosulfonated polymer (Nafion®), is combined directly with two electrodes. The PEM electrolyzer is considered an interesting alternative to the alkaline water electrolyzer [1, 5, 7], as it can be operated under higher current densities and work under a wide range of power inputs [1]. The possibilities of dynamic operation of PEMWEs, including a load-following mode [1, 7], make them ideal in an energy capture and storage system for intermittent energy sources like wind, solar and wave, typically at remote locations. The membrane in the PEM electrolyzer provides high proton conductivity, low gas crossover and compact system design [1]. No liquid caustic electrolyte is circulated in the cell stack, which makes the PEM electrolyzer both safer and more reliable compared to the alkaline electrolyzer [5].

One important component in a PEM electrolyzer stack is the Bipolar Plate (BPP) [4]. Its tasks are to separate single cells in a stack, conduct heat and current between single cells in a stack and distribute react agents within the electrolyzer [1, 4]. The BPP must have high corrosion resistance, possess high mechanical strength, high shock durability and be easy to manufacture allowing for mass production [4]. To the authors knowledge, there are currently no official targets for BPPs in PEMWEs, but the U.S. Department of Energy (DoE) [8] have set targets for BPPs in PEM fuel cells (PEMFCs). Their targets for 2020 include a maximum contact resistance of 0.01 Ω cm^2 and a maximum corrosion current density of 1 μA cm^{-2}. Even though

these targets were developed for PEMFCs, low contact resistance and corrosion current is equally important for BPPs in PEMWEs, as they affect the cost, performance and lifetime. The BPP stand for a large fraction of the stack cost [1, 7], and a reduction of BPP manufacturing costs could thus drastically decrease the total cost of a PEMWE stack. The high single cell voltage and anode electrode potential, sometimes exceeding 2.0 V in an operating electrolyzer, restrains the materials selection significantly. Metal BPPs are generally easy to mass produce, and they exhibit exemplary electrical- and thermal properties, but oxides formed on the metal surface can cause high ohmic resistance. Titanium is typically used as BPP in PEM water electrolyzers today [1, 4].

BPPs for PEMFCs have been thoroughly investigated [9-13], and in particular stainless steel BPPs [14-18]. In comparison, there are few published studies on BPPs for PEWE. Titanium as BPP material in PEMWEs and regenerative fuel cells has been investigated to some extent [4, 19-24], with a main focus on coatings. Lin et al. [23] looked into the corrosion behavior of (Ti, Zr)N coated titanium for use as bipolar plate material in regenerative fuel cells. They found the corrosion resistance of (Ti, Zr)N to outperform that of TiC, TiN and ZrN. Zang et al. [20] performed both corrosion-and Interfacial Contact Resistance (ICR) measurements on titanium with nanocomposite Ti-Ag-N. Zang et al. [19] investigated the corrosion properties, interfacial conductivity and surface energy of Ti-Ag coated titanium BPPs. They found the ICR to increase from 4.1 mΩ cm^2 to 22.2 mΩ cm^2 after polarization at 2.0 V_{SHE} for 4 hours.

Other materials have also been investigated for use as BPP material in electrolyzers [25-29]. Nikiforov et al. [25] tested the corrosion properties of several steel and nickel alloys in 85% phosphoric acid and at various temperatures for use in high temperature steam electrolyzers. Chisholm et al. [26] printed polypropylene flow plates for water electrolyzers by use of a 3D printer. They coated the printed plates with silver conductive paint. Gago et al. [27] tested titanium coatings and surface modification with platinum on stainless steel BPPs for PEWEs. Rasten et al. [29] suggested the use of highly alloyed stainless steel as BPP material for PEMEWEs. The recommended austenitic steel contained 20 weight % nickel, 20 weight % chromium, 3-5 weight % molybdenum, 0.5-2 weight % copper, 30-50 weight % iron and maximum 9 weight % other elements. Langemann et al. [28] measured the pH development over time on both anode and cathode side in a PEMWE equipped with corrosion resistant BPPs. They found the pH to decrease on both the cathodic and anodic side of the electrolyzer over a time span of 50 hours. The same authors performed polarization tests of AISI 304L coated with Au and TiN in a 0.50 M sulfuric

acid solution at 2.0 V_{SHE}, and studied the pH development in the feeding water during these measurements.

Niobium, molybdenum, chromium and titanium have all been investigated as possible alloying components for stainless steel bipolar plates for fuel cells [30-32]. Kim et al. [32] investigated the alloying effects of Cr and Mo for several commercial steels, and found that the transpassive transition of stainless steels become progressively like the one for chromium as their Pitting Resistance Equilibrium Number (PREN) increases. Feng et al. [30] found that by alloying AISI 316L with niobium, the dissolution rate of the material was significantly reduced.

A number of studies have been conducted with focus on the corrosion properties of metals such as AISI 316L, molybdenum, tungsten, niobium, tantalum, Inconel 625 and 254 SMO [33-42]. Very few of the studies conducted have been performed with conditions similar to what the materials are exposed to inside a PEMWE. As far as the authors are aware of, there are currently no studies of BPPs for PEMWEs, where both the corrosion properties and resistance development at relevant conditions for a selection of potential BPP plate materials have been compared to one another. The potential exhibited by a PEMWE can be even higher than 2.0 V_{SHE}, and this limits the number of fields where similar testing is relevant. Corrosion studies rarely focus on testing materials at such high potentials, but it would be highly relevant in the field of PEM water electrolysis.

In this work the suitability of various relevant bipolar plate materials has been examined, with emphasis on their durability under conditions similar to those experienced on the anode side of an operating PEMWE. Polarization, ICR and Scanning Electron Microscopy (SEM) imagining were used to characterize and compare the corrosion and conductivity properties for a selection of metallic BPP materials. Here, we emphasize the necessity of studying the substrate materials at relevant operating conditions. The materials were polarized as high as 2.0 V_{SHE}, and this study is thus unique for several of these materials. This information is highly relevant in the selection of appropriate materials for BPPs in electrolyzers, including substrate materials for various coatings with the ultimate goal of reducing cost and increasing lifetime.

4.3 Procedure and Materials

The materials tested in this study are listed in Table 4.1. In addition to the procedures described below, a Hitachi S-3400N SEM was used for characterization. The accelerating voltage was kept at 15 kV for all the imaging. Prior to testing, the materials were etched in order to remove non-conducting oxides on the materials surface.

Table 4.1: Surface area and etching procedure of all the materials in this study.

Material	Surface area [cm^2] *	Etching agent	Etching time
Tungsten	3/5.4	37 % HCl	15 min
254 SMO	3.1/12.3	25 % HCl	15 min
Titanium gr. 2	12.3	37 % HCl	60 min
AISI 316L	3.1/12.3	12.5 % HCl	15 min
AISI 304L	3.1/3.1	12.5 % HCl	20 min
Tantalum	12.3	42 % KOH	24 h
Niobium	12.3	37 % HCl	15 min
Molybdenum	2.1/4.2	37 % HCl	15 min
Inconel 625	3.2/12.3	25 % HCl	15 min

* The given area is for one side of the test samples. For some of the materials, the samples used for potentiostatic and potentiodynamic measurements had different surface areas. The potentiostatic area is listed to the left and the potentiodynamic area is listed to the right.

Table 4.2: Compositions of the alloys used in this study.

Elements	Alloys and weight % of elements			
	AISI 316 L [43]	AISI 304L [43]	254 SMO [44]	Inconel 625 [45]
Aluminum	-	-	-	0.4
Carbon	≤0.030	≤0.030	≤0.020	0.1
Chromium	16.0-18.0	18.0-20.0	19.5-20.5	20-23
Cobalt	-	-	-	1
Copper	-	-	0.5-1	-
Iron	Rest	Rest	Rest	5
Manganese	≤2.00	≤2.00	-	0.5
Molybdenum	2.0-3.0	-	6-6.5	8-10
Nickel	10.0-14.0	8.0-12.0	17.5-18.5	58
Niobium	-	-	-	3.15-4.15
Nitrogen	-	-	0.18-0.22	-
Phosphorus	≤0.045	≤0.045	-	-
Silicon	≤1	≤1	-	0.5
Sulfur	≤0.030	≤0.030	-	-
Titanium	-	-	-	0.4

The etching procedure for each material was adjusted in order to minimize the contact resistance after etching. The etching agent and time used to clean each material is listed in Table 4.1, along with the surface areas of each sample. The compositions of the alloys used in this work are listed in Table 4.2.

4.3.1 Polarization

A Gamry ref 600 potentiostat with a three-electrode-setup was used to polarize the metal samples, as described by Lædre et al.[46] A Biologic VMP3 potentiostat was used for the high current experiments. The electrolyte used was a 0.1 M Na_2SO_4 solution that was adjusted to pH 5.5 by addition of 1 mM H_2SO_4. Platinum was used as counter electrode and Hg/Hg_2SO_4 electrode was used as the reference electrode. This reference electrode was deliberately chosen to ensure no chloride migration into the electrolyte. Chloride ions are known to cause aggressive pitting corrosion on e.g. AISI 316L stainless steel and possibly impair the platinum counter electrode. The reference electrode was kept in a saturated K_2SO_4 solution, and was connected to the electrolyte via a salt bridge with the same solution as the electrolyte. Nitrogen gas (5.0 N_2. Yara) was bubbled into the solution both before and during the polarization tests, to minimize oxygen content in the electrolyte.

The parameters used during the polarization tests are presented in Table 4.3. The potentiostatic test was designed to simulate the potential experienced by a bipolar plate inside an operating PEM water electrolyzer on the anode side. The potentiodynamic test was designed to show the corrosion properties of the metals when polarized between 0 and 2.0 V_{SHE}. These potentials were chosen to study the corrosion bipolar plates could experience inside a PEMWE. IR compensation was performed by employing the ohmic resistance obtained from an electrochemical impedance spectrum (EIS) obtained prior to each test.

Table 4.3: Polarization parameters chosen for the potentiostatic and potentiodynamic tests.

Test	Temperature [°C]	pH	Potential [V]	Duration /sweep rate
Potentiostatic	70	5.5	2.0 V_{SHE}	3600 s
Potentiodynamic	70	5.5	0-2.0 V_{SHE}	1.0 mV s^{-1}

All of the materials were weighed before and after polarization on an accurate laboratory scale, in order to obtain the weight loss.

4.3.2 Interfacial Contact Resistance

Before and after each polarization test, the interfacial contact resistance was measured ex-situ. The setup used for ICR measurement is shown in Figure 4.1. The ICR was measured between the specimen and a Gas Diffusion Layer (GDL, Freudenberg H23C6), where the GDL was used to measure the contact resistance towards a known, conductive material. The specimen with the GDL on top was put in between two gold-coated copper plates, and a pneumatic piston was used to move the lower plate towards the upper one. A current of 2.0 A was applied between the two gold coated copper plates by use of a XDL 56-4 DC power supply (Xantex). A pin connected to a very sensitive spring was mounted in the middle of the bottom plate, in order to obtain measurements at a certain area of the test specimen. The corresponding voltage was measured between the upper gold-coated copper plate and the spring loaded pin using a Fluke 76 True RMS multimeter, and this voltage was used to calculate the ICR between the specimen and the GDL.

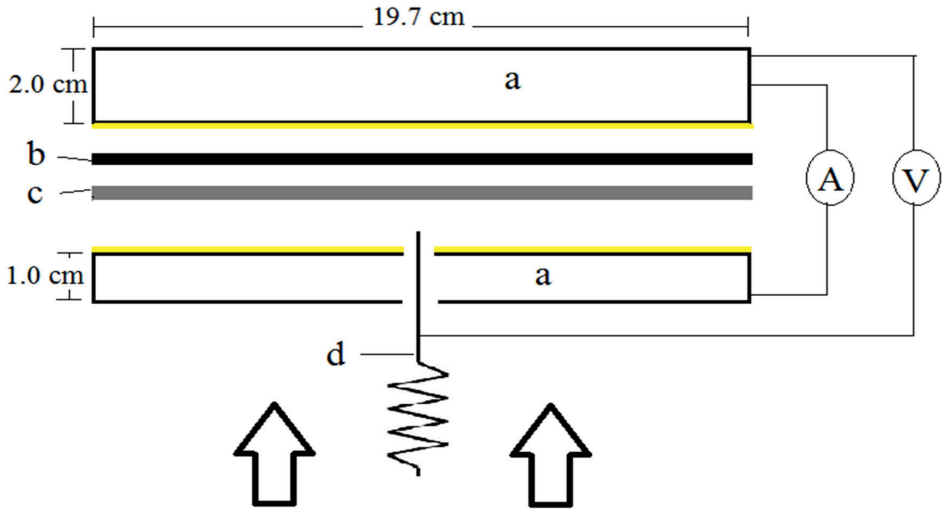

Figure 4.1: Setup for measuring of ICR ex situ with a) Gold coated copper plates, b) GDL, c) Bipolar test plate and d) spring loaded pin.

4.4 Results and Discussion

4.4.1 Potentiodynamic Polarization

PEM water electrolysis bipolar plates are exposed to demanding conditions such as high positive potentials, acidic membrane and liquid water feed. The conditions are significantly more demanding than for PEM fuel cells and polarization up to 2.0 V allow for several reactions one needs to be aware of. In addition to various corrosion reactions and oxide formation, oxygen evolution will also contribute to the overall current produced by the system.

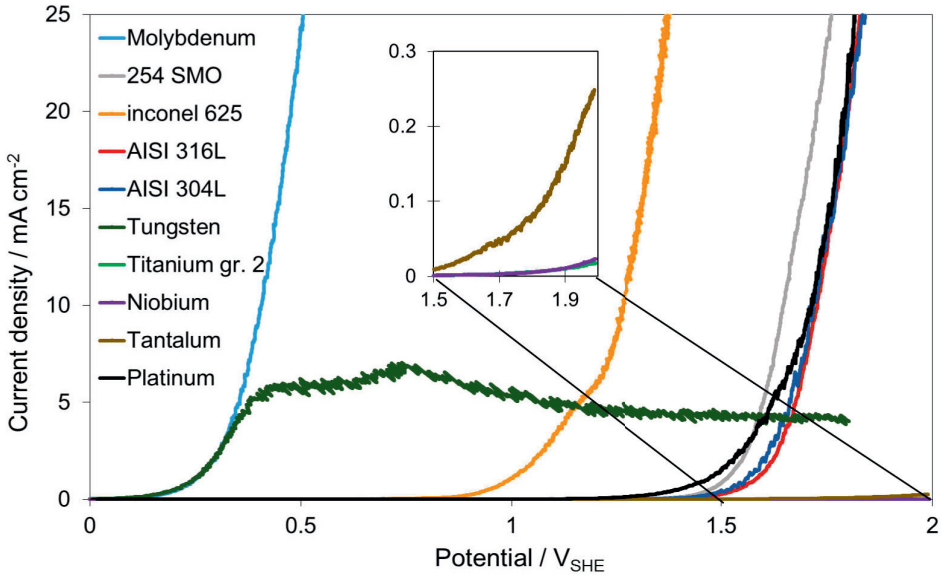

Figure 4.2: Currents produced by the various materials during potentiodynamic polarizations from 0-2.0 V_{SHE}.

Figure 4.2 displays the current-potential relation obtained from the potentiodynamic tests performed for all the materials. As several of the materials produced very high currents, all curves were cut at 25 mA cm^{-2}. Only the current onset and the initial current increase behavior are emphasized upon in the comparison between the materials studied in this work. In addition to the various bipolar plate materials tested, a platinum wire was put through the potentiostatic test as well for comparison reasons. For simplicity we neglect any corrosion and conductivity changes due to Pt oxide formation during anodic polarization above 0 V_{SHE}, and thus assume that the current observed was attributed entirely to oxygen evolution. The current onset potential and initial current intensification during

anodic polarization of the platinum electrode was then used to determine whether oxygen evolution or corrosion processes were the dominating process for the other sample materials.

Titanium, tantalum and niobium produced very low current densities throughout the entire sweep, and maximum current densities several order of magnitude lower than all the other materials in this study. The current density increased with increasing potential for all three materials. This increase could have been caused by corrosion, but it could also be a result of oxygen evolution on the sample surfaces.

For the molybdenum electrode, the current increased rapidly from approximately 0.25 V_{SHE}, and kept increasing throughout the entire test. This shows that accelerating current producing reactions took place on the material surface almost throughout the entire sweep. Oxygen evolution was to be expected only at higher potentials, in the same, or more positive potential region as oxygen evolution on the platinum electrode. Thus the early increase in current density at the molybdenum electrode, indicates corrosion processes occurring on the molybdenum surface during the early stages of the polarization. Not surprisingly, the same was also observed for the Inconel 625 sample, containing rather large amounts of both nickel and iron, known to corrode in acidic environment. However, it is worth noting that the observed current did not become excessive until about 1.0 V.

The three steel materials in this study, AISI 304L, AISI 316L and 254 SMO, did not show a clear current increase until approximately 1.5 V. A current increase at a lower potential was observed for the 254 SMO sample compared to the AISI 316L and AISI 304L steel samples. This was attributed to higher corrosion current at this sample, perhaps due to the higher fraction of molybdenum and nickel in this sample (Table 4.2). AISI 304L and AISI 316L were the two materials in this study with the most similar composition, and this is probably the reason why the curves for the two materials almost coincide in Figure 4.2. An interesting observation is that these same two steel materials produced currents very similar to platinum. This makes it difficult to determine which surface reactions that took place, as both oxygen evolution and corrosion processes were possible.

The potentiodynamic polarization of tungsten showed an increase in current density shortly after initiating the test, but then it stabilized at approximately 5.0 mA cm^{-2}. This is interesting, as none of the other materials experienced the same trend. One explanation could be that the rate-determining step for tungsten was a chemical reaction. Another explanation could be a limiting process strangling the current

density to low values, for example slow dissolution of inactive oxide exposing the vulnerable metal underneath.

4.4.2 Potentiostatic Polarization

The results from the potentiostatic polarization tests are shown in Figure 4.3. Both niobium and tantalum are widely known for their ability to resist corrosion in most environments. This is attributed to the stable oxides formed on the metal surfaces of these metals [47, 48]. Compared to the other materials investigated in this study, niobium and tantalum produced very low currents. Potentiostatic polarization of tantalum resulted in current densities that stabilized around 10 µA cm^{-2}, while for niobium they stabilized around 20 µA cm^{-2}. Titanium, which is one of the most common substrate material used as BPPs in PEMWEs today [1], also showed relatively low current densities (around 170 µA cm^{-2}) during the potentiostatic test. As with tantalum and niobium, titanium forms a stable oxide layer on the surface, which prevents corrosion. Tungsten produced currents higher than titanium, niobium and tantalum, but more than one order of magnitude lower than the rest of the materials. The currents from the polarization of tungsten stabilized at 3.7 mA cm^{-2}.

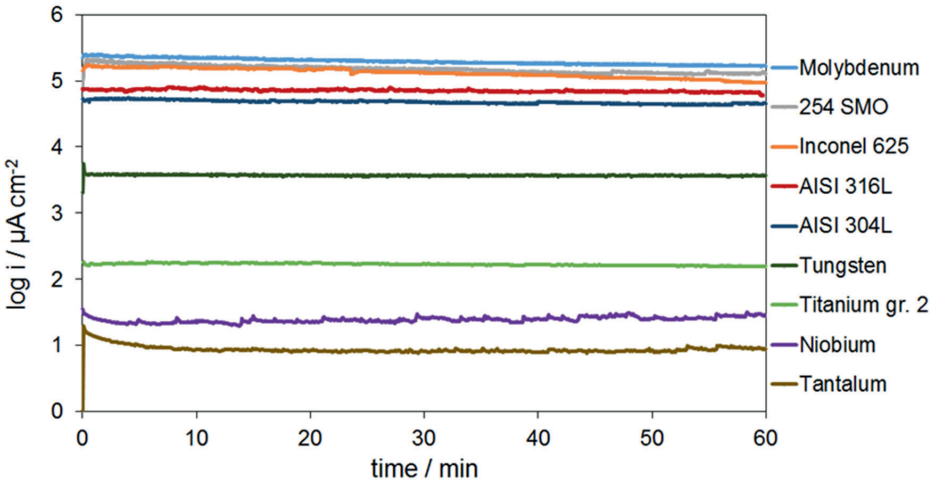

Figure 4.3: Currents produced by the various materials during the potentiostatic polarizations at 2.0 V_{SHE}.

The material that produced the highest current densities during the potentiostatic test was molybdenum, with currents around 200 mA cm^{-2}. The potentiostatic polarizations of the steel samples AISI 316L, AISI 304L, 254 SMO and Inconel 625 all resulted in currents lower than molybdenum, but several orders of magnitude higher than tantalum, niobium, titanium and tungsten. The currents produced by these materials all decreased over time, where Inconel 625 showed a steeper decrease than the other materials. This change in current could arise from the formation and alteration of oxide composition on the metal surface. When comparing the results in Figure 4.3 to the results in Figure 4.2, oxygen evolution cannot be excluded in the high currents observed for the AISI 304 and AISI 316L samples in Figure 4.3. For molybdenum, 254 SMO and Inconel 625, however, most of the currents contribution is due to corrosion processes.

As for the potentiodynamic test, the potentiostatic polarization of tungsten resulted in current densities higher than titanium, but lower than the alloys. The current density kept stable at about 4 mA cm^{-2} throughout the entire polarization, which can be explained by a chemical dissolution process as the rate determining step [49]. Based on the current-potential behavior alone (Figures. 4.2 and 4.3), titanium, tungsten and tantalum appear to be the most promising BPP materials for PEM water electrolysis. However, the contact resistance of the materials must also be considered and is reported and discussed in Section 4.4.4.

Figure 4.4 displays pictures after polarization (column 1) as well as SEM images obtained both before (column 3) and after polarization (column 2) of Inconel 625 and 254 SMO samples. The pictures and images from the potentiostatic polarizations of Inconel 625 (A) and 254 SMO (B) are shown, as well as the potentiodynamic polarization of 254 SMO (C). In all of the SEM images, heavy corrosion can be observed. The pictures and SEM images of the 254 SMO and Inconel 625 samples that had been put through the potentiostatic tests (Fig. 4 A1, A3, B1 and B3), revealed corroded surfaces, where corrosion had created deep cavities in the surface. The uneven structure of the sample surfaces indicates that a kind of non-uniform corrosion has happened. The corrosion may have been initiated as local pitting corrosion, inevitably progressing to the entire surface. Both of these materials have been found to experience pitting corrosion in certain environments [34, 50], even though they both should be pitting resistant in e.g. sea water [35, 51]. The picture and corresponding SEM image of the 254 SMO sample obtained after the potentiodynamic polarization clearly displays pitting corrosion. This kind of corrosion can be very harmful to the material as it progresses rapidly once initiated.

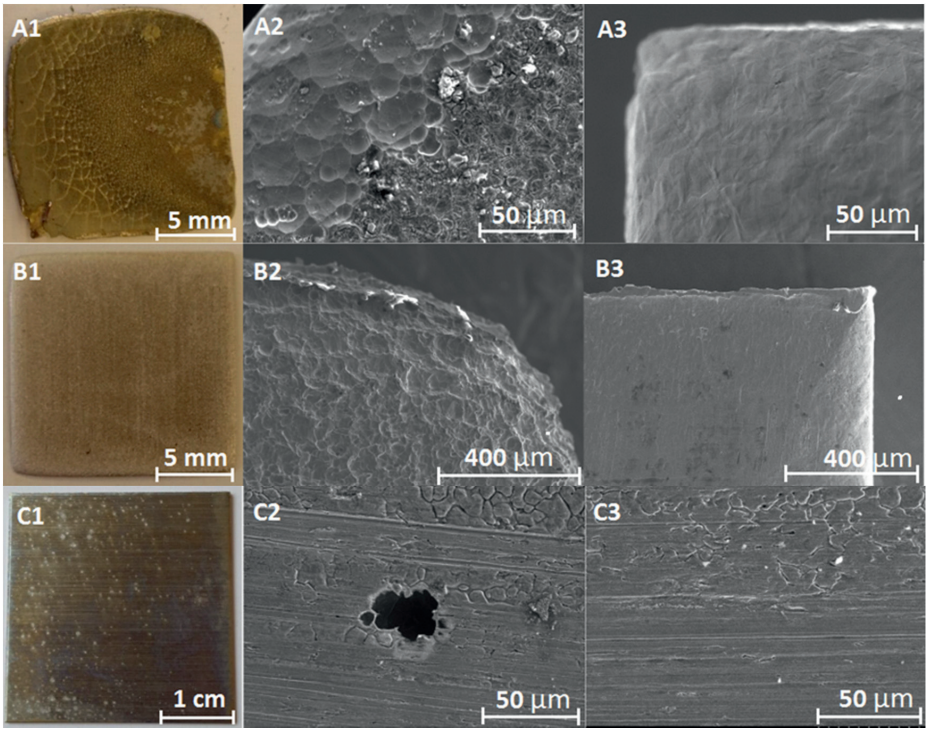

Figure 4.4: Pictures and SEM images of samples before and after the following tests: (A) Potentiostatic polarization of Inconel 625, (B) potentiostatic polarization of 254 SMO and (C) potentiodynamic polarization of 254 SMO. (1) Pictures of corroded samples, (2) SEM images of samples before polarization and (3) SEM images after polarization.

4.4.3 Corrosion and Weight Loss

Table 4.4 displays the results from weight measurements performed before and after each potentiostatic test, as well as weight calculations for each material from the current produced during polarization. By using Faradays law (equation 4) weight loss was calculated from the average currents produced by each material when polarized potentiostatically at 2.0 V_{SHE}. In this equation, m is the mass, Q is the charge, M is the molecular mass, F is Faradays constant and n_{avg} is the average number of electrons transferred. The n_{avg} and molar weights for the alloys were calculated from the n and M values of all the components in the alloys.

$$m = \frac{Q \cdot M}{n_{avg} \cdot F} \tag{4}$$

Table 4.4: Weight loss measurements and calculations from the potentiostatic tests performed at 2 V_{SHE}, along with oxides from Pourbaix diagrams of the various materials at 25 °C and pH= 5.5 [52].

Material	Possible oxide(s)	n_{avg}	Measured weight loss [mg]	Estimated weight loss from total current [mg]	Percentage of current from corrosion [%]
Titanium gr. 2	TiO_2	4.0	-1.70[a]	1.83	-
Tantalum	Ta_2O_5	5.0	-2.70[a]	0.29	-
Niobium	Nb_2O_5	5.0	-27.00[a]	0.42	-
AISI 316L	Fe_2O_3/$Cr_2O_7^{2-}$ /NiO_2	3.6	59.30	255.60	23.20
Tungsten	WO_3	6.0	5.00	25.52	19.59
AISI 304L	Fe_2O_3/ $Cr_2O_7^{2-}$ /NiO_2	3.7	40.29	155.00	27.67
Molybdenum	MoO_3	6.0	530.30	506.00	104.80
254 SMO	Fe_2O_3/ $Cr_2O_7^{2-}$ /NiO_2	3.9	609.20	518.70	117.50
Inconel 625	NiO_2/ $Cr_2O_7^{2-}$ /Fe_2O_3	4.5	619.20	429.80	144.00

[a] The negative weight losses were probably cause by oxide development on the surface.

Also included in Table 4.4 are oxides retrieved from Pourbaix diagrams at 25 °C, 2.0 V_{SHE} and pH=5.5 [52]. The temperature used during this study was higher than 25 °C, but the content of Table 4.4 still proved valuable for the analysis performed here. For the alloy materials, the oxides from the major components are included. The oxide compositions on metal surfaces are complex, and the results in Table 4.4 are not based on an in depth study of the oxides of the materials in this work, as this was not the main objective here.

The percentage of current produced by corrosion was included in the table, with the objective of distinguishing between corrosion and other surface reactions, such as oxygen evolution. All components in an alloy were assumed to corrode simultaneously in the estimation of weight loss from the observed current. It was further assumed that the weight increase due to oxide formation was negligible in comparison to the total weight loss for most of the materials tested. However, for the materials with close to no weight loss the oxide formation at the surface of the material could be of significance in the weight measurements.

In fact, niobium, titanium and tantalum all experienced negative weight loss during the potentiostatic test (Table 4.4), which means they gained weight. Low corrosion combined with oxide formation, could explain the weight increase, as the weight gains were minor compared to the weight losses observed for the other materials. From Figures 4.2 and 4.3 it can be seen that the currents from both tantalum and niobium where low compared to most of the other materials, which indicates less corrosion.

Tungsten, AISI 304L and AISI 316L produced currents corresponding to weight losses approximately five times higher than the measured weight losses, when assuming that all the current came from corrosion. This indicates that most of the current came from oxygen evolution, which is in agreement with the current-potential behavior reported in Figure 4.2 for the AISI 304L and AISI 316L steel samples. These curves almost overlap the one for platinum. The same trend was not observed for tungsten in the potentiodynamic test, but this does not exclude oxygen evolution, as the weight loss measurements were performed in conjunction with the potentiostatic tests.

The percentages of currents from corrosion were found to be more than 100% for 254 SMO, molybdenum and Inconel 625. All of these materials showed an increase in current at lower voltages than platinum in the potentiodynamic tests, and it is thus assumed that the contribution from corrosion was dwarfing the oxygen evolution. For molybdenum, the number is very close to 100, and the conclusion is that all of

the current produced during the polarization, came as a result of corrosion. For 254 SMO and Inconel 625, the high percentage also shows that corrosion was responsible for all of the current. The fact that the percentage was above 100, can be explained by the difficulty in determining which elements in the alloy that contributed to the corrosion.

4.4.4 Interfacial Contact Resistance

Figure 4.5 shows how the measured contact resistance varied with pressure. ICR values at very low pressures proved to be difficult as some of the samples tested were much smaller than the equipment used for the ICR measurements. This is the reason why some of the curves in Figure 4.5 have different starting pressures. Figure 4.6 compares ICR values for all the materials at a pressure of 140 N cm^{-2} obtained before and after each one hour potentiostatic polarization. There are two bars for each material in Figure 4.6, where the one to the left shows the ICR value after sample pretreatment involving oxide removal, but before polarization. The bar to the right shows the ICR value obtained after the polarization measurements. In order to understand these ICR results, it is important to compare them to the other measurements obtained in this study.

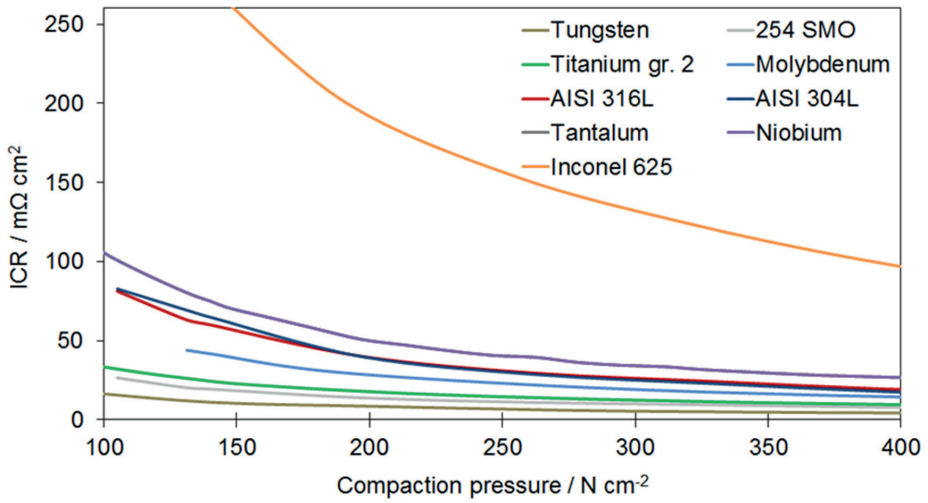

Figure 4.5: ICR measured at various pneumatic pressures for each material after potentiostatic polarization.

As can be seen from Figure 4.6, most of the materials showed an increase in ICR after they had been polarized. This was not the case for Tungsten, where the ICR even decreased from 13 mΩ cm² to 11 mΩ cm². This could come from a change of the tungsten surface resulting in a more conductive surface layer. Inconel 625 provided the highest ICR values after polarization (274 mΩ cm²), while tungsten the lowest (11 mΩ cm²). As the polarization and ICR measurements of Inconel 625 resulted in both high current densities and resistances, this material is a poor candidate for use as BPP in PEMWEs.

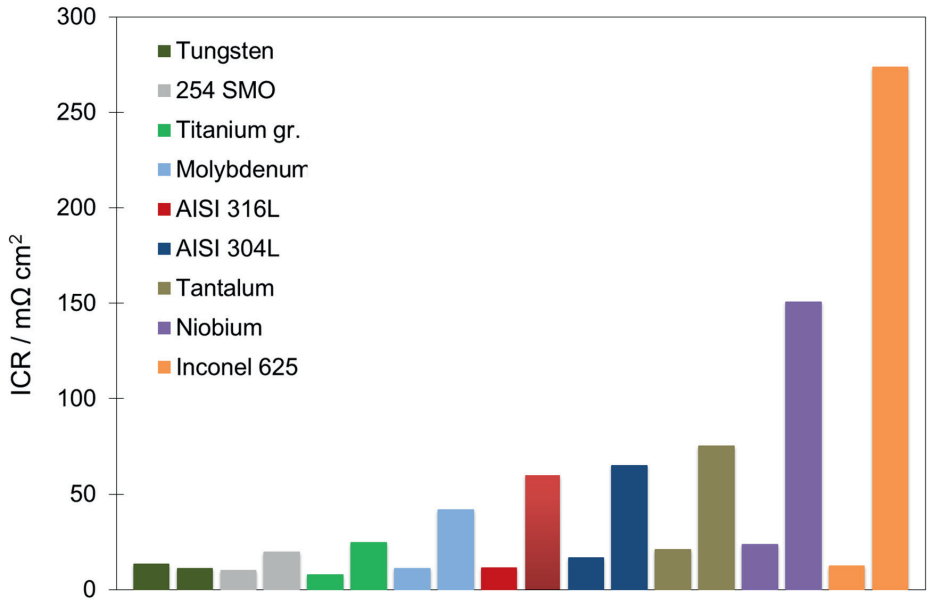

Figure 4.6: ICR values measured before (left) and after (right) each potentiostatic test at 140 N cm^{-2}.

The ICR of titanium, tantalum and niobium went from 8 mΩ cm², 21 mΩ cm² and 24 mΩ cm² to 24 mΩ cm², 75 mΩ cm² and 151 mΩ cm² during polarization, respectively. This resulted in an increase of 3, 3.6 and 6.3 times the before-values. This corresponds well with the assumption that passive oxides are formed on their surfaces during anodic polarization. The negative weight loss measurements and low current densities in both potentiostatic and potentiodynamic polarizations for these three materials also strengthens this assumption.

AISI 316L and AISI 304L produced currents in the same order of magnitude during both potentiostatic- and potentiodynamic polarization. The ICR values measured at

140 N cm^{-2} were 60 mΩ cm^2 for AISI 316L and 65 mΩ cm^2 AISI 304L. The main difference between these two materials is that the 316L steel contains molybdenum, while 304L does not. 254 SMO produced currents approximately one order of magnitude higher than both of the other steels, and the ICR value measured after polarization was 19 mΩ cm^2. High current density and low ICR indicate that this steel corroded more than 316L and 304L, and that the surface oxide formed was thinner or had a different composition than the other steels. 254 SMO contains higher amounts of both molybdenum and nickel compared to both of the other steels, which could explain the difference in both current density and ICR.

The current densities from the potentiostatic polarization of tungsten were higher than for some of the other metals. This combined with a minimal ICR change, indicates that tungsten did not form a thick protective oxide during polarization. The Pourbaix diagram for tungsten at 25 °C suggests formation of either WO_3 or WO_4^{2-}, depending on concentration of ions [52]. All of the results combined support the idea that a reaction limiting process took place, which caused the low, but steady, current densities and the low ICR values for tungsten.

4.4.5 ICR Development over Time for Titanium

The duration of the potentiostatic test for titanium was prolonged to study how the ICR developed over time. Titanium samples were pretreated and put through a potentiostatic test at 2.0 V_{SHE} of various lengths. The resulting current densities and ICR values are displayed in Figure 4.7 and Figure 4.8, respectively. The absolute values of the current densities are all in the same order of magnitude, although slightly lower for the 122 h test indicating the expected variations at such low absolute values of the currents. The currents measured were all in the μA range, and at such low currents minor variations could lead to relatively large deviations. For all the tests the current density stabilized at the beginning of the tests, and kept stable throughout the test. For the 122 h test a very small increase in currents was observed towards the end of the test, but the low absolute values of the currents makes it difficult to determine whether it is a result of surface reactions or just instabilities in the measurements. The focus was thus put on the ICR measurements, which showed interesting development of the ICR over time. From the curve in Figure 4.8, it is evident that the ICR increased as the length of the test increased. This is crucial when considering titanium as a potential BPP material for PEMWEs. If the ICR continues to increase, this would inevitably result in a continuous decrease in electrolyzer performance.

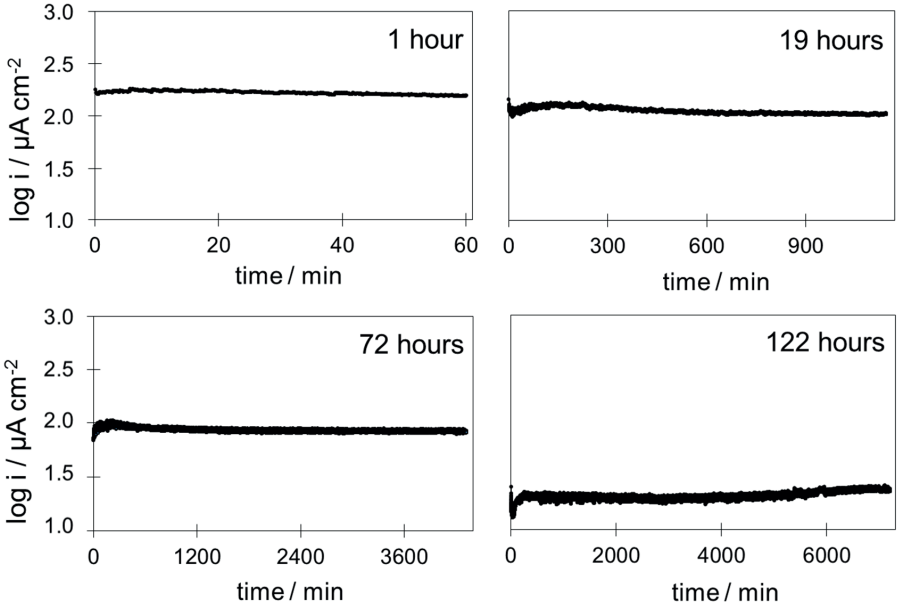

Figure 4.7: Polarization of titanium at 2.0 V_{SHE} over different time spans.

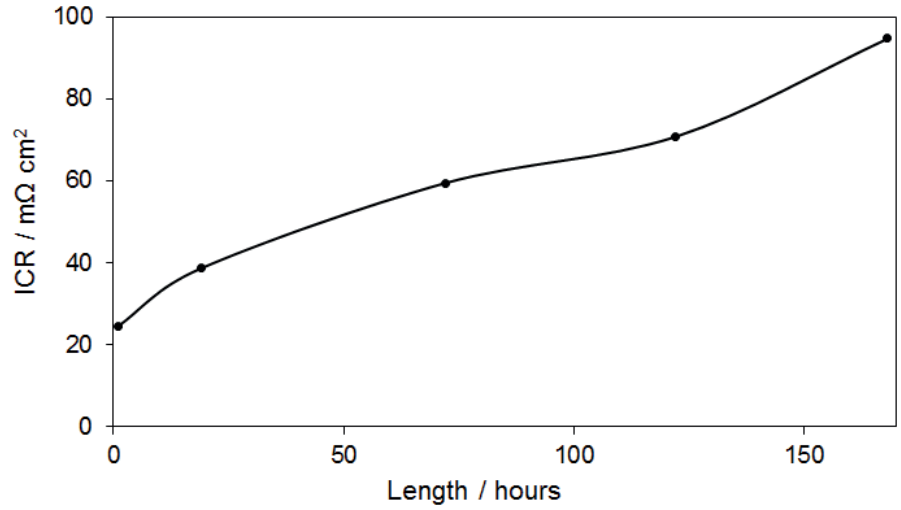

Figure 4.8: ICR at 140 N cm^{-2} after potentiostatic polarization of titanium at 2.0 V_{SHE} over different time spans.

4.5 Conclusions

In both the potentiostatic- and potentiodynamic polarization tests, tantalum, niobium and titanium produced low current densities compared to the other materials. Neither of these materials experienced any weight loss during polarization, which indicates that they did not corrode. On the other hand, both niobium and tantalum showed a significant increase in ICR, as compared to the negligible increase for titanium during the one-hour potentiostatic test. Nevertheless, a longer polarization at 2.0 V showed that the ICR increased also for titanium with time.

Weight measurements indicated that only approx. 20% of the overall current produced by the AISI 304L and 316L samples was related to corrosion. This suggested that these materials were catalytically active towards oxygen evolution at 2.0 V. Even though some of the materials tested in this study, showed promising qualities, neither of them fulfilled the conductivity and corrosion requirements set by DoE for PEM fuel cells. It is worth pointing out that these targets were set for BPPs in PEM fuel cells, and used only as guidelines in this work as there is not yet put forth similar targets for BPPs in PEM water electrolyzers. For both systems, it is crucial that the materials do not corrode, do not poison the electrolyte or electrocatalysts and maintain a low interfacial contact resistance. As there appears to be a lack of literature describing polarization up to 2.0 V_{SHE} for several of the materials tested in this study, the results presented here provide an important basis when choosing substrates for BPP coatings.

4.6 Acknowledgements

Norwegian University of Science and Technology (NTNU) financed this work together with SINTEF materials and chemistry and the COATELY project. Sigrid Lædre acknowledges NTNU for the award of a PhD-scholarship.

4.7 Literature

1. Carmo, M., et al., *A comprehensive review on PEM water electrolysis.* International Journal of Hydrogen Energy, 2013. **38**(12): p. 4901-4934.
2. Barbir, F., *PEM electrolysis for production of hydrogen from renewable energy sources.* Solar Energy, 2005. **78**(5): p. 661-669.
3. Dunn, S., *Hydrogen futures: toward a sustainable energy system.* International Journal of Hydrogen Energy, 2002. **27**(3): p. 235-264.
4. Wang, J.-T., et al., *Corrosion behavior of three bipolar plate materials in simulated SPE water electrolysis environment.* International Journal of Hydrogen Energy, 2012. **37**(17): p. 12069-12073.
5. Millet, P., F. Andolfatto, and R. Durand, *Design and performance of a solid polymer electrolyte water electrolyzer.* International Journal of Hydrogen Energy, 1996. **21**(2): p. 87-93.
6. Grigoriev, S.A., et al., *Optimization of porous current collectors for PEM water electrolysers.* International Journal of Hydrogen Energy, 2009. **34**(11): p. 4968-4973.
7. Ayers, K.E., et al., *Research Advances towards Low Cost, High Efficiency PEM Electrolysis.* ECS Transactions, 2010. **33**(1): p. 3-15.
8. *U.S. Department of Energy, Fuel Cell Technologies Office Multi-Year Research, Development, and Demonstration Plan*. 2012. p. 29.
9. Hermann, A., T. Chaudhuri, and P. Spagnol, *Bipolar plates for PEM fuel cells: A review.* International Journal of Hydrogen Energy, 2005. **30**(12): p. 1297-1302.
10. Wang, H. and J.A. Turner, *Reviewing Metallic PEMFC Bipolar Plates.* Fuel Cells, 2010. **10**(4): p. 510-519.
11. Tawfik, H., Y. Hung, and D. Mahajan, *Metal bipolar plates for PEM fuel cell - A review.* Journal of Power Sources, 2007. **163**(2): p. 755-767.
12. Antunes, R.A., et al., *Corrosion of metal bipolar plates for PEM fuel cells: A review.* International Journal of Hydrogen Energy, 2010. **35**(8): p. 3632-3647.
13. Hamilton, P.J. and B.G. Pollet, *Polymer Electrolyte Membrane Fuel Cell (PEMFC) Flow Field Plate: Design, Materials and Characterisation.* Fuel Cells, 2010. **10**(4): p. 489-509.
14. André, J., L. Antoni, and J.-P. Petit, *Corrosion resistance of stainless steel bipolar plates in a PEFC environment: A comprehensive study.* International Journal of Hydrogen Energy, 2010. **35**(8): p. 3684-3697.
15. André, J., et al., *Electrical contact resistance between stainless steel bipolar plate and carbon felt in PEFC: A comprehensive study.* International Journal of Hydrogen Energy, 2009. **34**(7): p. 3125-3133.
16. Papadias, D.D., et al., *Degradation of SS316L bipolar plates in simulated fuel cell environment: Corrosion rate, barrier film formation kinetics and contact resistance.* Journal of Power Sources, 2015. **273**: p. 1237-1249.
17. Wang, H.L., M.A. Sweikart, and J.A. Turner, *Stainless steel as bipolar plate material for polymer electrolyte membrane fuel cells.* Journal of Power Sources, 2003. **115**(2): p. 243-251.
18. Yang, Y., L.-j. Guo, and H. Liu, *Corrosion characteristics of SS316L as bipolar plate material in PEMFC cathode environments with different acidities.* International Journal of Hydrogen Energy, 2011. **36**(2): p. 1654-1663.
19. Zhang, H., et al., *Performance of Ti–Ag-deposited titanium bipolar plates in simulated unitized regenerative fuel cell (URFC) environment.* International Journal of Hydrogen Energy, 2011. **36**(9): p. 5695-5701.
20. Zhang, M., et al., *Honeycomb-like nanocomposite Ti-Ag-N films prepared by pulsed bias arc ion plating on titanium as bipolar plates for unitized regenerative fuel cells.* Journal of Power Sources, 2012. **198**(0): p. 196-202.

21. Jung, H.-Y., et al., *Performance of gold-coated titanium bipolar plates in unitized regenerative fuel cell operation.* Journal of Power Sources, 2009. **194**(2): p. 972-975.
22. Jung, H.-Y., S.-Y. Huang, and B.N. Popov, *High-durability titanium bipolar plate modified by electrochemical deposition of platinum for unitized regenerative fuel cell (URFC).* Journal of Power Sources. **195**(7): p. 1950-1956.
23. Lin, M.-T., C.-H. Wan, and W. Wu, *Comparison of corrosion behaviors between SS304 and Ti substrate coated with (Ti,Zr)N thin films as Metal bipolar plate for unitized regenerative fuel cell.* Thin Solid Films, 2013. **544**(0): p. 162-169.
24. Toops, T.J., et al., *Evaluation of nitrided titanium separator plates for proton exchange membrane electrolyzer cells.* Journal of Power Sources, 2014. **272**: p. 954-960.
25. Nikiforov, A.V., et al., *Corrosion behaviour of construction materials for high temperature steam electrolysers.* International Journal of Hydrogen Energy, 2011. **36**(1): p. 111-119.
26. Chisholm, G., et al., *3D printed flow plates for the electrolysis of water: an economic and adaptable approach to device manufacture.* Energy & Environmental Science, 2014. **7**(9): p. 3026-3032.
27. Gago, A.S., et al., *Protective coatings on stainless steel bipolar plates for proton exchange membrane (PEM) electrolysers.* Journal of Power Sources, 2016. **307**: p. 815-825.
28. Langemann, M., et al., *Validation and characterization of suitable materials for bipolar plates in PEM water electrolysis.* International Journal of Hydrogen Energy, (0).
29. Rasten, E., et al., *Use of Austenitic Stainless Steel as Construction Material in a Device or Structural Component Which is Exposed to an Oxygen and/or Hydrogen and/or Hydrofluoric Acid Environment*, in *Patent application*. 2010. p. Patent application number: 20100133096.
30. Feng, K., et al., *Corrosion behavior and electrical conductivity of niobium implanted 316L stainless steel used as bipolar plates in polymer electrolyte membrane fuel cells.* Surface and Coatings Technology, 2010. **205**(1): p. 85-91.
31. Lee, S.-H., et al., *Effects of niobium and titanium addition and surface treatment on electrical conductivity of 316 stainless steel as bipolar plates for proton-exchange membrane fuel cells.* Journal of Power Sources, 2009. **187**(2): p. 312-317.
32. Kim, J.S., et al., *Effect of alloying elements on the contact resistance and the passivation behaviour of stainless steels.* Corrosion Science, 2002. **44**(4): p. 635-655.
33. Abd El Meguid, E.A. and A.A. Abd El Latif, *Electrochemical and SEM study on Type 254 SMO stainless steel in chloride solutions.* Corrosion Science, 2004. **46**(10): p. 2431-2444.
34. Abd El Meguid, E.A. and A.A. Abd El Latif, *Critical pitting temperature for Type 254 SMO stainless steel in chloride solutions.* Corrosion Science, 2007. **49**(2): p. 263-275.
35. Cooper, K.P., P. Slebodnick, and E.D. Thomas, *Seawater corrosion behavior of laser surface modified Inconel 625 alloy.* Materials Science and Engineering: A, 1996. **206**(1): p. 138-149.
36. Fujii, T., K. Sue, and S.-i. Kawasaki, *Effect of pressure on corrosion of Inconel 625 in supercritical water up to 100 MPa with acids or oxygen.* The Journal of Supercritical Fluids, 2014. **95**(0): p. 285-291.
37. Patrick, E., et al., *Corrosion of tungsten microelectrodes used in neural recording applications.* Journal of Neuroscience Methods, 2011. **198**(2): p. 158-171.
38. Wang, P., et al., *Solution chemistry of Mo(III) and Mo(IV): Thermodynamic foundation for modeling localized corrosion.* Corrosion Science, 2010. **52**(5): p. 1625-1634.

39. Zhu, Y., J. Zhuang, and X. Zeng, *Mechanism of (NH4)S2O8 to enhance the anti-corrosion performance of MoCe inhibitor on X80 steel in acid solution.* Applied Surface Science, 2014. **313**(0): p. 31-40.
40. Freitas, M.B.J.G., C. Eiras, and L.O.S. Bulhões, *Breakdown of the niobium oxide film under galvanostatic polarisation and in acid solutions.* Corrosion Science, 2004. **46**(5): p. 1051-1060.
41. Asselin, E., T.M. Ahmed, and A. Alfantazi, *Corrosion of niobium in sulphuric and hydrochloric acid solutions at 75 and 95 °C.* Corrosion Science, 2007. **49**(2): p. 694-710.
42. Petrushina, I., et al., *Corrosion behavior of highly austenitic stainless steels and Ni-based alloys at elevated temperatures in concentrated phosphoric acid solutions.* International Conference on Hydrogen Material Science and Chemistry of Carbon Nanomaterials, August 25-31, 2009, Yalta, Ukraine, 2009: p. 162-163.
43. Bernstein, I.M. and D. Peckner, *Handbook of stainless steels*. 1977, New York: McGraw-Hill.
44. Covino, B.S. and S.D. Cramer, *Corrosion : fundamentals, testing and protection*. [Rev. ed.]. ed, ed. B.S. Covino, S.D. Cramer, and A.S.M.I.H. Committee. 2003, Materials Park, OH: ASM International.
45. Committee, A.S.M.I.H., *ASM Handbook, Volume 02 - Properties and Selection: Nonferrous Alloys and Special-Purpose Materials*. 1990, ASM International. p. 1118-1128.
46. Lædre, S., et al., *The effect of pH and halides on the corrosion process of stainless steel bipolar plates for proton exchange membrane fuel cells.* International Journal of Hydrogen Energy, 2012. **37**(23): p. 18537-18546.
47. Revie, R.W. and H.H. Uhlig, *Tantalum*, in *Corrosion and Corrosion Control*. 2008, John Wiley & Sons, Inc. p. 441-443.
48. Mishra, B., *Review of Extraction, Processing, Properties, and Applications of Reactive Metals : 1999 TMS Annual Meeting, San Diego, CA, February 28-March 15, 1999*. 2013, Somerset, NJ, USA: John Wiley & Sons.
49. Drazic, D.M. and J.P. Popic, *Anomalous dissolution of metals and chemical corrosion.* Journal of the Serbian Chemical Society, 2005.
50. Scully, J.R., B.A. Kehler, and G. Ilevbare, *Crevice Corrosion Stabilization and Repassivation Behavior of Alloys 625 and 22*. NACE International.
51. Olsson, J. and B. Wallen, *Experience with a high molybdenum stainless steel in saline environments.* Desalination, 1983. **44**(1–3): p. 241-254.
52. Pourbaix, M., *Atlas of electrochemical equilibria in aqueous solutions*. 1966, Oxford; New York: Pergamon Press.

5 Ta-ITO Coated Titanium Bipolar Plates for Proton Exchange Membrane Electrolyzers

Authors: Sigrid Lædre[a], Lucia Mendizabal[b] Ole Edvard Kongstein[c], Anders Oedegaard[c], Håvard Karoliussen[a] and Frode Seland[a]

a Norwegian University of Science and Technology (NTNU), Norway

b IK4-TEKNIKER, Spain

c SINTEF Materials and Chemistry, Norway

This manuscript has been prepared for publication.

5.1 Abstract

Titanium is a common Bipolar Plate BPP material for use in Polymer Electrolyte Membrane Water Electrolyzers (PEMWEs). However, the oxide formed on its surface during anodic polarization causes a relatively high electrical resistance, which has been shown to increase with time. A novel bi-layer coating composed of a tantalum base layer with a Tin doped Indium Oxide (ITO) top layer was applied to titanium substrates. Several coated plates were polarized ex situ in a parameter study, where pH, potential and temperature of the electrolyte was altered, as well as the duration of the polarization. The Interfacial Contact Resistance (ICR) for the Ta-ITO coated titanium was measured to 10 mΩ cm^2 before polarization. The ICR after polarization showed an increase with time for the first 24 hours, and then a stabilization of the ICR at approx. 30 mΩ cm^2. Minor variations were seen in the ICR after polarization at 1.4 V_{RHE} and 2.0 V_{RHE}, but after polarization at 2.5 V_{RHE} and 2.6 V_{RHE}, the ICR increased to 102 mΩ cm^2 and 503 mΩ cm^2, respectively. XPS analysis revealed that the oxygen to metal ratio on the Ta-ITO coated sample surfaces increased with increasing polarization potential. The In/Tin ratio on the surface of the Ta-ITO coated titanium tripled during polarization at 2.6 V_{RHE}. The surfaced of the samples polarized at 2.5 V_{RHE} and 2.6 V_{RHE} showed lower concentrations of oxygen vacancies, an increase in hydroxides and a decrease in metallic character compared to the non-coated and baseline samples. This study showed that ITO is a promising candidate for use as coating on BPPs in PEMWEs.

5.2 Introduction

As the world's energy consumption grows, and it becomes evident that the anthropogenic influence on the atmospheric greenhouse effect causes irreparable damages, the need for renewable energy sources becomes evident [1-3]. Hydrogen, which is one of the most abundant elements on the earth's surface, is considered one of the most promising energy carriers for the future [4-6]. There are several methods for producing hydrogen, but today it is predominantly produced by steam reforming of natural gas (methane) or gasification of coal and oil [3, 4]. These methods are cost effective, but result in the production of CO_2, impeding the transition to renewable energy sources. Water electrolysis powered by renewable energy is a more environmentally friendly method for producing hydrogen, as it does not depend on fossil fuels, nor does it result in Greenhouse gas emissions. Alkaline water electrolyzers dominate the market today [2, 4] with their relatively cheap components, long life time and low maintenance costs. Even though there are many advantages to the alkaline electrolyzer, it is associated with a low partial load range, limited current density and low operating pressures [4].

Several of the drawbacks associated with the alkaline electrolyzer were overcome when the first Proton Exchange Membrane Water Electrolyzer (PEMWE) was developed by General electric in the 1960s [7]. With a thin (20-300 μm) polymer electrolyte membrane (e.g. Nafion®, fumapem®), this electrolyzer obtains high proton conductivity, low gas crossover, compact system design and high pressure operation [4]. The PEMWE is considered an interesting alternative to the alkaline water electrolyzer [8, 9], as it can operate under higher current densities and work under a wide range of power inputs [4]. Another advantage over the alkaline electrolyzer, is the lack of liquid caustic electrolyte, making the PEMWE both safer and more reliable. The PEMWE can operate dynamically, including a load following mode [10], which make it very attractive in energy capture and storage systems where the electrical energy is obtained from e.g. wind power.

The Bipolar Plates (BPP) are essential components in a PEMWE stack [6], and their tasks are to separate single cells in a stack, distribute water and produced gases within the electrolyzer and conduct heat and current between single cells in a stack [4]. In addition to being electrically conducting, the BPP must have high corrosion resistance, be easy to manufacture, possess high shock durability and high mechanical strength [6]. These demands have limited the material selection for BPPs, and thus made it an expensive part of the PEMWE [4, 10]. Carmo et al. [4] estimated the separator plates and current collectors to be responsible for 48 % of the total stack cost. If this is the case, the cost reduction of a PEMWE stack are very

much dependent on the development of new and better BPP solutions. Compared to e.g. PEM fuel cells (PEMFC), the conditions inside a PEMWE is far more challenging for the BPP. The cell voltage and anode electrode potential in a PEMWE can under some circumstances reach 2.0 V, which restrains the material selection significantly. In commercial electrolyzers today, titanium is typically used as BPPs [4, 6]. As metals are easy to mass produce and exhibit high electrical- and thermal properties, they are good candidates for BPPs. The oxides formed on the metal surface can, however, contribute to high ohmic resistances.

With its low initial resistivity, high initial thermal conductivity, low permeability and excellent strength [4], titanium is a good candidate for BPPs in PEMWE. However, titanium is prone to degradation at the anode side of the electrolyzer, and the development of oxides on its surface causes an increase of Interfacial Contact Resistance (ICR). Coated titanium has been studied as BPP material for electrolyzers and regenerative fuel cells [4, 6, 11-16]. Lin et al. [13] investigated the corrosion behavior of titanium coated with (Ti, Zr)N, with the objective of using it as bipolar plate material in regenerative fuel cells. Zhang et al. [14] worked with a silver-containing coating for titanium, Ti-Ag, where they tested the corrosion properties, interfacial conductivity and surface energy. Zhang et al [15] coated titanium with Honeycomb-like nanocomposite Ti-Ag-N by use of a DSHP-700 arc ion plating system. X-ray diffraction (XRD), Scanning Electron Microscopy (SEM) and ICR were used to characterize the coating, and the samples were put through both potentiostatic and potentiodynamic polarizations. Other materials and coatings have also been investigated as possible BPP solutions in electrolyzers [16-19]. For example, Langemann et al. [17] and Gago et al. [18]tested coatings for stainless steel BPPs in PEMWE. Rasten et al. [19] investigated highly alloyed stainless steel as BPP material for PEM water electrolyzers. They recommended the use of austenitic steel containing 20 % nickel, 20 % chromium, 3-5 % molybdenum, 0.5-2 % copper, 30-50 % iron and maximum 9 % other elements.

Tantalum and tantalum oxides have been used for various applications in the past [20-28]. Due to tantalums biocompatibility, ductility and excellent corrosion resistance, it has been investigated for use in in-vivo applications. [23, 25, 28]. Tantalum oxide's (Ta_2O_5) high dielectric constant, high refractive index, low optical absorption coefficient and high chemical stability has made it attractive for use in memory devices, coatings for photographic lenses, electrochromic devices, switchable mirror foil film, photocatalysis [24, 27].

Indium Tin Oxide (ITO) is a tin-doped indium oxide (In_2O_3:Sn) and an n-type semiconductor which exhibits high optical transmittance in the visible region, high

electrical conductivity, surface uniformity and process compatibility [29, 30]. These properties have led to the use of ITO films as transparent electrodes in e.g. flat panels displays and solar cells, surface heaters for automobile windows, camera lenses and mirrors [30]. ITO films have been deposited by vacuum evaporation [31], spray pyrolysis [32], Chemical Vapor Deposition (CVD) [33], sol-gel process [34], Direct Current sputtering (DC) [35] and Radio Frequency (RF) [36] sputtering. These studies have shown the great importance of deposition technique and process parameters on microstructural, optical and electrical properties of ITO films [29]. For example, ITO films exhibit resistivity values ranging from $1{\cdot}10^{-4}$ Ω cm up to $1{\cdot}10^{-2}$ Ω cm [37, 38] dependent upon growing characteristics. Magnetron sputtering is considered as the state-of-the-art ITO industrial production method in terms of ITO opto-electronic properties, process control and reproducibility [39].

The pH experience by a BPP inside an operating electrolyzer is difficult to measure, but there are studies trying to determine how the pH develops over time inside a PEMWE. Langemann et al. [17] measured the pH on both anode and cathode side during operation in a PEMWE, where the BPPs had been coated with noble metals to avoid corrosion.. Over a time span of 50 hours, the pH values in the inlet water were found to decrease from 5.6 to 3.5 on the anodic side and from 5.6 to 4.7 on the cathodic side of the water electrolyzer.

In this work a novel corrosion-resistant and electrically conductive bi-layer coating made to improve the performance of titanium BPPs in PEMWE is presented. The bi-layer coating is composed of a tantalum layer (Ta) deposited by High Power Pulsed Magnetron Sputtering (HPPMS) followed by a successive deposition of thin ITO layer by pulsed dc Magnetron Sputtering (PMS). HPPMS technique is a variation of conventional dc magnetron sputtering with much higher ionization degree of sputtered particles due to the application of high peak power short pulses with low frequency and duty cycle [40]. The increased ionization obtained by HPPMS has been utilized in this study to grow well-adherent, high density and low defect Ta layer [41]. Coatings development by HPPMS on BPPs for PEMWE have not yet been reported. The deposition of a thin ITO film on top of the Ta layer is intended to block the probable growth on non-conductive tantalum oxides at the anode during high voltage PEMWE operation. In addition, ITO exhibits high electrical conductivity and good corrosion resistance making it a good coating for BPPs in PEMWE. The purpose of this work was to study Ta-ITO coated titanium under conditions similar to the ones inside an operating PEMWE, with the objective of using the coating on both BPPs and sinters in PEMWE. The high potential and harsh conditions used for these tests separate this study from previous investigations of ITO for other purposes.

5.3 Procedure and Materials

5.3.1 Coatings and Substrates

Titanium gr. 2 coupons (3.5×3.5 cm) were used as substrate materials for the Ta-ITO coating in this study. A closed field unbalanced magnetron sputtering (CFUBMS) system equipped with two rectangular magnetrons (500 x 125 mm) were used for the deposition of both tantalum and ITO. The substrates were placed in a double rotational planetary substrate holder (8 rpm) at a distance of 120 mm from the magnetrons. The bi-layer Ta-ITO coatings were deposited by successive sputtering of a metallic Ta target and a ceramic ITO (In_2O_3: SnO_2, 90:10 wt. %) target by HPPMS and PMS, respectively.

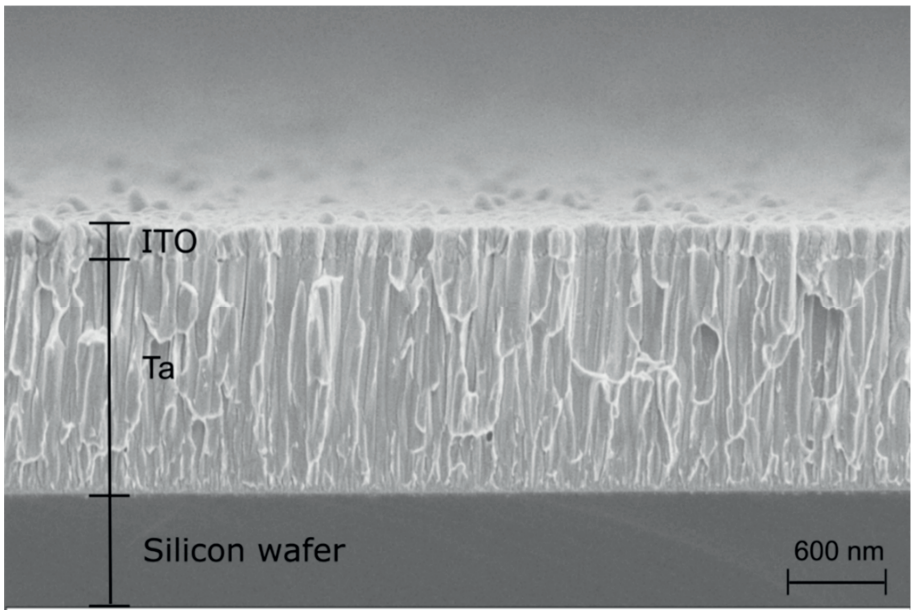

Figure 5.1: Cross section of a silicon wafer coated with Ta-ITO.

The titanium substrates were etched for 1 hour in 25 % HCl, pre-heated to 250 °C and sputter etched in an Ar+H_2 mixture for 10 minutes in the sputtering system prior to coating deposition. The etching and sputtering was done to clean the surface and remove oxides. The Ta film was grown by HPPMS in Ar atmosphere at 0.7 Pa and 4 kW average power. The HPPMS pulse shape was a 1500 µs pulse with a peak power of 80 kW, a peak current of 90 A, a peak voltage of 855 V and a repetition frequency of 120 Hz. Deposition time was set to 60 minutes and -50 V bias voltage was applied. The ITO film was reactively sputtered by PMS at 0.3 Pa and 1.5 kW average power.

Argon and oxygen flows were maintained constant at 75 and 3 Standard Cubic Centimeters per Minute (SCCM), respectively. The pulsing frequency was 75 kHz and the duty cycle 70 %. Deposition time was 10 min, and no bias was applied. The thickness of the tantalum and ITO coatings applied to the titanium substrates were 1.5 μm and 190 nm, respectively. Figure 5.1 shows a cross section image of the Ta-ITO coating on top of a silicon wafer. The silicon wafer was used for this imaging, as it is easier to cut than titanium.

5.3.2 Polarization

A Gamry ref 600 potentiostat was used to polarize the plates in a three-electrode-conventional electrochemical cell. In order to limit and control the exposed area of the working electrode sample, it was placed in a custom made sample holder exposing only a circular area on one side. A platinum wire was used as counter electrode, and a Reversible Hydrogen Electrode (RHE) was used as a reference. The electrolyte was made by a 0.1 M Na_2SO_4 solution, where the pH was adjusted by use of H_2SO_4 and NaOH. To minimize oxygen content in the electrolyte, Nitrogen gas (5.0 N_2. Aga) was bubbled into the solution both before and during most of the polarization tests. As the coating proved to be catalytic towards oxygen evolution at 2.0 V_{RHE}, nitrogen bubbling was minimized during the long term tests, to avoid loss of the electrolyte by evaporation.

Various operation parameters where altered in the ex situ polarization experiments performed in this study: Temperature, pH, electrode potential and duration of polarization. The parameters used during the polarization tests are presented in Table 5.1. The baseline parameters were chosen as they were assumed to be close to the conditions normally experienced by a BPP inside an operating electrolyzer. Most of the tests performed were at a fixed potential (potentiostatic), but potentiodynamic polarization between 0 and 2.0 V_{RHE} were also carried out. This range should cover most of the potentials experienced inside an electrolyzer. In addition to the Ta-ITO coated titanium, non-coated titanium, gold coated titanium, non-coated gold and non-coated platinum were tested at the baseline conditions. Electrochemical Impedance Spectroscopy (EIS) was performed prior to each polarization test, to obtain ohmic resistances, which were used for IR compensation.

Table 5.1: Polarization parameters used for the potentiostatic and potentiodynamic polarizations in this study

Name	Substrate	Coating	Temperature [°C]	pH	Potential [V_{RHE}]	Duration/ sweep rate
Baseline	Ti	Ta + ITO	60	5.5	2.0	3600 s
Ta-ITO sweep	Ti	Ta + ITO	60	5.5	0-2.0	1 mV s^{-1}
1.4 V	Ti	Ta + ITO	60	5.5	1.4	3600 s
2.4 V	Ti	Ta + ITO	60	5.5	2.4	3600 s
2.5 V	Ti	Ta + ITO	60	5.5	2.5	3600 s
2.6 V	Ti	Ta + ITO	60	5.5	2.6	3600 s
pH 3	Ti	Ta + ITO	60	3	2.0	3600 s
pH 8	Ti	Ta + ITO	60	8	2.0	3600 s
Room temp	Ti	Ta + ITO	20	5.5	2.0	3600 s
4 h	Ti	Ta + ITO	60	5.5	2.0	4h
12 h	Ti	Ta + ITO	60	5.5	2.0	12 h
24 h	Ti	Ta + ITO	60	5.5	2.0	24 h
72 h	Ti	Ta+ ITO	60	5.5	2.0	72 h
Non coated Ti	Ti	None	60	5.5	2.0	3600 s
Gold chrono	Au	None	60	5.5	2.0	3600 s
Gold sweep	Au	None	60	5.5	0-2.0	1 mV s^{-1}
Platinum chrono	Pt	None	60	5.5	2.0	3600 s
Platinum sweep	Pt	None	60	5.5	0-2.0	mV s^{-1}

5.4 Contact Resistance Measurements

ICR was measured before and after each test. A schematic of the ICR setup was shown by the author in Section 4.2.2 of this thesis. The resistance was measured between the test plate and a Gas Diffusion Layer (GDL). Carbon GDL is not used on the anode side in an operating electrolyzer, as it would corrode, but for these ex situ tests carbon GDLs were used to obtain comparable ICR values. The test plate and GDL were placed between two gold-coated copper plates, and a current of 2.0 A (Xantex, XDL 56-4 DC power supply) was passed through the system. The pressure between the two gold plates was controlled by applying a pneumatic pressure to the bottom plate. The voltage was measured between the top gold coated copper plate and a spring loaded gold pin in the middle of the bottom gold coated copper plate using a Fluke 76 True RMS multimeter. From this voltage, the ICR was calculated by Ohms law.

5.4.1 Surface Analysis Methods

Scanning Electron Microscopy (SEM, Hitachi S-3400N), Field Emission Gun Scanning Electron Microscopy (FEGSEM, Zeiss Ultra), Auger electron spectroscopy (AES, JEOL JAMP-9500) and X-ray Photoelectron Spectroscopy (XPS, Axis Ultra^{DLD}) was used to characterize the coated plates both before and after polarization.

5.5 Results and discussion

5.5.1 Parameter Variations

A set of test parameters were defined as baseline polarization conditions during this study (Table 5.1). Temperature, pH, cell potential and test duration were altered in order to study the effect this would have on the current and ICR. Note that only one parameter was altered at the time. Alteration of working electrode potential and duration of polarization was studied in depth, as these parameters proved to have the most impact on both polarization currents and ICR.

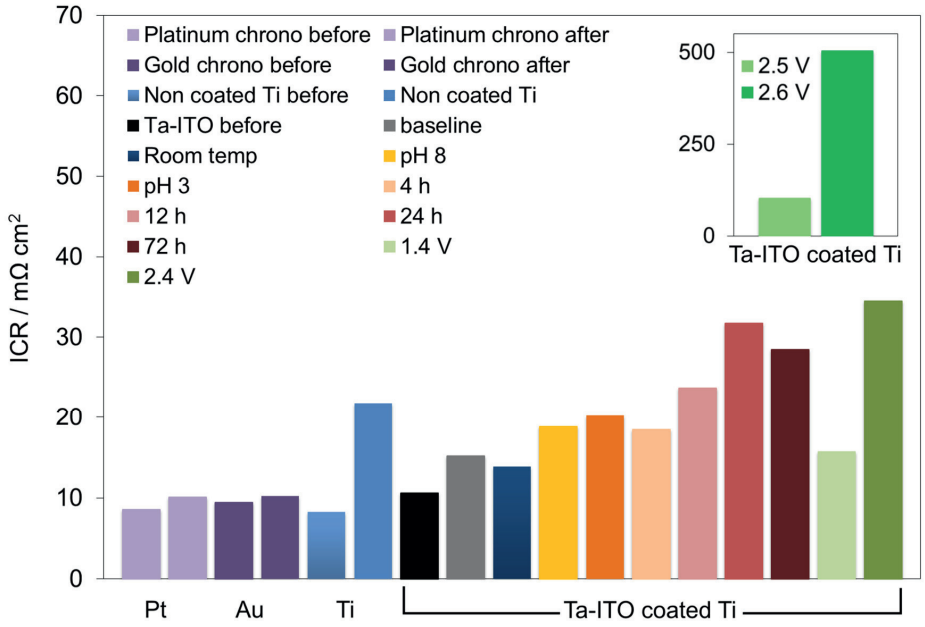

Figure 5.2: ICR values obtained from the plates used in all the potentiostatic tests in this study (Table 5.1) before and after polarization at 2.0 V_{RHE} for 1 hour. A compaction pressure of 140 Ncm^{-2} was used for all the ICR measurements, and when the material is not specified, it is Ta-ITO coated titanium.

At high potentials, the measured cell current arose from both degradation of the material and oxygen evolution. Weight loss was measured for each sample with a digital scale, but neither of the Ta-ITO coated titanium samples showed significant weight loss during polarization. It was thus assumed that most of the current produced during polarization of the Ta-ITO coated titanium samples were caused by oxygen evolution. The ICR results were therefore assumed to provide more accurate information about the alteration in the Ta-ITO coating during polarization.

The ICR values obtained at 140 N cm^{-2} after polarization of all the samples in the parameter study are displayed in Figure 5.2. The black bar in the chart shows the ICR of an unpolarized Ta-ITO coated titanium plate. Polarization of non-coated gold, platinum and titanium are also included in the figure as references.

For bipolar plates in fuel cells, the US Department of Energy (DoE) [42] has set forth targets including currents below 1 μA cm^{-2} and ICR below 10 mΩ cm^2. Even though these targets do not apply for BPPs in PEMWE, they provide an indication of the order of magnitude acceptable for current and resistance. The interfacial contact resistance measured before polarization of the Ta-ITO coated titanium plate was 10 mΩ cm^2, and after polarization at baseline conditions it was 15 mΩ cm^2. These values are both close to DoE's target for ICR. As can be seen from Figure 5.2, the highest ICR value obtained was measured on the Ta-ITO coated titanium that had been polarized at 2.6 V_{RHE} (503 mΩ cm^2). The lowest value for the Ta-ITO coated samples after polarization was obtained from the sample that had been polarized at room temperature. This was to be expected, as temperature is known to accelerate corrosion processes on the surface, resulting in alteration of the oxide layer conductivity.

As expected, both gold and platinum showed lower ICR after polarization than any of the other samples in this study. Neither of these materials are known to corrode to any significance when polarized in the anodic direction. When comparing non-coated titanium to the Ta-ITO coated titanium, it is evident that the non-coated titanium experienced a higher increase in ICR after the baseline test. This is particularly interesting considering the fact that titanium is most commonly used as BPP in PEMWE today.

Zhang et al. [15] measured ICR on Ti-Ag-N coated titanium for use in regenerative fuel cells. After polarization at 2.0 V_{SCE} in 0.5 M H_2SO_4 + 2 ppm F^-, the ICR of the Ti-Ag-N coated titanium was reported to be between 2.3 and 7.0 mΩ cm^2. Zhang et al. [14] coated titanium with Ti-Ag and found the ICR to increase from 4.1 mΩ cm^2 to 22.2 mΩ cm^2 after polarization at 2.0 V_{NHE} in 0.5 M H_2SO_4 + 5 ppm F^-. These numbers are all in the same order of magnitude as the ICR obtained from the Ta-ITO coatings.

Figure 5.3 shows pictures and SEM images of Ta-ITO coated plates both before and after polarization. The circular mark on the polarized samples were from the O-ring in the working electrode setup, and only the area inside this circle was exposed to the electrolyte. The SEM images in the middle column were obtained at a magnification of 1000x, and the images at the right were obtained at a magnification of 10 000x. The images in the same rows are from the same sample. Figure 5.3A

shows the unpolarized sample, 5.3B shows the sample that had been polarized at baseline conditions, 5.3C shows the sample that had been polarized for 24 hours and Figure 5.3D shows the sample that had been polarized at 2.6 V_{RHE}.

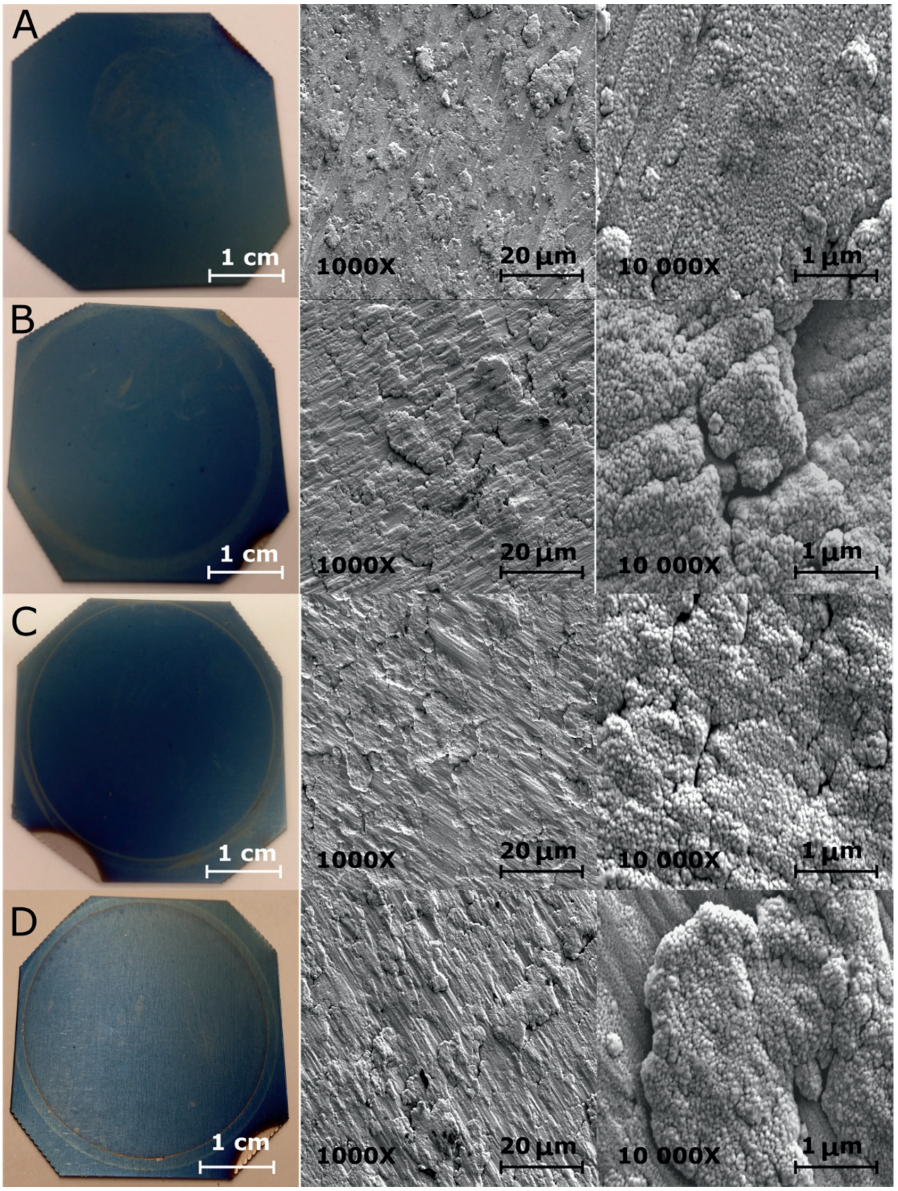

Figure 5.3: Pictures and SEM images of Ta-ITO coated Ti obtained A) Before polarization, B) After polarization at baseline conditions, C) After polarization for 24 h and D) After polarization at 2.6 V_{RHE}.

These samples were chosen as they showed great variation in ICR values obtained after polarization. From both the pictures and SEM images it is evident that the surfaces of the samples are very similar. The SEM images show a similar surface structure on all four samples. Assessment of the pictures and SEM images separately gave no indication of any corrosion or surface alterations after polarization.

Time Variations

Figures 5.4 and 5.5 show results obtained from the Ta-ITO coated titanium samples that had been polarized for various durations of time. One hur tests can be used for screening of materials and coatings, but as electrolyzers should operate for much longer periods of time, it is important to extend such tests to see how the current and ICR develop over time. Figure 5.4 shows how the current density develops over time for a series of Ta-ITO coated titanium samples. The current densities are of similar size and in general quite low, with a similar continuous and slow decline with time. As mentioned earlier, the current on most materials at 2.0 V_{RHE} in acidic aqueous electrolytes, is greatly influenced by oxygen evolution at the surface. Furthermore, none of the samples in this study showed significant weight loss during polarization, and it was thus assumed that most of the current observed originated from other surface reactions than corrosion. As mentioned, nitrogen bubbling was not used during the long term polarizations, to avoid evaporation of electrolyte. The presence of oxygen was probably higher at the beginning of the long term tests (12 h, 24 h, and 72 h).

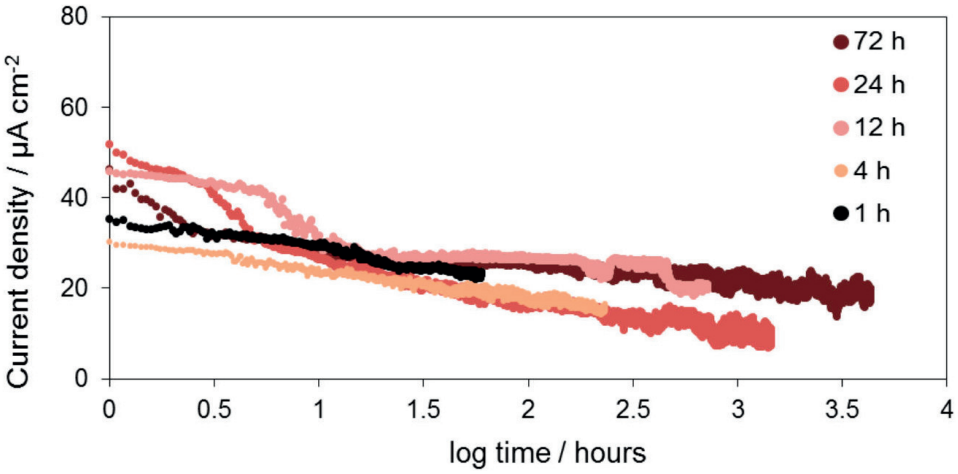

Figure 5.4: Current development over time for the Ta-ITO coated titanium when polarized potentiostatically at 2.0 V_{RHE}.

Figure 5.5 shows the development of ICR with time, and it is evident that the ICR stabilizes somewhere between 12 and 24 hours. This is interesting, as this indicates that the ICR will remain stable over time. The small decrease from 24 to 72 hours is most likely an indication of the experimental spread in such measurements. The error bars only reflect the experimental uncertainty in the ICR measuring device. It is important to note that the ICR does increase from 15 mΩ cm^2 after 1 hour to 32 mΩ cm^2 after 24 hours, but the absolute values are still small compared to the highest ICR values obtained in this study (Figure 2).

Figure 4.8 Section 4.4.5 shows how the ICR developed over time for non-coated titanium when polarized at 2.0 V_{RHE}. The ICR for non-coated titanium increased continuously with time, and was still increasing after 122 h of polarization at 2.0 V_{SHE}. This is not the same trend seen for the Ta-ITO coated samples, where the current stabilized around 24 hours. In addition, the absolute values of the ICR in Figure 4.8 are higher than the values in Figure 5. These results show a very promising trend for the Ta-ITO coating, and might be a better option than the non-coated Ti used today.

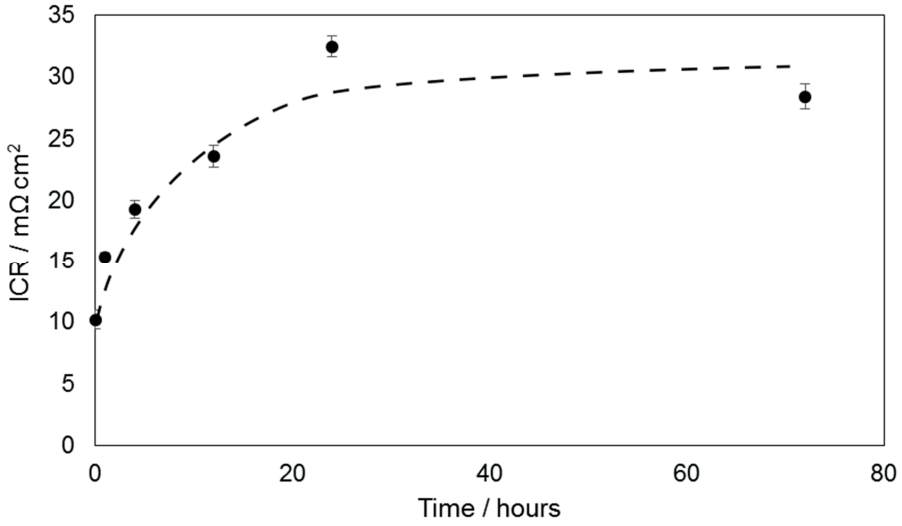

Figure 5.5: Development of ICR with time for the Ta-ITO coated titanium when polarized potentiostatically at 2.0 V_{RHE}.

Potential variations

Figure 5.6 shows the contact resistances obtained after polarization of the Ta-ITO coated titanium plates at various potentials. The Ta-ITO plates that had been polarized at 1.4 V_{RHE} and 2.0 V_{RHE} showed very similar resistances, as can be seen in both Figures. When the potential was increased to 2.4 V_{RHE}, the ICR started to increase. As displayed in Figure 5.6, the slope of the curve changes drastically after 2.4 V_{RHE}. When the potential is changed from 2.4 V_{RHE} to 2.5 V_{RHE}, the ICR value was tripled. Between 2.5 V_{RHE} and 2.6 V_{RHE} the ICR increased by a factor of 5 (Figure 5.2). It is thus evident that even higher potentials cause significant changes in the surface properties of the coated samples, leading to a much reduced electronic conductivity. This change was not evident in the pictures and images presented in Figure 5.3, where the 2.0 V_{RHE} and 2.6 V_{RHE} samples were compared.

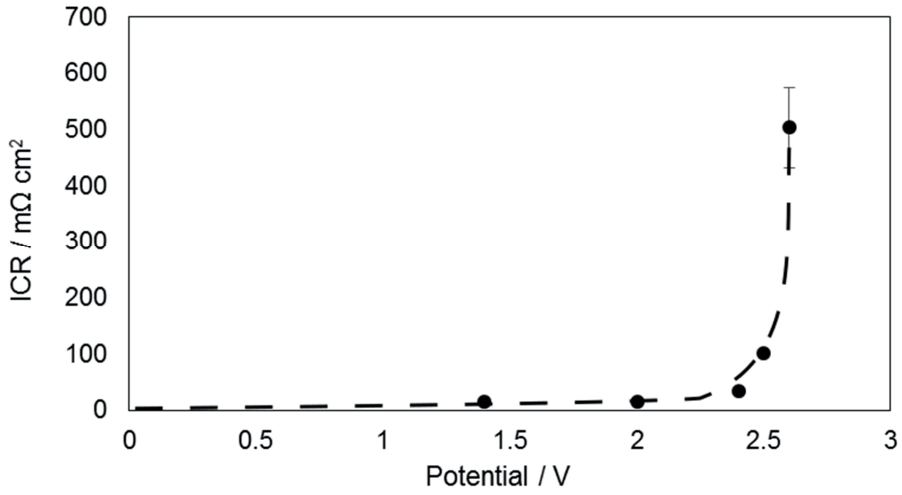

Figure 5.6: ICR values obtained from the Ta-ITO coated titanium plates after polarization at different potentials. All the ICR values were obtained at a compaction pressure of 140 N cm^{-2}.

5.5.2 Potentiodynamic Polarization

In addition to the potentiostatic polarizations in this study, potetiodynamic polarization curves were obtained for gold, platinum and Ta-ITO coated titanium. The results from the polarization are presented in Figure 5.7, while the ICR obtained before and after each sweep is presented in Table 5.2. The currents produced during the polarizations of all three materials, were most likely caused by oxygen evolution. The onset of current increase is a bit different for the three materials, but for all of them the current increases drastically after 1.7 V. As no significant weight loss was observed for the Ta-ITO coated sample, it was assumed that it did not corrode significantly. The observed small difference between the three linear sweeps could be attributed to the variations of the electrochemical nature for oxygen evolution at the surface of the three materials. The ICR did not change during polarization for gold or platinum, and the change for the Ta-ITO coated titanium was similar to the ICR obtained after the potentiostatic polarization.

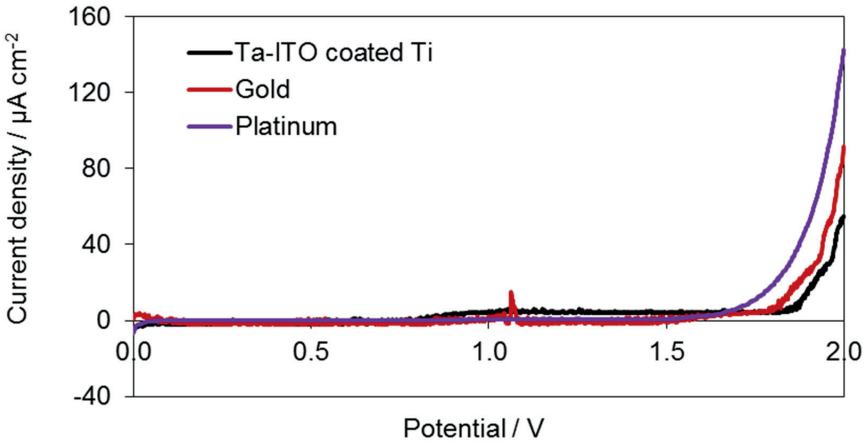

Figure 5.7: Potentiodynamic polarization curves for gold, platinum and Ta-ITO coated Ti at baseline conditions.

Table 5.2: ICR values at 140 N cm^{-2} obtained from platinum, gold and Ta-ITO before and after potentiostatic polarization at 2 V_{RHE}.

Material	ICR at 140 N cm^{-2} [mΩ cm^2]	
	Before Polarization	After Polarization
Platinum	9	9
Gold	10	10
Ta-ITO coated titanium	10	16

5.5.3 AES and XPS Characterization

Auger electron spectroscopy was used in order to understand why such a substantial increase in ICR was observed for the samples that had been polarized at 2.5 V_{RHE} and 2.6 V_{RHE} for one hour. AES provided relative amounts of each component (tantalum, indium, oxygen and tin) as a function of depth in four different Ta-ITO coated titanium samples. The 2.5 V_{RHE} plate and the 2.6 V_{RHE} plate were chosen as they showed the highest ICR values after polarization of all the tested plates, with 102 mΩ cm^2 and 503 mΩ cm^2, respectively. An unpolarized plate and the baseline sample were also analyzed by AES, as they had shown relatively low ICR values compared to the two other samples.

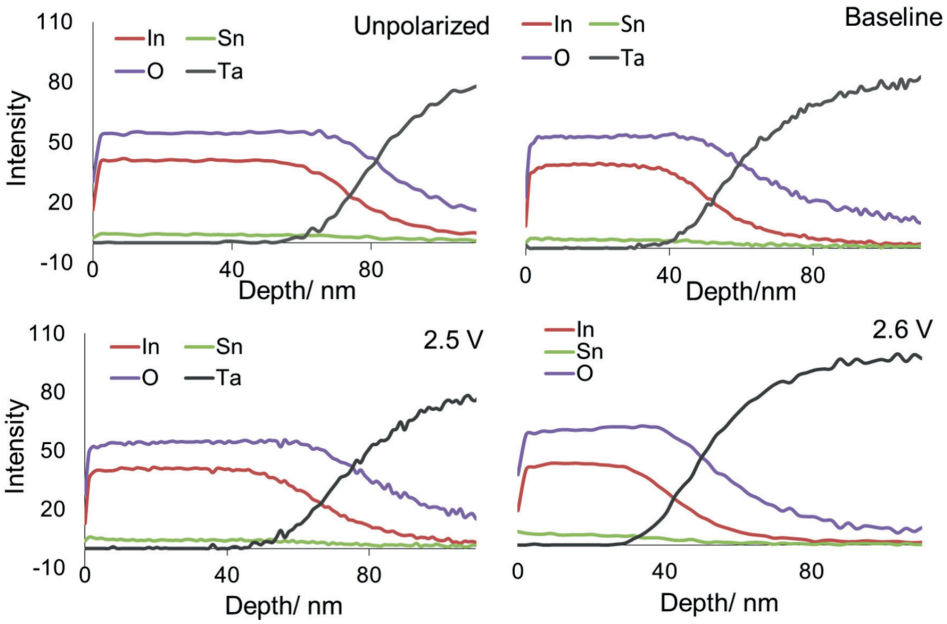

Figure 5.8: AES analysis performed on four Ta-ITO plates, one unpolarized and three polarized as described in table 5.1.

The results are presented in Figure 5.8, where the oxide thickness can be estimated based on the oxygen intensity with depth. From this, it looks like the unpolarized sample and the 2.5 V_{RHE} sample had a thicker oxide than the other two, and that the 2.6 V_{RHE} sample obtained the thinnest oxide layer. In addition, no significant change in composition was observed for either of the samples. Based on the ICR measurements, these findings were surprising as one would assume that the oxide layer on the sample surfaces possessed the same properties with respect to conductivity, and that a thicker oxide would be expected to result in a higher rather

than lower ICR. There is not a clear trend when the AES and ICR results are compared for the four samples below, and it became evident that further analysis was necessary to understand the increase in ICR for the 2.5 V_{RHE} and 2.6 V_{RHE} samples.

As the AES analysis was inconclusive, XPS was performed on the same four samples. The results are shown in Table 5.3 and Figure 5.9. Table 5.3 shows the composition of the coatings and the relationship between indium and tin. The ratio between oxygen content and (indium + tin) in the 2.5 V_{RHE} and 2.6 V_{RHE} samples are higher than for the unpolarized and baseline samples. This means that there is more oxygen compared to metal in the top most part of the samples polarized at higher voltages, which could explain the higher ICR values obtained from the 2.5 V_{RHE} and 2.6 V_{RHE} samples. The XPS analysis also showed a decrease in the indium/tin ratio from top to bottom in the table. The unpolarized sample has 8.9 times more indium than tin, the baseline sample has 6.15, the 2.5 V_{RHE} sample has 3.83 and the 2.6 V_{RHE} sample has only 2.69 times more indium than tin.

Table 5.3 Composition of oxygen, carbon, indium and tin in the samples analyzed by XPS. The oxygen/metal ratio and indium/tin ratio is also included.

Sample	Core level	Composition (atom %)	O/(In+Sn) ratio	In/Sn ratio
Unpolarized	In 3d	25.0	1.42	8.88
	O 1s	39.6		
	C 1s	32.9		
	Sn 3d	2.8		
Baseline	In 3d	14.6	1.82	6.15
	O 1s	31.0		
	C 1s	52.0		
	Sn 3d	2.5		
2.5 V	In 3d	13.1	1.93	3.83
	O 1s	31.9		
	C 1s	51.6		
	Sn 3d	3.4		
2.6 V	In 3d	10.6	2.10	2.69
	O 1s	30.5		
	C 1s	55.0		
	Sn 3d	3.9		

The trend in the In/Sn ratio is opposite of the ICR values in Table 5.2, indicating that a low indium/tin ration correlated with a high ICR value. The reason for the ratio decrease in the 2.5 V_{RHE} and 2.6 V_{RHE} samples is due to an enrichment of Sn and a removal of In from surface of the samples. Indium could dissolve into the electrolyte due to selective dissolution from e.g. selective corrosion, and this would also explain in part why the AES measurements showed a decrease in ITO thickness. Thirumoorthi and Prakash [43] found the resistivity of ITO to decrease with increasing Sn weight percent, from 0.9 mohm cm with 0 wt % Sn to 0.4 mohm cm at 30 wt % Sn. However, this is a minor decrease compared to the increase in ICR found in this study, and other effects are thus assumed to be responsible for the observed increase in the ICR values for the 2.5 V_{RHE} and 2.6 V_{RHE} samples.

Figure 5.9 shows the XPS spectrums of oxygen (O 1s), indium (In $3d_{5/2}$) and tin (Sn $3d_{5/2}$) obtained from the unpolarized, baseline, 2.5 V_{RHE} and 2.6 V_{RHE} samples. The peaks are each related to the binding energy between the various elements on the surface of the samples. Three peaks were observed for oxygen in in this analysis (Figure 5.9A). O1 and O3 are present in all four samples, and they both increase in height from bottom to top in Figure 5.9 A. The O1 peak is associated with the oxygen found in the ITO layer as it was deposited on the titanium surface [44]. The O3 peak is associated with hydroxides, indicating that the amount of hydroxides on the surface of the samples increase from bottom to top [44-46]. The O2 peak is only present in the unpolarized and baseline samples. This peak is associated with oxygen in a configuration where it is adjacent to oxygen vacancies in the structure [47]. This indicates that the number of oxygen vacancies on the surfaces of the 2.5 V_{RHE} and 2.6 V_{RHE} samples were lower than the other two samples. Oxygen vacancies are known for increasing the electrical conductivity of a material [30], and the high ICR obtained from the 2.5 V_{RHE} and 2.6 V_{RHE} could thus be partially caused by the lower number of oxygen vacancies.

Two peaks can be seen for indium in the spectrums shown in Figure 5.9 B. In1 is found in the spectras obtained from all four samples, but In2 is only found in the spectras from the unpolarized and baseline samples. In 1 is associated with In^{3+} in In_2O_3 like species [47]. The In1 peak loosed its asymmetry from bottom to top in Figure 5.9B, which indicates that the metallic character of indium is weakened from bottom to top. Smaller degrees of asymmetry could result in lower conductivity [48, 49], which can explain the higher ICR observed for the 2.5 V_{RHE} and 2.6 V_{RHE} samples. The In2 peak is associated with indium in e.g. In-OH and In-OOH species [44, 47], which coincides well with the O2 peak.

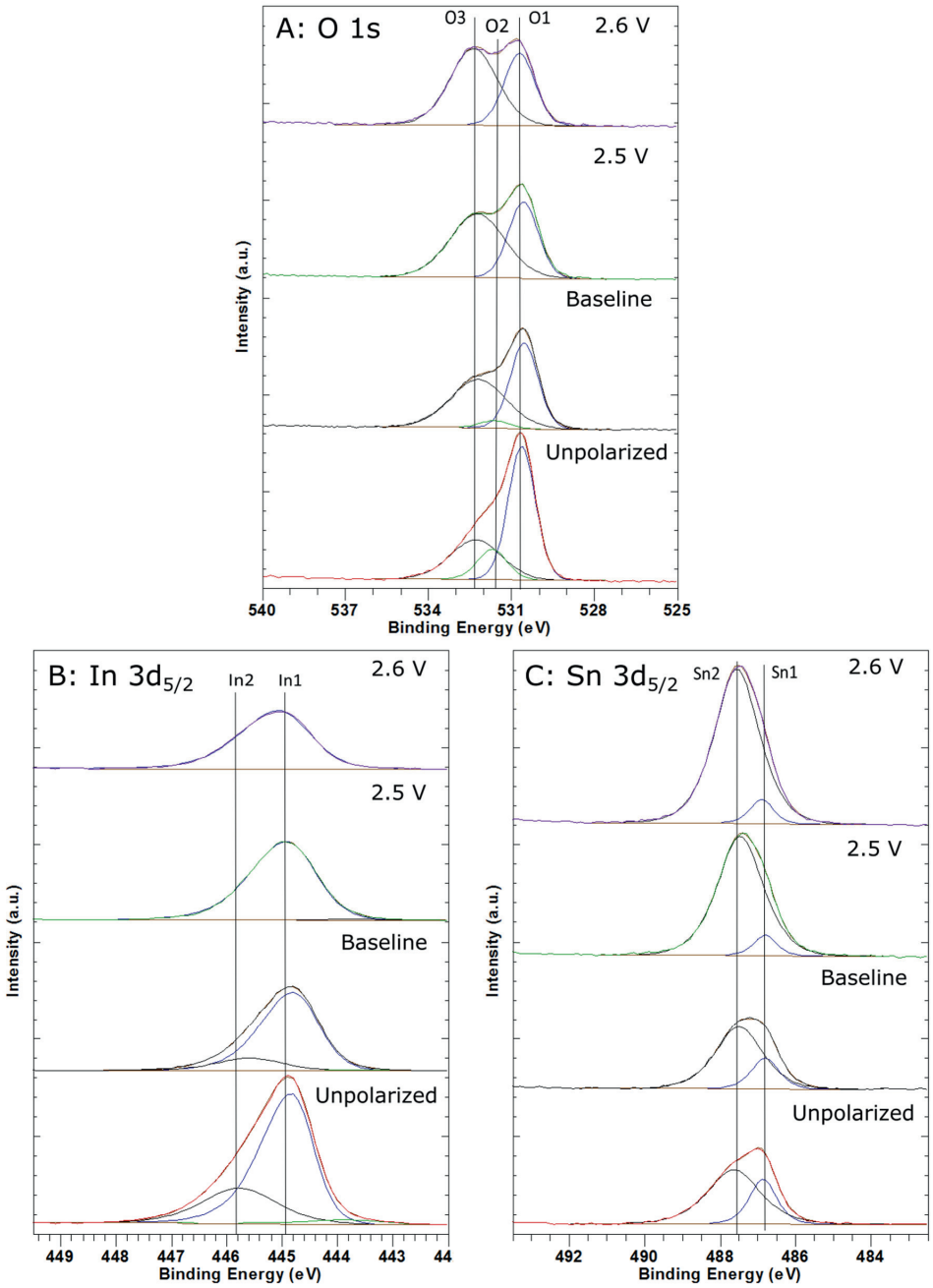

Figure 5.9: XPS spectrums obtained from four of the samples in this study (table 5.1) showing binding energies of oxygen, indium and tin.

The spectrums obtained showed two tin peaks (Figure 5.9C), Sn1 and Sn2. The first one is associated with Sn in SnO_2 like species [46, 47]. The Sn2 peak can be associated with different compounds, but in this case it correspond well with the with the O3 peak, indicating that it is from a tin hydroxide.

When looking at all the XPS spectrums combined, it is clear that there was an increase in hydroxides on the surface of samples compared to the other two, which increases with polarization potential. In addition, there is a decrease in oxygen adjacent to oxygen vacancies for the same two samples, as well as a decrease in metallic character for indium. All of these factors explain why the ICR for the samples were so high compared to all the other Ta-ITO coated titanium samples in this study.

5.6 Conclusions

The Ta-ITO bi-layer coating was successfully applied to the titanium surface by use of DC magnetron sputtering. The coating was polarized under various conditions, resulting in very low corrosion currents. As the weight loss measured for all the samples were lower than the error of the measurements, it was assumed that the current produced during polarization was caused by oxygen evolution. Pictures and SEM images obtained before and after polarization showed no changes on the coated surfaces, even after polarization at 2.6 V_{RHE}. Alteration of pH and temperature proved to have little or no effect on the interfacial contact resistance. Potentials above 2.0 V_{RHE} and polarization longer than 1 h resulted in higher ICR value. The Ta-ITO coated titanium plate that had been polarized at 2.6 V_{RHE} showed an ICR value of 503 mΩ cm^2 compared to 15 for the sample polarized at 2.0 V_{RHE}.

XPS analysis showed that there was an increase in hydroxides on the surface of the 2.5 V_{RHE} and 2.6 V_{RHE} samples compared to the unpolarized and baseline samples, and that the increase was related to higher polarization potentials. For the same two samples, there was a decrease in oxygen vacancies and a decrease in metallic character for indium. The oxygen to metal ratio on the Ta-ITO coated samples surfaces were found to increase on the 2.5 V_{RHE} and 2.6 V_{RHE}, and the indium to tin relationship was found to decrease. The latter was probably caused by selective dissolution of indium. Combined, all of these factors could explain why the ICR values for the 2.5 V_{RHE} and 2.6 V_{RHE} were so much higher than for all the other samples in this study. However, polarization at such high potentials are not realistic for BPPs in PEMWE. When the Ta-ITO coated titanium plates were polarized at 2.0 V_{RHE} for more than one day, the ICR leveled out at about 30 mΩ cm^2. This means that Ta-ITO films are very promising as BPP material in the harsh PEMWE environment.

5.7 Acknowledgements

Norwegian University of Science and Technology is greatly acknowledged for the award of scholarship. The work was also funded by SINTEF materials and chemistry through the COATELY project. Thank you John Walmsley and Ingeborg-Helene Svenum for helping out with the AES and XPS analysis.

5.8 Literature

1. Winter, C.-J., *Hydrogen energy — Abundant, efficient, clean: A debate over the energy-system-of-change.* International Journal of Hydrogen Energy, 2009. **34**(14, Supplement 1): p. S1-S52.
2. Ursua, A., L.M. Gandia, and P. Sanchis, *Hydrogen Production From Water Electrolysis: Current Status and Future Trends.* Proceedings of the IEEE, 2012. **100**(2): p. 410-426.
3. Millet, P., et al., *Cell failure mechanisms in PEM water electrolyzers.* International Journal of Hydrogen Energy, 2012. **37**(22): p. 17478-17487.
4. Carmo, M., et al., *A comprehensive review on PEM water electrolysis.* International Journal of Hydrogen Energy, 2013. **38**(12): p. 4901-4934.
5. Barbir, F., *PEM electrolysis for production of hydrogen from renewable energy sources.* Solar Energy, 2005. **78**(5): p. 661-669.
6. Wang, J.-T., et al., *Corrosion behavior of three bipolar plate materials in simulated SPE water electrolysis environment.* International Journal of Hydrogen Energy, 2012. **37**(17): p. 12069-12073.
7. Russell, J., L. Nuttall, and A. Fickett, *Hydrogen generation by solid polymer electrolyte water electrolysis.* American Chemical Society Division of Fuel Chemistry Preprints, 1973. **18**(3): p. 24e40.
8. Millet, P., F. Andolfatto, and R. Durand, *Design and performance of a solid polymer electrolyte water electrolyzer.* International Journal of Hydrogen Energy, 1996. **21**(2): p. 87-93.
9. Grigoriev, S.A., et al., *Optimization of porous current collectors for PEM water electrolysers.* International Journal of Hydrogen Energy, 2009. **34**(11): p. 4968-4973.
10. Ayers, K.E., et al., *Research Advances towards Low Cost, High Efficiency PEM Electrolysis.* ECS Transactions, 2010. **33**(1): p. 3-15.
11. Jung, H.-Y., et al., *Performance of gold-coated titanium bipolar plates in unitized regenerative fuel cell operation.* Journal of Power Sources, 2009. **194**(2): p. 972-975.
12. Jung, H.-Y., S.-Y. Huang, and B.N. Popov, *High-durability titanium bipolar plate modified by electrochemical deposition of platinum for unitized regenerative fuel cell (URFC).* Journal of Power Sources. **195**(7): p. 1950-1956.
13. Lin, M.-T., C.-H. Wan, and W. Wu, *Comparison of corrosion behaviors between SS304 and Ti substrate coated with (Ti,Zr)N thin films as Metal bipolar plate for unitized regenerative fuel cell.* Thin Solid Films, 2013. **544**(0): p. 162-169.
14. Zhang, H., et al., *Performance of Ti–Ag-deposited titanium bipolar plates in simulated unitized regenerative fuel cell (URFC) environment.* International Journal of Hydrogen Energy, 2011. **36**(9): p. 5695-5701.
15. Zhang, M., et al., *Honeycomb-like nanocomposite Ti-Ag-N films prepared by pulsed bias arc ion plating on titanium as bipolar plates for unitized regenerative fuel cells.* Journal of Power Sources, 2012. **198**(0): p. 196-202.
16. Nikiforov, A.V., et al., *Corrosion behaviour of construction materials for high temperature steam electrolysers.* International Journal of Hydrogen Energy, 2011. **36**(1): p. 111-119.
17. Langemann, M., et al., *Validation and characterization of suitable materials for bipolar plates in PEM water electrolysis.* International Journal of Hydrogen Energy, (0).
18. Gago, A.S., et al., *Protective coatings on stainless steel bipolar plates for proton exchange membrane (PEM) electrolysers.* Journal of Power Sources, 2016. **307**: p. 815-825.
19. Rasten, E., et al., *Use of Austenitic Stainless Steel as Construction Material in a Device or Structural Component Which is Exposed to an Oxygen and/or Hydrogen*

and/or Hydrofluoric Acid Environment, in *Patent application*. 2010. p. Patent application number: 20100133096.
20. Cacucci, A., et al., *Interdependence of structural and electrical properties in tantalum/tantalum oxide multilayers.* Surface and Coatings Technology, 2013. **227**: p. 38-41.
21. Jagadeesh Chandra, S.V., et al., *Structural and electrical properties of radio frequency magnetron sputtered tantalum oxide films: Influence of post-deposition annealing.* Materials Science in Semiconductor Processing, 2010. **13**(4): p. 245-251.
22. Chang, Y.-Y., et al., *Antibacterial properties and cytocompatibility of tantalum oxide coatings.* Surface and Coatings Technology, 2014. **259, Part B**: p. 193-198.
23. Frandsen, C.J., et al., *Tantalum coating on TiO2 nanotubes induces superior rate of matrix mineralization and osteofunctionality in human osteoblasts.* Materials Science and Engineering: C, 2014. **37**: p. 332-341.
24. Kumar, K.J., N.R.C. Raju, and A. Subrahmanyam, *Properties of pulsed reactive DC magnetron sputtered tantalum oxide (Ta2O5) thin films for photocatalysis.* Surface and Coatings Technology, 2011. **205, Supplement 2**: p. S261-S264.
25. Meng, F., Z. Li, and X. Liu, *Synthesis of tantalum thin films on titanium by plasma immersion ion implantation and deposition.* Surface and Coatings Technology, 2013. **229**: p. 205-209.
26. Rahmati, B., et al., *Development of tantalum oxide (Ta-O) thin film coating on biomedical Ti-6Al-4V alloy to enhance mechanical properties and biocompatibility.* Ceramics International, 2016. **42**(1, Part A): p. 466-480.
27. Tajima, K., et al., *Electrochemical evaluation of Ta2O5 thin film for all-solid-state switchable mirror glass.* Solid State Ionics, 2009. **180**(6–8): p. 654-658.
28. Black, J., *Biologic performance of tantalum.* Clinical Materials, 1994. **16**(3): p. 167-173.
29. Lien, S.-Y., *Characterization and optimization of ITO thin films for application in heterojunction silicon solar cells.* Thin Solid Films, 2010. **518**(21, Supplement): p. S10-S13.
30. Kim, H., et al., *Electrical, optical, and structural properties of indium–tin–oxide thin films for organic light-emitting devices.* Journal of Applied Physics, 1999. **86**(11): p. 6451-6461.
31. Liu, X.D., E.Y. Jiang, and D.X. Zhang, *Electrical transport properties in indium tin oxide films prepared by electron-beam evaporation.* Journal of Applied Physics, 2008. **104**(7): p. 073711.
32. Korotcenkov, G., et al., *The influence of film structure on In2O3 gas response.* Thin Solid Films, 2004. **460**(1–2): p. 315-323.
33. Maruyama, T. and K. Fukui, *Indium tin oxide thin films prepared by chemical vapour deposition.* Thin Solid Films, 1991. **203**(2): p. 297-302.
34. Daoudi, K., et al., *Densification of In2O3:Sn multilayered films elaborated by the dip-coating sol–gel route.* Thin Solid Films, 2003. **445**(1): p. 20-25.
35. Cho, S.H., et al., *Effects of O2 addition on microstructure and electrical property for ITO films deposited with several kinds of ITO targets.* Journal of Physics and Chemistry of Solids, 2008. **69**(5–6): p. 1334-1337.
36. Kerkache, L., et al., *Physical properties of RF sputtered ITO thin films and annealing effect.* Journal of Physics D: Applied Physics, 2006. **39**(1): p. 184.
37. Juhn-Jong, L. and L. Zhi-Qing, *Electronic conduction properties of indium tin oxide: single-particle and many-body transport.* Journal of Physics: Condensed Matter, 2014. **26**(34): p. 343201.
38. Bierwagen, O., *Indium oxide—a transparent, wide-band gap semiconductor for (opto)electronic applications.* Semiconductor Science and Technology, 2015. **30**(2): p. 024001.

39. Nadel, S.J., et al., *Equipment, materials and processes: a review of high rate sputtering technology for glass coating.* Thin Solid Films, 2003. **442**(1–2): p. 11-14.
40. Sarakinos, K., J. Alami, and S. Konstantinidis, *High power pulsed magnetron sputtering: A review on scientific and engineering state of the art.* Surface and Coatings Technology, 2010. **204**(11): p. 1661-1684.
41. Lin, J., et al., *Effect of Negative Substrate Bias on the Structure and Properties of Ta Coatings Deposited Using Modulated Pulse Power Magnetron Sputtering.* IEEE Transactions on Plasma Science, 2010. **38**(11): p. 3071-3078.
42. *U.S. Department of Energy, Fuel Cell Technologies Office Multi-Year Research, Development, and Demonstration Plan*. 2012. p. 29.
43. Thirumoorthi, M. and J. Thomas Joseph Prakash, *Structure, optical and electrical properties of indium tin oxide ultra thin films prepared by jet nebulizer spray pyrolysis technique.* Journal of Asian Ceramic Societies, 2016. **4**(1): p. 124-132.
44. Nunes de Carvalho, C., et al., *Effect of substrate temperature on the surface structure, composition and morphology of indium–tin oxide films.* Surface and Coatings Technology, 2000. **124**(1): p. 70-75.
45. Zhu, J., et al., *Nanocrystalline anatase TiO2 photocatalysts prepared via a facile low temperature nonhydrolytic sol–gel reaction of TiCl4 and benzyl alcohol.* Applied Catalysis B: Environmental, 2007. **76**(1–2): p. 82-91.
46. Montilla, F., et al., *Preparation and Characterization of Antimony-Doped Tin Dioxide Electrodes. 3. XPS and SIMS Characterization.* The Journal of Physical Chemistry B, 2004. **108**(41): p. 15976-15981.
47. Thøgersen, A., et al., *Elemental distribution and oxygen deficiency of magnetron sputtered indium tin oxide films.* Journal of Applied Physics, 2011. **109**(11): p. 113532.
48. Gassenbauer, Y. and A. Klein, *Electronic and Chemical Properties of Tin-Doped Indium Oxide (ITO) Surfaces and ITO/ZnPc Interfaces Studied In-situ by Photoelectron Spectroscopy.* The Journal of Physical Chemistry B, 2006. **110**(10): p. 4793-4801.
49. Gassenbauer, Y., A. Wachau, and A. Klein, *Chemical and electronic properties of the ITO/Al2O3 interface.* Physical Chemistry Chemical Physics, 2009. **11**(17): p. 3049-3054.

6 Overall Conclusions

The main objectives in this work have been to develop techniques to study the ICR development and corrosion resistance of bipolar plate materials and coatings for PEM systems under various operating conditions, both in situ and ex situ. A more in-depth understanding allows for the development of cost efficient and durable bipolar plate materials for PEM systems.

In most existing literature, evaluation of BPP materials is performed by ex situ polarization in a conventional three electrode glass cell in a low pH aqueous electrolyte. Highly acidic environments are usually chosen in order to accelerate the degradation of materials and reduce test duration. pH in the water from an operating PEMFC was measured to be below 3.75, which corresponded well with previous literature. Results presented in this work, showed that altering the electrolyte pH from 3.7 to 0.5 resulted in a decrease in ICR values as a result of a reduction in the passivating and less conductive oxide layer thickness exposing bare metal. Auger Electron Spectroscopy analysis confirmed this relationship. Long term (ex situ) testing at a pH of 3.71 did not affect the ICR, as it seemed to stabilize in less than an hour. This indicated that accelerated testing should not be done by decreasing the pH as far as 0.51. Addition of Cl^- and F^- in the amounts expected in an operating PEMFC did not result in an increase in currents or ICR, but when the Cl^- amount was increased from 10 to 100 ppm, the stainless steel plates (AISI 316L) showed clear signs of pitting.

Investigating bipolar plate materials at near operating conditions are challenging and thus this thesis work has also focused on method development for both ex situ and in situ characterization. All the ex situ tests in this work have been designed and improved continuously in order to establish reliable and reproducible testing conditions for both polarization and ICR measurements. However, the most extensive method development was the one for in situ ICR measurements. The principle of this method is simple, relying on thin gold wires welded and placed strategically between the BPP and GDL for accurate ICR measurements during fuel cell operation. The average ICR obtained from three measuring points on the BPP surface proved to be more accurate than just one, as this value correlated well with the ex situ measurements obtained after polarization. Ex situ ICR measurements performed on smaller areas of the plates, with a point measuring setup, showed that the variation between the three in situ measuring points were probably caused by uneven current distribution in the cell. The in situ ICR was measured to be 5 $m\Omega\ cm^2$

for the gold coated AISI 316L BPP, and the corresponding ICR measured ex situ after operation was 7 mΩ cm^2. A non-coated AISI 316L BPP that had been operated at OCV 50 % of the time showed the highest ICR values in both ex situ and in situ measurements at approx. 30 mΩ cm^2 and 35 mΩ cm^2, respectively. The method presented here is more than good enough for evaluating whether new coatings are promising enough for further research.

The earlier work in this PhD focused on BPPs for PEMFCs, and the work performed in the second part was focused on BPPs for PEMWE. As there were few studies on BPPs for PEMWE, and a lack of studies comparing several substrate materials for BPPs, a material study was performed. Out of the nine materials tested, tantalum, niobium and titanium produced the lowest current densities when polarized both potentiostatically at 2.0 V_{SHE} and potentiodynamically from 0-2.0 V_{SHE}. As expected, both niobium and tantalum showed substantial increases in ICR after one hour polarization at 2.0 V_{SHE}. For titanium, the ICR kept increasing with time up to 122 hours.

By comparing weight loss measurements with the measured currents produced by AISI 316L and AISI 304L during polarization, it was found that only approx. 20 % of the current was related to corrosion. This was less than for any of the other materials. When polarizing materials at 2.0 V_{SHE}, oxygen evolution is unavoidable. However, the catalytic properties of each material towards oxygen evolution will differ. Even though some of the results from this study may be expected, there appears to be a lack of literature describing polarization up to 2.0 V_{SHE} for several of the materials tested in this study. Several of the materials investigated in this study could potentially be used as BPP materials, but in order to obtain a low enough ICR, coating is necessary.

A bi-layer coating consisting of tantalum and ITO was successfully applied to titanium substrates by DC magnetron sputtering with the objective of polarizing it under conditions similar to the conditions inside a PEM electrolyzer. Altering the pH and temperature of the electrolyte showed little or no effect on the ICR after polarization. ICR values obtained from Ta-ITO coated titanium polarized potentiostatically at potentials between 1.4 V_{RHE} and 2.0 V_{RHE} were very similar. However, after polarization at even higher potentials, an increase in ICR values was observed. The Ta-ITO coated titanium plate that had been polarized at 2.6 V_{RHE} showed an ICR value of 503 compared to 15 for the sample polarized at 2.0 V_{RHE}. The duration of polarization did affect the ICR, and an increase in ICR was observed for the first 24 hours. After 24 hours the ICR stabilized, and the ICR values obtained for the plates that had been polarized at 2.0 V_{RHE} for 24 hours and 72 hours showed very

similar ICR values. This shows that the bi-layer Ta-ITO coating is very promising as BPP material in the harsh PEMWE environment.

From XPS analysis it was found that the surface of the samples that had been polarized at 2.5 V_{RHE} and 2.6 V_{RHE} contained higher amounts of hydroxides than the unpolarized and baseline samples. A decrease in oxygen vacancies and a decrease in the metallic character of Sn were also found on the surface of the 2.5 V_{RHE} and 2.6 V_{RHE} samples when compared to the unpolarized and baseline samples. The oxygen to metal ratio on the Ta-ITO coated samples surfaces were found to increase on the 2.5 V_{RHE} and 2.6 V_{RHE}, whereas the indium to tin relationship was found to decrease. The latter could have been caused by selective dissolution of indium. All of these factors combined could explain why the ICR values for the 2.5 V_{RHE} and 2.6 V_{RHE} were so much higher than for all the other samples in this study.

All of the objectives presented in the introduction have been proceeded, and it is believed that the work described in this thesis is of interest to the relevant field. Some of the results have been published, and some have been prepared for publication.

7 Further work

The ex situ methods developed during both of the studies involving BPPs for PEMFCs were also used during the work on BPPs for PEMWEs described in this thesis. The use of the polarization- and ICR setup is versatile, and can be used for studies of materials and coatings for PEMFC, PEMWE and other applications. They will be used in the COATELY project, and they will probably be used in other future SINTEF projects as well.

The ex situ ICR setup works very well, and will probably not be altered. The potentiostatic setup has already been altered several times throughout this PhD, to obtain reliable conditions and as few experimental errors as possible. A smaller test cell could be used, and it would be a good idea to mount all the electrodes in a permanent setup where they are in the exact same distance from one another in all polarization tests. This would probably involve the construction of a new electrochemical cell, and was not done in this PhD work, as it would be too time consuming.

The in situ method for ICR measurements should be used for testing of ICR in future projects. Even though the method was developed for measuring ICR between the BPP and the GDL in a PEMFC, the method is easily transferrable to testing of ICR between all components in both PEMFCs and PEMWEs. Several projects on both PEMFCs and PEMWEs are currently running at both SINTEF and NTNU, and the method could be a good way of testing materials for such systems.

The next step for the Ta-ITO coating is to test it in situ in an operating PEMWE. This work has already been initiated, and SINTEF will continue with further in situ testing in the COATELY project. Preliminary ex situ investigations have shown that even thinner tantalum layers might provide lower ICR values, and this should also be further investigated.

As tantalum is rare and relatively expensive, titanium might be used as the adhesive layer under the ITO.

Another way of cutting the cost, is to use AISI 316L as substrate instead of titanium. However, this material corrodes when polarized at 2.0 V, and the surface coverage of the applied coating would have to be 100 %. This is difficult to achieve, and in addition, small scratches from handling the plates will be detrimental. One idea is to use a multilayer coating, consisting of several very thin coatings. It is believed that

such a coating would provide better surface coverage. Partners in the COATELY project have already started with this next step, and it will continue.

Appendices

Appendix A: Scientific papers

Paper 1:

Lædre S, Kongstein OE, Oedegaard A, Seland F, Karoliussen H. *The effect of pH and halides on the corrosion process of stainless steel bipolar plates for proton exchange membrane fuel cells.* International Journal of Hydrogen Energy. 2012;37:18537-46.

Paper 2:

Ladre S, Kongstein OE, Oedegaard A, Seland F, Karoliussen H. *In Situ and Ex Situ Contact Resistance Measurements of Stainless Steel Bipolar Plates for PEM Fuel Cells.* ECS Transactions. 2013;50:829-39.

INTERNATIONAL JOURNAL OF HYDROGEN ENERGY 37 (2012) 18537–18546

Available online at www.sciencedirect.com

SciVerse ScienceDirect

journal homepage: www.elsevier.com/locate/he

The effect of pH and halides on the corrosion process of stainless steel bipolar plates for proton exchange membrane fuel cells

Sigrid Lædre [a,c,*], *Ole Edvard Kongstein* [b], *Anders Oedegaard* [b], *Frode Seland* [c], *Håvard Karoliussen* [a]

[a] *Department of Chemical Engineering and Materials Technology, Sør-Trøndelag University College, 7004 Trondheim, Norway*
[b] *SINTEF Materials and Chemistry, 7465 Trondheim, Norway*
[c] *Department of Materials Science and Engineering, Norwegian University of Science and Technology, 7491 Trondheim, Norway*

ARTICLE INFO

Article history:
Received 18 May 2012
Received in revised form
31 August 2012
Accepted 4 September 2012
Available online 6 October 2012

Keywords:
PEM fuel cell
Stainless steel bipolar plate
Contact resistance
Corrosion
Halides
pH

ABSTRACT

Stainless steel is attractive as material for bipolar plates in proton exchange membrane fuel cells, due to its high electrical conductivity, high mechanical strength and relatively low material and processing cost. Potentiostatic and potentiodynamic tests were performed in H_2SO_4 solutions on AISI 316L stainless steel bipolar plates with etched flow fields. The effect of pH and presence of small amounts of fluoride and chloride on the corrosion rate and interfacial contact resistance of the stainless steel bipolar plate were investigated. The tests performed in electrolytes with various pH values revealed that the oxide layer was thinner and more prone to corrosion at pH values significantly lower than the pH one expects the bipolar plate to experience in an operating proton exchange membrane fuel cells. The use of solutions with very low pH in such measurements is thus probably not the best way of accelerating the corrosion rate of stainless steel bipolar plates. By use of strongly acidic solutions the composition and thickness of the oxide layer on the stainless steel is probably altered in a way that might never have happened in an operating proton exchange membrane fuel cell. Additions of fluoride and chloride in the amounts expected in an operating fuel cell (2 ppm F^- and 10 ppm Cl^-) did not cause significant changes for neither the polarization- nor the contact resistance measurements. However, by increasing the amount of Cl^- to 100 ppm, pitting was initiated on the stainless steel surface.

1. Introduction

The Bipolar Plate (BPP) accounts for about 80% of the total cell-weight and about 25% of the total cell cost in a Proton Exchange Membrane Fuel Cell (PEMFC) [1,2]. The principle tasks for a bipolar plate is to distribute the gas in the cell, manage the water in the cell, remove heat from active areas, prevent leakage and to conduct the current away from each single cell in a stack [3]. Furthermore, a bipolar plate needs to be electrically conducting, corrosion resistant, easy to produce, relatively cheap and both chemically and mechanically stable [4]. Most commercialized bipolar plates made

* *Corresponding author*. Department of Chemical Engineering and Materials Technology, Sør-Trøndelag University College, NO-7004 Trondheim, Norway. Tel.: +47 97750663, +47 73559637; fax: +47 73559631.
E-mail address: sigrid.ladre@hist.no (S. Lædre).
0360-3199/$ – see front matter
http://dx.doi.org/10.1016/j.ijhydene.2012.09.021

today are carbon based, but they are expensive and time consuming to manufacture. Metal bipolar plates, on the other hand, are cheaper and easier to produce, and they are in general very good electrical and thermal conductors. However, metal plates tend to degrade over time, mainly due to corrosion or electronic passivation of the surface layer due to oxide formation. Furthermore, common metals possess rather high thermal expansion coefficients, which is undesirable. A bipolar plate needs to have a low electrical resistivity in order to conduct the current between individual Membrane Electrode Assemblies (MEAs) in a stack. Passivity, which protects the metal from corrosion by formation of a thin surface film under oxidizing conditions at high anodic polarization, can result in high contact resistance between the metal and the Gas Diffusion Layer (GDL) in a PEMFC.

Several studies have investigated the possibility of using stainless steel as bipolar plate material [1,4–9]. Stainless steel has a relatively high strength, low gas permeability, high chemical stability, a wide range of alloy choices and it is relatively cheap to produce into desired shape and size [3]. The U.S. Department of Energy (DOE) has established some development targets for various properties of bipolar plates for PEM fuel cells [10]. These are given in Table 1 for the years 2005, 2010 and 2015.

Previous studies on the corrosion resistance of stainless steel bipolar plates have been conducted, both in-situ and ex-situ [4,11–14], and various electrolytes have been used for the polarization of these plates. Feng et al. [11] carried out potentiodynamic, potentiostatic and Electrochemical Impedance Spectroscopy (EIS) measurements of AISI 316L under both simulated fuel cell conditions (pH from 3 to 6) and accelerated conditions (0.5 M and 1 M H_2SO_4). $1{\cdot}10^{-4}$ M F^-, $2{\cdot}10^{-6}$ M SO_4^{2-} and $2{\cdot}10^{-6}$ M Cl^- was also added to some of the electrolytes. It was found that the nature of the passive film depends on both pH and applied potential during polarization. Wang et al. [4] polarized different grades of stainless steel, from Open Circuit Voltage (OCV) in both anodic and cathodic direction, using a 1 M H_2SO_4 solution with 2 ppm F^- as electrolyte. They also performed potentiostatic measurements at 0.6 V_{SCE} and −0.1 V_{SCE} to simulate the cathode and anode potentials, respectively, in an operating fuel cell. They suggested that the thickness of the passive film formed on stainless steel during potentiostatic polarization remains constant throughout the polarization. Kumagai et al. [13] used a 0.05 M H_2SO_4 electrolyte to study the behavior of various austenitic steels as a function of pH, where the pH was adjusted by addition of 0.5 M Na_2SO_4. It was found that at pH values below 3.3, relatively thin films enriched with chromium oxide was formed, while the films formed at higher pH were thicker and mainly consisted of iron oxide.

Nafion membranes are made from a copolymer of two different fluoride containing compounds [15], and when used in PEM fuel cells, fluoride in the form of HF is susceptible to be released. Agneaux et al. [16] analyzed solutions gathered from both anodic and cathodic outlets of PEM fuel cells operated with bipolar plates made from different grades of stainless steel, and the fluoride content in the water from the anode and cathode outlets were found to be $5.7{\cdot}10^{-4}$ M and $4.1{\cdot}10^{-4}$ M, respectively. Healy et al. [17] found that the amount of F^- in the fuel cell product water, when operated at temperatures between 75 and 82 °C and current densities of 0.2–0.8 A cm^{-2}, varied between approximately $1.58{\cdot}10^{-4}$ M and $5.62{\cdot}10^{-6}$ M. Borup and Vanderborgh [18] suggested that both fluoride and chloride facilitates the initiation of corrosion of bipolar plate materials. Yang et al. [12] performed potentiodynamic and potentiostatic experiments in $1{\cdot}10^{-5}$ M H_2SO_4 solutions with addition of different amounts of F^-. Although all currents measured satisfied DOEs target, these tests indicated that the corrosion current, and also pitting corrosion, increases with F^- concentrations. Rivas et al. [19] characterized the corrosion resistance of AISI 316 coated with molybdenum oxide films by potentidynamic and potentiostatic test in 0.5 M sulfuric acid solutions with 2 ppm fluoride. They found that the deposited Mo oxides offer a high degree of protection against corrosion on specific areas of the stainless steel. Matsuoka et al. [20] found no effect on MEA performance (voltage degradation and loss of ESA) with additions of small amounts of F^- (3 mM solutions) to the fuel stream during operating conditions (70 °C and 0.3 A cm^{-2}). On the other hand, a significant change was observed with addition of similar amounts of Cl^-, as reported in the same work.

There are several possible resources to the Cl^- found in PEM fuel cells. Hydrogen, produced as a bi-product in the chlorine-alkali industry [21], contains ppm levels of Cl_2. Cl^- can also be found in PEM fuel cells operated in marine environment because they might take up the chloride ions from this environment through the fuel and/or air. Schmidt et al. [22] claimed that high-surface area fuel cell catalysts, which are often synthesized from halide-containing educts, can release halides into the fuel cell. They also suggested that water in the feed streams can contain traces of Cl^-. Previous research has shown that Cl^- can contaminate a PEM fuel cell by adsorbing to the active sites of the catalyst [22], and by accelerating the catalyst dissolution [23]. Ageneaux et al. [16] found the chloride concentrations for anodic and cathodic media in PEM fuel cells to be $9{\cdot}10^{-7}$ M and $1{\cdot}10^{-6}$ M respectively. Li et al. [21] performed in-situ experiments by operating

Table 1 – DOEs targets for PEMFC bipolar plates [10].

Properties	Units	2005 Status	2010	2015
Cost[a]	$ kW^{-1}	10[b]	5	3
Weight	kg kW^{-1}	0.36	<0.4	<0.4
H_2 permeation flux	cm^3 s^{-1} cm^{-2} @ 80 °C, 3 atm	$<2{\cdot}10^{-6}$	$<2{\cdot}10^{-6}$	$<2{\cdot}10^{-6}$
Corrosion	μA cm^{-2}	<1[c]	<1[c]	<1[c]
Electrical conductivity	S cm^{-1}	<600	<100	<100
Resistivity[d]	Ω cm^2	<0.02	<0.01	<0.01
Flexural strength	MPa	<34	<25	<25
Flexibility	% Deflection at mid-span	1.5–3.5	3–5	3–5

a Based on 2002 dollars and costs projected to high volume production (500,000 stacks per year).
b Status is from 2005 TIAX study.
c May have to be as low as 1 nA cm^{-2} if all corrosion product ions remain in ionomer.
d Includes contact resistance.

a Teldyne single fuel cell where Cl^- was added in various amounts as HCl to the fuel and air. Their aim was to understand the impacts and mechanisms of chlorine contamination on the MEA and they found the severity of contamination to be independent of injection side (fuel vs. air). Ofstad et al. [24] evaluated the stability of different types of platinum surfaces in the presence of chloride. They added 10, 20 and 50 ppm chloride as hydrochloric acid to a 0.5 M H_2SO_4 solution, and found the dissolution rate of the Pt/C catalyst to be up to 170 times larger with the addition of chloride in these amounts.

Abd El Meguid et al. [25] explored the potentiodynamic anodic polarization behavior of AISI 304 in 0.1 M NaCl with addition of several anions. It was found that the sulfate ion increases the pitting potential of AISI 304, which reveals that the competition between Cl^- and SO_4^{2-} to adsorb to the surface may inhibit the pitting attack. Pujar et al. [26] performed electrochemical noise (EN) measurements on AISI 316 in deaerated solutions of sodium chloride and sodium sulfate. They reported that the sulfate ions strengthen the passive film by being incorporated into it, as opposed to the chloride ions, which adsorb to the passive film and initiate pitting corrosion.

The oxide layer formed on AISI 316L is a chromium oxide (Cr_2O_3), and can be formed in air, without anodic polarization. This layer is what makes the stainless steel protected against corrosion, but when stainless steel is used as bipolar plate material, the oxide layer also impedes the flow of current between individual cells in a stack. Wang et al. [4] and Lee and Lim [27] tested the interfacial contact resistance (ICR) of stainless steel. Their setups were similar, with carbon paper next to the sample on both top and bottom, and copper plates as an outer structure where the current was sent through. Wang et al. [4] measured the contact resistance of stainless steel bipolar plates after pre-treating them under potentiostatic conditions at 0.6 V_{SCE} for different periods of time. They found the contact resistance after 60 min of polarization at 0.6 V_{SCE} to be 250 mΩ cm^2 at 140 N cm^{-2} (14 bar), and the tests performed over different time spans showed similar results. Several studies have been conducted where Auger Electron Spectroscopy (AES) have been used as a method for investigating oxide layers on stainless steel [28,29]. Davies et al. [30] performed surface analyzes of the passive film on AISI 316L by use of AES as part of their investigation of AISI 316L as material for bipolar plates in solid polymer fuel cells. Their research showed that the oxygen content decreases with increasing depth.

Our aim in this study was to investigate AISI 316L bipolar plates when polarized in solutions with different molarities, in order to study the influence of pH on the corrosion rate and contact resistance. There was also an interest to study the effect F^- and Cl^- have on the performance of stainless steel bipolar plates. Previous studies have been performed on bipolar plates with respect to F^- [15–17], where significant effects were reported. However, previous studies on Cl^- additions to PEM fuel cells have primarily been focused on the overall effect on the fuel cell, and/or on the polymer membrane [21,24]. Sulfate was not added to the electrolyte because previous research has suggested that the ion has a corrosion inhibiting effect [25,26], which was not desirable during this work. To get a better understanding of how the thickness of the chromium oxide layer changes under different polarization conditions, ICR measurements, AES analyses and Scanning Electron Microscopy (SEM) imaging were also performed.

2. Experimental

AISI 316L bipolar plates were used for the tests. The surface area of the plates was 16 cm^2 before the flow field was etched in, and the surface of the non-etched area was 8.059 cm^2. Potentiostatic, potentiodynamic and ICR measurements were performed during this study, as well as SEM (Hitachi S-3400N) and AES (JEOL JAMP-9500) analyses.

2.1. Electrochemical measurements of the bipolar plates

A three-electrode system was used to perform the potentiostatic and potentiodynamic measurements. Concentrated sulfuric acid (Merck, 95–97%) was mixed with Millipore water (18.2 MΩ) until the desired acid concentration and used as electrolyte. A potentiostat (IM6 Zahner electric) was used to polarize the stainless steel bipolar plate acting as the working electrode vs. a Mercury/mercury sulfate (Hg/Hg_2SO_4) reference electrode. The reference electrode was placed in a separate compartment containing a solution of saturated K_2SO_4, which was connected to the electrolyte via a salt bridge made of sulfuric acid of the same molarity as used in the electrode compartment. The counter electrode, a platinum foil, was placed in the electrolyte along with the working electrode and a temperature gauge, which was connected to a heating plate controlling the temperature in the test cell. The temperature in the cell was set to 75 °C, and nitrogen gas (5.0 N_2, Yara) was continuously bubbled into the electrolyte during the experiments. Two predesigned experiments, a potentiodynamic scan and the other a potentiostatic test, were used to measure the corrosion rate. They are both described in Table 2.

2.1.1. pH variations and addition of fluoride and chloride

Both potentiostatic and potentiodynamic measurements (Table 2) were performed in sulfuric acid solutions with molarities of 0.1 mM, 1 mM, 0.1 M and 1 M. The same measurements were also performed in electrolytes made from 1 mM H_2SO_4 with 2 ppm fluoride, 1 mM H_2SO_4 with

Table 2 – The predesigned potentiodynamic and potentiostatic experiments designed to measure corrosion currents.

Test	Potentials [V_{SHE}]	Duration/ speed	Description
Potentiodynamic	−0.25 to 1.05	2 mV s^{-1}	A potential scan covering the potentials of both anode and cathode reactions in a PEMFC.
Potentiostatic	0.951	60 min	Potential close to the cathode potential in a PEMFC at OCV.

10 ppm chloride and 1 mM H_2SO_4 with 100 ppm. The fluoride was added as NaF (Merck, 99%) and the chloride was added as NaCl (Merck, 99.5%). AES analyses were performed on the plates that had been polarized in solutions with various pH values in order to estimate the effect pH has on the thickness of the oxide layer.

2.2. *Interfacial contact resistance (ICR) measurements*

The ICR of the AISI 316L bipolar plates was measured before and after each corrosion test, and the setup of the contact resistance equipment is shown in Fig. 1. The setup was designed in such way as to enforce the bipolar plates for similar conditions as in a real fuel cell. A gold coated bipolar plate was used as standard, and the contact resistance was measured between this plate, the backing and the bipolar test plate.

A XDL 56-4 DC power supply (Xantex) was connected to the copper plates in order to send current through the whole setup, and the resulting voltage was measured with a multimeter (Fluke 76 True RMS) between the two bipolar plates. A current of 2 A was used in the experiments, and the compaction pressure was controlled by a pneumatic cylinder (Camozzi, QP2A080A010).

3. Results and discussion

The potentiostatic and potentiodynamic tests were chosen to match relevant potentials in an operating PEM fuel cell to study the effect of acidity (pH) an additives (Cl^- and F^-). The first test was a linear polarization, where the potential was set to run from −0.25 V_{SHE} to 1.05 V_{SHE} at 2 mV s^{-1} .1.05 V_{SHE} was chosen because in an operating fuel cell, even with maximum overpotential, the voltage is rarely higher than 1 V_{SHE}. The lowest potential was set to −0.25 V_{SHE} to cover the anode potential in an operating PEM fuel cell. The potential used in the second corrosion test was chosen to simulate the open circuit voltage in a PEM fuel cell, which is typically slightly below 1 V.

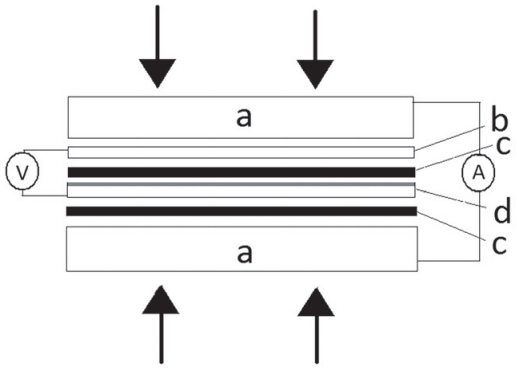

Fig. 1 – Setup for measuring ICR a) copper plates. b) bipolar test plate. c) carbon backing. d) gold coated stainless steel plate (standard).

Table 3 – Acid concentrations and the corresponding pH values used in this work.

Concentration H_2SO_4	0.0001 M	0.001 M	0.1 M	1 M
pH	3.72	2.87	1.01	0.51

3.1. *Variation of pH*

In order to study the effect of acid concentration and evaluate whether or not it is possible to accelerate ex-situ tests by simply increasing the acidity, tests were performed in electrolytes with different molarities. The molarities and corresponding pH values are presented in Table 3. The local pH variations inside an operating fuel cell is hard to measure, but measurements done (Fig. 2) on the water leaving the fuel cell, shows that the pH is always higher than 3.75. Healy et al. [17] found the minimum pH in the PEM fuel cell product water to be around 3.8. The pH close to the bipolar plate is probably slightly lower than in the water leaving the fuel cell. Among the four acid concentrations tested during this study, the 1 mM solution was assumed to be the one that lies closest to the actual pH experienced by the bipolar plate. Several previous studies have been conducted in 1 M or 0.5 M H_2SO_4 electrolytes [4,27,31]. Some authors used electrolytes with low pH values to accelerate the degrading rate of the plates, but this introduces the possibility of altering the kinetics of the existing surface processes. Furthermore, a too high pH might initiate processes that are unlikely to occur in an operating fuel cell with only moderate pH values.

The majority of the polarization tests, both potentiostatic and potentiodynamic, produced small currents, sometimes not much larger than the general noise. Figs. 3 and 4 show the potentiostatic and potentiodynamic results, respectively, for the various acidities used in this work. The polarizations performed in 1 M solutions show the highest corrosion currents in both figures.

When a strong acidic solution is used, the passivated oxide layer is susceptible to be destabilized, especially at the lower potential. If this happens, the oxide layer could start to

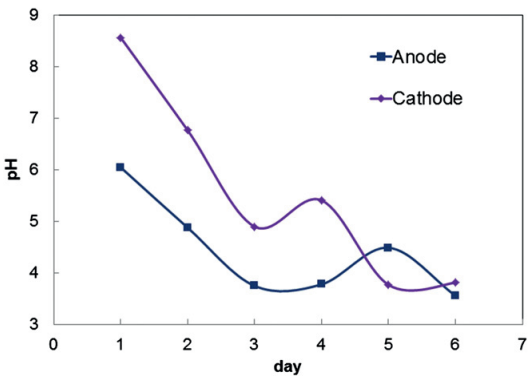

Fig. 2 – pH values measured in the effluent of a fuel cell operating at 75 °C for several days.

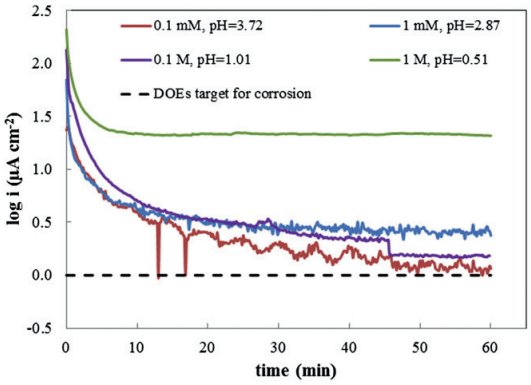

Fig. 3 – Potentiostatic measurements at 0.951 V_{SHE} for 1 h, variation in pH.

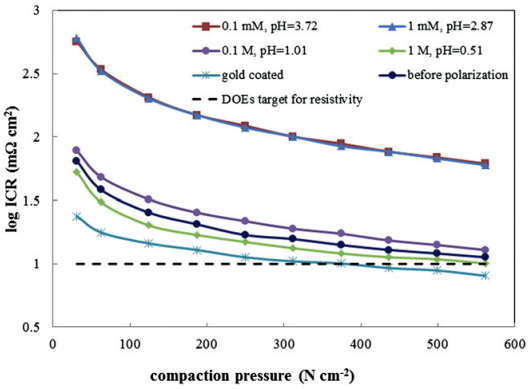

Fig. 5 – ICR results after the potentiostatic measurements at 0.951 V_{SHE}, variation in pH.

reduce, or even dissolve, and the bare stainless steel surface might come in direct contact with the electrolyte. This could in turn initiate corrosion processes at the stainless steel surface that would not have taken place in an electrolyte with lower acidity. From the potentiostatic measurements in Fig. 3 performed at 0.951 V_{SHE}, a significant steady corrosion current, just below 22 μA cm^{-2}, can be observed for the curve representing the 1 M electrolyte about 5 min into the test. The other current transients slowly decay to low values depending on acidity. This effect is also visualized in the potentiodynamic measurements in Fig. 4. Once again the "passive" region observed between about 0.3 and 0.9 V depends on acidity, where the 1 M solution obtains a markedly increased current compared to the other three acid concentrations. The corrosion current observed for lower potentials, about 0–0.2 V_{SHE}, increased with acidity as expected, although a negligible difference was observed for the lowest acid concentrations. Nevertheless, the trend is that a higher acid concentration induces higher corrosion current densities at all relevant potentials, but only small variations are observed when the acid concentration becomes low enough.

DOEs target for corrosion current for bipolar plates in PEM fuel cells is set to less than 1 μA cm^{-2} [32]. Non-coated stainless steel in 0.1 mM, 1 mM and 0.1 M solutions (Fig. 3) showed current densities close to this value in the potentiostatic tests. These low values are most likely a result of the passivated oxide layer formed on the surface of the plates. It is worth pointing out that an increased passivity, hence lower corrosion current, by lowering the acidity could possibly increase the contact resistance beyond the target put forward by DOE for bipolar plates.

The contact resistance measurements performed after the potentiostatic and potentiodynamic tests for various acid concentrations are presented in Figs. 5 and 6, respectively. From both these figures it becomes obvious that the bipolar plates that had been polarized in solutions with mild pH conditions produced higher contact resistances than the

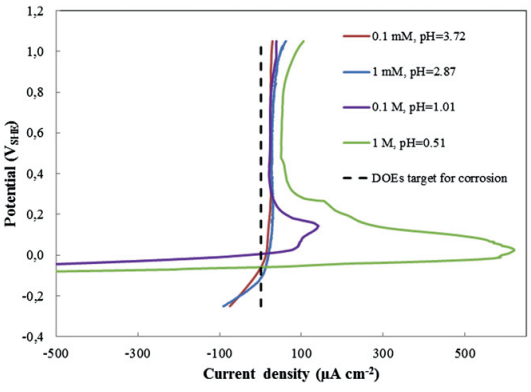

Fig. 4 – Current–potential relation during the potentiodynamic measurements from −0.25 V to 1.05 V_{SHE}, at 2 mV s^{-1} with a variation in pH.

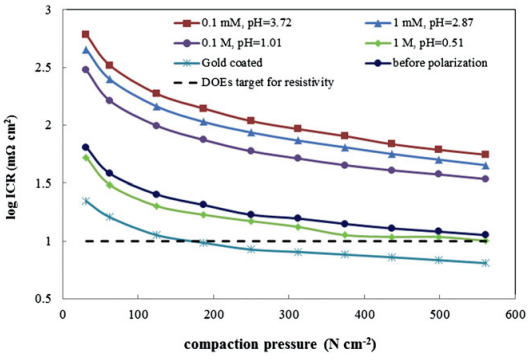

Fig. 6 – ICR results after the potentiodynamic measurements from −0.25 V to 1.05 V_{SHE}, with a variation in pH.

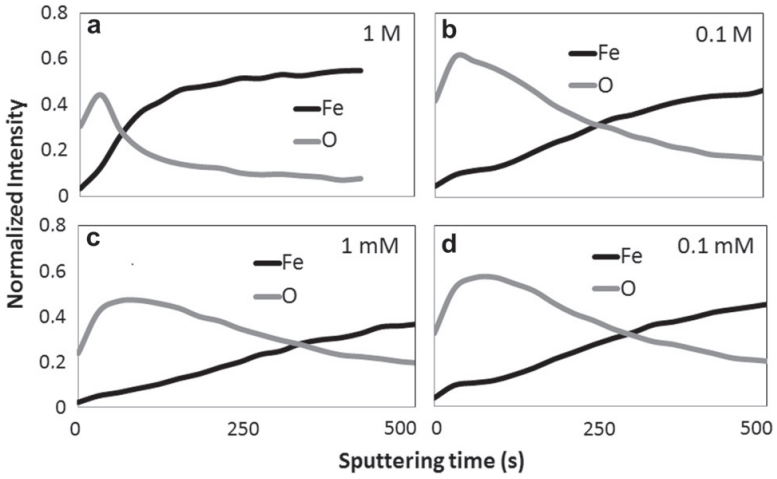

Fig. 7 – AES results showing the change in oxygen and Iron intensity as a function of sputtering time into the oxide layers on the stainless steel samples that had been polarized in solutions with molarities of a) 1 M. b) 0.1 M c) 1 mM and d) 0.1 mM.

plates polarized in solutions with low pH (very acidic). The low contact resistances measured on the plates used in the 0.1 M and the 1 M tests indicates that there is a difference in oxide layer thickness between the plates polarized in high acidity solutions compared to the ones that had been polarized in lower acidity solutions. To confirm this relationship, AES analysis were performed to measure the relative oxide layer thickness on the stainless steel plates. The results are presented in the graphs a, b, c and d in Fig. 7. The sputtering was performed at a constant rate, and the sputtering time is thus equivalent to the thickness of the oxide layer. Note that the oxygen intensity does not reach zero because of small amounts of oxygen present in the SEM chamber. All four graphs show a decrease in oxygen content and a corresponding increase in iron content with oxide layer thickness. The AES results from the stainless steel plates that had been polarized in 1 M and 0.1 M sulfuric acid solutions both show a faster decrease in oxygen intensity and a corresponding faster increase in iron intensity than any of the other plates. This shows that the polarization of stainless steel plates in highly acidic solutions produce thinner oxide layers on the plates than if they were polarized in solutions with lower acidities. The thickness of the oxide layer on the stainless steel bipolar plates is thus amongst other characteristics controlled by the acidity of the sulfuric acid electrolyte the plates are tested in. At higher acidities the oxide layer becomes thinner than at lower acidities, which would in turn support the ICR values obtained.

By using Ohm's Law in its simplest form, $U = R_{contact} \cdot I$, high contact resistance value have a potentially huge impact on the overall losses in an operating fuel cell. For example, a 100 mΩ cm^2 contact resistance corresponds to a 100 mV voltage loss if the current drawn from the fuel cell is set to 1 A cm^{-2}. At high currents, the voltage loss can be significant even for rather low ICR values.

ICR measurements were performed on gold coated stainless steel bipolar plates that had experienced the same test history as the ordinary stainless steel samples, i.e. they had gone through the potentiostatic- and potentiosdynamic tests in a 1 mM H_2SO_4 electrolyte. The corresponding current-potential values are displayed together with the stainless steel curves in Figs. 5 and 6. These plates produced very low contact resistances, as is to be expected for gold plated surfaces. This pattern coincides with the high current densities produced during the potentiostatic and potentiodynamic tests. The absolute values of the contact resistances (Table 4) are all higher than DOEs requirements (Table 1). Both gold coated steel and steel tested in 1 M H_2SO_4 showed ICR results in the same order of magnitude as DOEs target. The bipolar plates tested in 1 mM H_2SO_4 showed ICR results between 134.5

Table 4 – Contact resistance results at 140 N cm^{-2} (14 bar) after all the polarization tests. All the contact resistances values are given in mΩ cm^2.

What was tested	Test 1: −0.25 V to 1.05 V_{SHE}	Test 2: 0.951 V_{SHE}
Gold coated stainless steel	10.65	14
0.1 mM/pH=3.72	170.5	186.5
1 mM/pH=2.87	134.2	183
0.1 M/pH=1.01	90.6	29.8
1 M/pH=0.51	18.8	18.8
Addition of 2 ppm fluoride	157.5	171.9
Addition of 10 ppm chloride	185	201.3
Addition of 100 ppm chloride	194.5	268

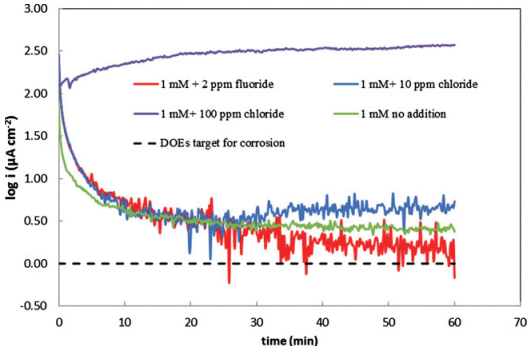

Fig. 8 – Potentiostatic measurements at 0.951 V_{SHE} for 1 h, addition of F^- and Cl^-.

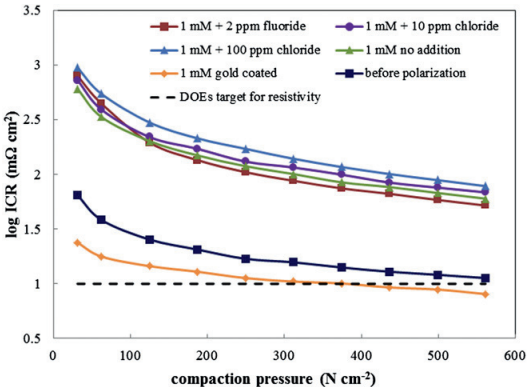

Fig. 10 – ICR results after the potentiostatic measurements at 0.951 V_{SHE}, addition of F^- and Cl^-.

and 183 mΩ cm^2 after the polarization tests, which is almost 20 times higher than DOEs target for contact resistance (<10 mΩ cm^2). In fact, contact resistance measurements itself rules out regular stainless steel as bipolar plate material, when assuming that the pH experienced by the bipolar plate is around 2.87 (1 mM H_2SO_4).

What is evident from the polarization tests performed at different acidities and the ICR measurements done before and after each electrochemical test is that the acidity of the electrolyte in which the tests are performed in, is crucial. There are great differences in contact resistance measurements and the current densities produced in the solutions with different acidities. From the results obtained during this work it is suggested to choose a pH value that lies close to the real pH in an operating PEM fuel cell, which is typically milder than what is chosen for accelerated degradation/corrosion tests. Lowering of the pH might not only speed up the reactions that normally takes place on a stainless steel surface in an operating fuel cell. It may also alter the relative rate of the reactions as well as introducing new processes on the plates (e.g. severe pitting at high electrode potentials), which is perhaps insignificant, or of low impact in a real PEM fuel cell operated under normal conditions.

3.2. *Fluoride and chloride additions to the electrolyte*

Previous research performed in electrolytes containing chloride [21,24] were not focused on the degradation of the bipolar plate, but rather on degradation of the expensive electrocatalyst (typically platinum) and the polymer membrane. The low amounts of fluoride (2 ppm) and chloride (10 ppm) added to the electrolyte in this work, were chosen in accordance with the amounts discussed in relevant literature [4,17,24]. The 100 ppm addition of Cl^- was done to investigate the effect that high amounts of chloride could have on the bipolar plate. A piece of gold coated glass was put through the potentiodynamic measurement to find the corrosion current of pure gold, and the results are included in Fig. 10 as a reference. The

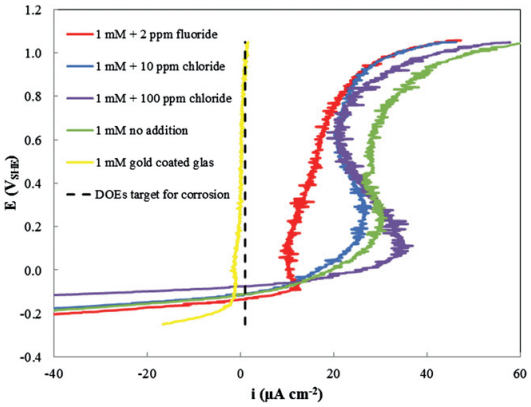

Fig. 9 – Potentiodynamic measurements from −0.25 V to 1.05 V_{SHE}, addition of F^- and Cl^-.

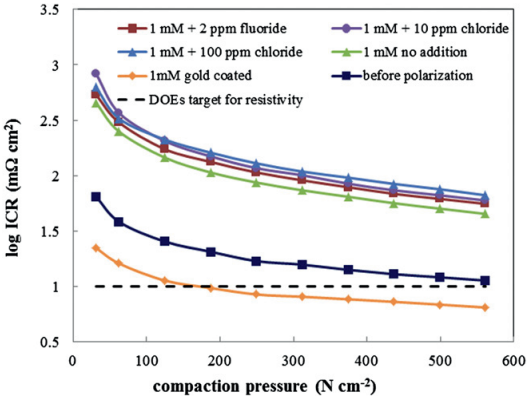

Fig. 11 – ICR results after the potentiodynamic measurements from −0.25 V to 1.05 V_{SHE} addition of F^- and Cl^-.

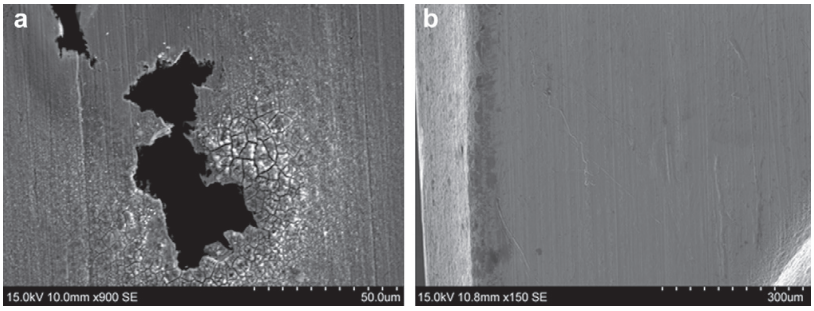

Fig. 12 – SEM imaging performed with an accelerating voltage of 15 kV a) A new, pristine, stainless steel plate. b) Pitting corrosion on the stainless steel surface after the polarization test performed at 0.951 V_{SHE} for 1 h with 100 ppm Cl^- added to the electrolyte.

current for the gold coated glass piece was found to be essentially zero in the relevant potential window, as expected. In this study, the addition of 2 ppm fluoride and 10 ppm chloride to the 1 mM H_2SO_4 electrolyte did not result in substantial changes for neither the polarization tests (Figs. 8 and 9) nor the ICR measurements (Figs. 10 and 11) compared to the tests done in electrolytes without these ions. Addition of 2 ppm fluoride or 10 ppm chloride to the electrolyte seems to produce corrosion currents in the same range as similar electrochemical tests performed without additions. This indicates that such low amounts of fluoride and chloride, which can be expected to be found in an operating PEM fuel cell, does not seem to promote corrosion processeses. Even though the absolute values of the current density appears to be low for the stainless steel bipolar plates, they are substantial compared to the current produced during the gold coated glass polarization.

From Fig. 8 (1 h at 0.951 V_{SHE}) it is clear that the 100 ppm chlorine addition to the electrolyte influences the current density in the potentiostatic measurements, and the current produced is much higher than similar tests without this addition. The current density toward the end of the test was close to 300 times the current density produced in any of the other tests presented in Fig. 8. SEM imaging revealed obvious signs of pitting corrosion on the plate used for this test (Fig. 12), and it proves how fatal pitting corrosion can be for a material. This could explain the high currents produced during the potentiostatic tests, because pitting corrosion usually accelerates rapidly when first initiated [33]. However, 100 ppm is too high a concentration likely to occur in a PEM fuel cell under normal operation.

Fig. 9 shows the potentiodynamic measurements performed in 1 mM H_2SO_4 containing either fluoride or chloride, along with measurements performed in a 1 mM H_2SO_4 electrolyte without additions. The shape of the 2 ppm fluoride and 10 ppm chloride curves are almost identical to the curves obtained from tests performed in 1 mM H_2SO_4 electrolyte without additions. The 100 ppm chloride curve is a little different, with a more emphasized current peak at around 0.1 V. This peak indicates a higher corrosion current, and confirms that 100 ppm chloride affects the corrosion rate of the steel.

The ICR measurements (Figs. 10 and 11) seem to agree with the polarization test results since the 2 ppm fluoride and 10 ppm chloride ICR values are in the same order of magnitude as the values obtained after polarization of AISI 316L in 1 mM sulfuric acid solutions without additions. This indicates that the amounts of chloride and fluoride found in a fuel cell do not affect the surface reactions taking place on the stainless steel bipolar plate. The ICR results obtained after the potentiostatic and potentiodynamic tests where 100 ppm of F^- was added to the electrolyte do not show a change in contact resistance compared to the other test presented in Figs. 10 and 11. The general thickness of the oxide layer on the stainless steel surface does not necessarily change when pitting occurs, because pitting attacks the oxide layer in very small fractions of the surface area [33]. This could in turn explain why the contact resistance measurements of the 100 ppm Cl^- test do not seem all that different from the other tests presented in Figs. 10 and 11.

4. Conclusions

Both electrochemical- and ICR measurements were performed to study the effect pH and halide additions have on the corrosion of AISI 316L bipolar plates for PEM fuel cells. Highest corrosion currents where measured when the steel was tested in electrolytes with the lowest pH (0.51), and the corresponding contact resistances were low enough to satisfy DOEs targets. DOE's requirements for corrosion current is less than 1 $\mu A\ cm^{-2}$, which were obtained in the high voltage tests performed in 0.1 mM and 1 mM solutions. AES analyses showes that the passivated oxide layer created during the polarization test was disintegrated at higher molarities, which was also expected as the formation of chromium oxides depends on the pH in the electrolyte. If the oxide layer got thin enough or was completely removed, the surface of the stainless steel could easily have reacted with the electrolyte and corrosion reactions could have taken place which would be unlikely to take place in an operating fuel cell. Use of electrolytes with lower pH than what is found in an operating PEM fuel cell, with the aim of accelerating the reactions on the

bipolar plates, might not produce the desired results. Other factors may also be altered if the objective is to accelerate reactions taking place in an operating fuel cell.

The polarization tests performed in the 1 mM solutions containing either 2 ppm F^- or 10 ppm Cl^- did not produce higher corrosion currents than the tests performed without these additions, and the contact resistances measured after the polarizations were also in the same order of magnitude. The stainless steel plates polarized in the electrolytes containing 100 ppm chloride revealed clear signs of pitting corrosion after the 1 h polarization at 0.951 V_{SHE}. This confirms that high amounts of Cl^- does initiate pitting, but the amounts experienced by the bipolar plates in a PEM fuel cell, at least up to 10 ppm, does not seem to cause any more corrosion than what was detected in the similar test without Cl^-.

Out of all the ICR measurements performed during this study, very few of the contact resistance measurements were satisfying according to DOE's requirements of less than 10 mΩ cm^2. Gold coated stainless steel showed the best results, with values right above 10 mΩ cm^2, but the price of gold makes it unattractive as coating for stainless steel bipolar plates. The general trend is that the bipolar plates used for the polarizations resulting in low current densities, are the same plates showing high ICR. Avoiding formation of such a layer through e.g. complete coverage of the surface with a highly conductive, and corrosion resistive material, is highly desired before making stainless steel bipolar plates a viable alternative for large-scale production.

Acknowledgments

This work was financially supported by Sør-Trøndelag University College (HIST), Norwegian University of Science and Technology (NTNU), SINTEF and Nordic Innovation. Nordic innovation is greatly acknowledged for funding the NORCOAT project (09051). S.L. thanks HIST for the award of a PhD-scholarship.

REFERENCES

[1] Antunes RA, Oliveira MCL, Ett G, Ett V. Corrosion of metal bipolar plates for PEM fuel cells: a review. Int J Hydrogen Energy 2010;35:3632–47.
[2] Wang H, Turner JA. Reviewing metallic PEMFC bipolar plates. Fuel Cells 2010;10:510–9.
[3] Hermann A, Chaudhuri T, Spagnol P. Bipolar plates for PEM fuel cells: a review. Int J Hydrogen Energy 2005;30:1297–302.
[4] Wang HL, Sweikart MA, Turner JA. Stainless steel as bipolar plate material for polymer electrolyte membrane fuel cells. J Power Sources 2003;115:243–51.
[5] Heras NDL, Roberts EPL, Langton R, Hodgson DR. A review of metal separator plate materials suitable for automotive PEM fuel cells. Energy Environ Sci 2009;2:206–14.
[6] Tawfik H, Hung Y, Mahajan D. Metal bipolar plates for PEM fuel cell – a review. J Power Sources 2007;163:755–67.
[7] Wang Y, Northwood DO. Effects of O_2 and H_2 on the corrosion of SS316L metallic bipolar plate materials in simulated anode and cathode environments of PEM fuel cells. Electrochim Acta 2007;52:6793–8.
[8] Lafront AM, Ghali E, Morales AT. Corrosion behavior of two bipolar plate materials in simulated PEMFC environment by electrochemical noise technique. Electrochim Acta 2007;52:5076–85.
[9] Yang Y, Guo L-j, Liu H. Corrosion characteristics of SS316L as bipolar plate material in PEMFC cathode environments with different acidities. Int J Hydrogen Energy 2011;36:1654–63.
[10] U.S.D.o. energy, Hydrogen, Fuel Cells & Technologies Program. In: Multi-year research, development and demonstration Plan. D.O. Energy. Ch. 3.4.4, p. 26, http://www1.eere.energy.gov/hydrogenandfuelcells/mypp/; 2005.
[11] Feng K, Wu GS, Li ZG, Cai X, Chu PK. Corrosion behavior of SS316L in simulated and accelerated PEMFC environments. Int J Hydrogen Energy 2011;36:13032–42.
[12] Yang Y, Guo LJ, Liu HT. Effect of fluoride ions on corrosion behavior of SS316L in simulated proton exchange membrane fuel cell (PEMFC) cathode environments. J Power Sources 2010;195:5651–9.
[13] Kumagai M, Myung ST, Kuwata S, Asaishi R, Yashiro H. Corrosion behavior of austenitic stainless steels as a function of pH for use as bipolar plates in polymer electrolyte membrane fuel cells. Electrochim Acta 2008;53:4205–12.
[14] Yang Y, Guo L, Liu H. Influence of fluoride ions on corrosion performance of 316L stainless steel as bipolar plate material in simulated PEMFC anode environments. Int J Hydrogen Energy 2012;37:1875–83.
[15] Curtin DE, Lousenberg RD, Henry TJ, Tangeman PC, Tisack ME. Advanced materials for improved PEMFC performance and life. J Power Sources 2004;131:41–8.
[16] Agneaux A, Plouzennec MH, Antoni L, Garnier J. Corrosion behaviour of stainless steel plates in PEMFC working conditions. Fuel Cells 2006;6:47–53.
[17] Healy J, Hayden C, Xie T, Olson K, Waldo R, Brundage M, et al. Aspects of the chemical degradation of PFSA ionomers used in PEM fuel cells. Fuel Cells 2005;5:302–8.
[18] Borup RL, Vanderborgh NE. Design and testing criteria for bipolar plate materials for PEM fuel cell application, MRS Proceedings 1995;393:151–155.
[19] Rivas SV, Belmonte MR, Pérez-Quiroz JT, Cortes MA, Morón LE, Torres J, et al. Evaluation of materials for bipolar plates in simulated PEM fuel-cell cathodic environments. J New Mater Electrochem Syst 2008;11:81–5.
[20] Matsuoka K, Sakamoto S, Nakato K, Hamada A, Itoh Y. Degradation of polymer electrolyte fuel cells under the existence of anion species. J Power Sources 2008;179:560–5.
[21] Li H, Wang HJ, Qian WM, Zhang SS, Wessel S, Cheng TTH, et al. Chloride contamination effects on proton exchange membrane fuel cell performance and durability. J Power Sources 2011;196:6249–55.
[22] Schmidt TJ, Paulus UA, Gasteiger HA, Behm RJ. The oxygen reduction reaction on a Pt/carbon fuel cell catalyst in the presence of chloride anions. J Electroanal Chem 2001;508:41–7.
[23] Yadav AP, Nishikata A, Tsuru T. Effect of halogen ions on platinum dissolution under potential cycling in 0.5 M H_2SO_4 solution. Electrochim Acta 2007;52:7444–52.
[24] Ofstad AB, Thomassen MS, Gomez de la Fuente JL, Seland F, Møller H, Sunde S,S. Assessment of platinum dissolution from Pt/Cfuel cell catalyst: an electrochemical Quartz Crystal Microbalance Study. J Electrochem Soc 2010;157:B621–7.
[25] Abd El Meguid EA, Mahmoud NA, Abd El Rehim SS. The effect of some sulphur compounds on the pitting corrosion of type 304 stainless steel. Mater Chem Phys 2000;63:67–74.
[26] Pujar MG, Anita T, Shaikh H, Dayal RK, Khatak HS. Use of electrochemical noise (EN) technique to study the effect of sulfate and chloride ions on passivation and pitting

corrosion behavior of 316 stainless steel. J Mater Eng Perform 2007;16:494–9.
[27] Lee YB, Lim DS. Electrical and corrosion properties of stainless steel bipolar plates coated with a conduction polymer composite. Curr Appl Phys 2010;10:S18–21.
[28] Vesel A, Drenik A, Mozetic M, Zalar A, Balat-Pichelin M, Bele M. AES investigation of the stainless steel surface oxidized in plasma. Vacuum 2007;82:228–31.
[29] Mandrino D, Donik Č. Chemical-state information obtained by AES and XPS from thin oxide layers on duplex stainless steel surfaces. Vacuum 2011;86:18–22.
[30] Davies DP, Adcock PL, Turpin M, Rowen SJ. Bipolar plate materials for solid polymer fuel cells. J Appl Electrochem 2000;30:101–5.
[31] Dur E, Cora ON, Koc M. Experimental investigations on the corrosion resistance characteristics of coated metallic bipolar plates for PEMFC. Int J Hydrogen Energy 2011;36:7162–73.
[32] Hamilton PJ, Pollet BG. Polymer electrolyte membrane fuel cell (PEMFC) flow field plate: design, materials and characterisation. Fuel Cells 2010;10:489–509.
[33] Talbot EJ, Talbot DR. Corrosion science and technology. CRC Press Taylor and Francis Group; 2007.

ECS Transactions, 50 (2) 829-839 (2012)
10.1149/05002.0829ecst ©The Electrochemical Society

In Situ and Ex situ Contact Resistance Measurements of Stainless Steel Bipolar Plates for PEM Fuel Cells

S. Ladre[a], O. E. Kongstein[b], A. Oedegaard[b] F. Seland[c], H. Karoliussen[a]

[a] Sør-Trøndelag University College, Department of Technology, 7004 Trondheim, Norway
[b] SINTEF Materials and Chemistry, Trondheim, 7491 Norway
[c] Norwegian University of Science and Technology, Department of Materials Science and Engineering, 7491 Trondheim, Norway

Passivation of stainless steel caused by the formation of an oxide layer on the surface is one of the main concerns when it comes to using stainless steel as bipolar plate material. Interfacial Contact Resistance (ICR) between the bipolar plate and the gas diffusion layer was measured both in situ and ex situ. A method for measuring ICR in situ was developed, and initial results showed that the ICR measured in situ is close to the ICR measured ex situ, for both non-coated and gold coated stainless steel bipolar plates. At a compaction pressure of 205.79 N cm^{-2}, the in situ ICR was found to be close to 50 mΩ cm^2 and the ex situ measurement performed on the same plate ex situ was found to be approximately 40 mΩ cm^2. The in situ method for ICR measurements enables direct studies of the passivation processes at the bipolar plate interface, while the cell is in operation, under the actual fuel cell conditions.

Introduction

Hydrogen based energy converters such as Polymer Electrolyte Fuel Cells (PEMFCs) are forecasted to play a significant role in a future sustainable society. Critical economic and durability issues needs to be resolved before the fuel cell can be introduced to the mass marked. Bipolar Plates (BPPs) are essential components in a fuel cell stack, where they assist with the distribution of the fuel and air, water management, cooling and current collection (1). In addition to being electrically conductive, the BPPs need to be corrosion resistant, easy to produce, relatively cheap and both chemically and mechanically stable (2). With the current technology they account for about 80% of the total stack-weight and about 25% of the total stack cost (3, 4). The U.S. Department of Energy (DOE) has put forth a set of development targets for bipolar plates for PEM fuel cells (Table I), where the most important ones in this work have been Interfacial Contact Resistance (ICR). The near future aim (2015) of the ICR is set to be less than 10 mΩ cm^2 (5).

Table I: DOEs targets for PEMFC bipolar plates (5).

Properties	Units	2005 status	2010	2015
Cost[a]	\$ kW^{-1}	10[b]	5	3
Weight	kg kW^{-1}	0.36	<0.4	<0.4
H_2 permeation flux	cm^3 s^{-1} cm^{-2} @ 80 °C, 3 atm	$<2\cdot10^{-6}$	$<2\cdot10^{-6}$	$<2\cdot10^{-6}$
Corrosion	µA cm^{-2}	<1[c]	<1[c]	<1[c]
Electrical conductivity	S cm^{-1}	<600	<100	<100
Resistivity[d]	Ω cm^2	<0.02	<0.01	<0.01
Flexural strength	MPa	<34	<25	<25
Flexibility	% deflection at mid-span	1.5-3.5	3-5	3-5

a Based on 2002 dollars and costs projected to high volume production (500,000 stacks per year)
b status is from 2005 TIAX study
c May have to be as low as 1 nA cm^{-2} if all corrosion product ions remain in ionomer.
d includes contact resistance

Up until now, most of the commercially available bipolar plates have been carbon-based due to the stability and performance demands for bipolar plates, which are exposed to the acidic environment introduced by the Nafion® membrane. However, there is a desire to move away from carbon based plates due to the rather expensive and time-consuming processing. In general, metal bipolar plates possess high electrical- and thermal conductivities, but non-noble metals tend to degrade over time, mainly due to corrosion. Introducing metallic impurities to the MEA will potentially give consequences for both catalyst activity and membrane conductivity. In addition, some metals will form a protective passive oxide layer at the surface under oxidizing conditions, e.g. high anodic polarization, which tend to increase the ICR between the metal bipolar plate and the attached Gas Diffusion Layer (GDL) in a PEMFC. Furthermore, common metals possess rather high thermal expansion coefficients, which are undesirable for use in fuel cells designed for flexible (varying) operating temperatures.

Stainless steel of various grades has previously been investigated for use as bipolar plate material (2, 3, 6-10) because it possesses a number of beneficial properties. Relatively high strength, high chemical stability, low gas permeability and a wide range of alloy choices are some of these. Furthermore, stainless steel bipolar plates are relatively cheap to process, and can easily be made with various designs, shapes and sizes (1).

Even though stainless steel possesses key properties well suited for bipolar plates in PEMFC (e.g. low corrosion current, low overall weight and easy and cheap to mass produce), it is impeded by the protective, and poorly conductive oxide layer formed in contact with oxygen in the surrounding environment. In particular, chromium that is present in the steel forms a thin, chromium oxide (Cr_2O_3) layer at the surface, with very low conductivity, which hamper the through-layer conductivity and significantly increases the overall resistivity. Interfacial contact resistance of stainless steel was measured ex-situ by Lee et al. (11) and Wang et al. (2) in a configuration where a stainless steel sample was sandwiched between two carbon papers with copper plates in an outer structure. An ICR of 50 mΩ cm^2 at 140 N cm^{-2} (14 bar) was measured by Wang et al. (2) after 60 minutes of polarization at 0.6 V_{SCE}. They observed similar results for tests performed over different time spans. Lee et al. (11) measured ICR values between 25 mΩ cm^2 and 850 mΩ cm^2 on stainless steel bipolar plates coated with a polymer-based coating containing various amounts of carbon black as electrical filler. High carbon contents provided the lowest ICR values. Wang et al. (12) also performed ICR

measurements of stainless steels with and without coating. A contact resistance of about 210 mΩ cm^2 was reported for the bare steel surface.

Several studies have been done where the contact resistance between the bipolar plate and other components in the fuel cell has been measured both ex situ (2, 4, 11) and estimated by various models (13-15). In situ measurement of ICR in a fuel cell is not as frequently described in the literature. In situ ICR measurements provide continuously measurements of the ICR, and make it easier to study how the contact resistance varies over a period of time. When in situ measurements are conducted, both gas flow inside the cell and water produced in the electrochemical reaction as well as humidification of the gases might influence the contact resistance. In addition, in situ ICR measurements provide the opportunity of studying the effect of parameter variations. One can e.g. study how the ICR changes with relative humidity, gas flow and gas pressure**.**

Makkus et. al. (16) performed various in situ measurements on stainless steel bipolar plates for Solid Polymer Fuel Cell (SPFC), including ICR measurements at different compaction pressures. Their objective was to determine the contact resistance between the flow plate and the backing, and this was done by placing a thin gold wire between the E-tek backing plus electrode and the membrane during assembly of the MEA. The voltage drop between this gold wire and the flow plate was measured during cell operation. At high compaction pressure, ICR values were found to be as low as in the case of graphite bipolar plates. At low compaction pressures, ICR values were found to be higher. Ihonen et. al. (17) developed a PEM fuel cell assembly where the contact resistance could more easily be measured. Their cell was made from Polyether-etherketone, and potential probes were connected to both gas backing and current collectors. They found that the cell they developed gave good reproducibility of the measurements, but also revealed that the placing of the probes were crucial for measuring the correct contact resistance. It was also found that stainless steel bipolar plates produce non-stable contact resistances, which changes with operating parameters.

The objective of the work described here was to develop a reliable approach to investigate and evaluate metal bipolar plate coatings through in situ and ex situ measurements. Several studies exist, where the contact resistance was measured ex situ. However, not much effort has yet been put into evaluating the in situ contact resistance, and this work strives to bridge in situ measurements performed in a PEMFC during operation with the ex situ measurements obtained from electrochemical half-cell experiments under similar acidic conditions. Thus, the main focus of this work has been to develop a method for measuring of interfacial contact resistance in situ, and some introductory results are presented and evaluated with respect to ex situ measurements and operating conditions.

Experimental

In situ ICR measurements

The in situ setup for measuring of contact resistance is shown in Figure 1. The setup was made from a PEM fuel cell, where 0.025 mm thin gold wires (99.95% pure gold, Goodfellow) were used to measure the contact resistance between the bipolar test plate

and the GDL. The plates used were made from 316 L stainless steel. The ICR was measured on the cathode side of the fuel cell. One gold wire was welded to each end of the bipolar plate (Figure 2), and for each of these a gold wire was put in between two GDLs as shown in Figure 1. The potential was thus measured between the gold wires welded to the bipolar plate and the gold wires put in between the two GDLs. This resulted in two measured potentials, one from each side of the setup. Note that when the cell was put into the station, it was tilted in a way which gave one measuring point at the top, and one at the bottom of the fuel cell. By welding the wires to the gold plate instead of just placing it on top of the plate, one makes sure the wires stays where they should throughout the measurements.

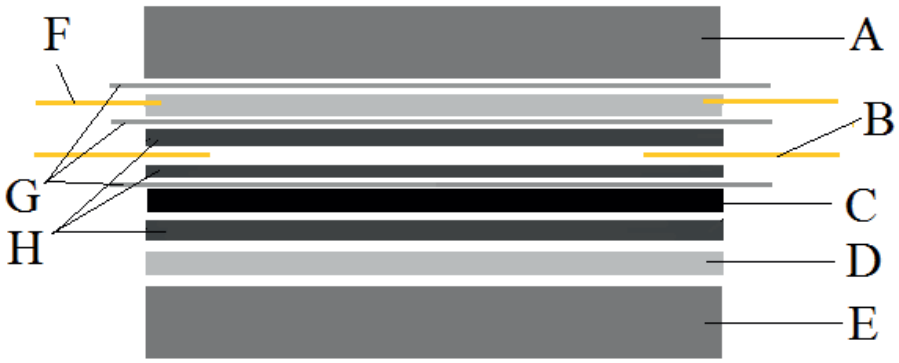

Figure 1: Setup for in situ measurements of ICR. A) Cathode housing. B) Gold wires placed in between to sheets of GDL. C) MEA. D) Bipolar plate. E) Anode housing. F) Gold wires welded to bipolar plate. G) Gasket, preventing contact between gold wires and other electrically conducting parts of the fuel cell. H) GDL.

In addition to the bipolar plate and the two GDLs, three layers of gasket were used on the cathode side of the fuel cell to make sure none of the gold wires came into contact with each other or the cell housing. The gold wires were reinforced on the outside of the cell house with conductive tape, and connected to a data acquisitions/switch unit of brand Agilent (34470A). The ICR was not measured on the anode side of the fuel cell, and thus only one GDL was needed in addition to the bipolar plate and gaskets on the anode side of the fuel cell.

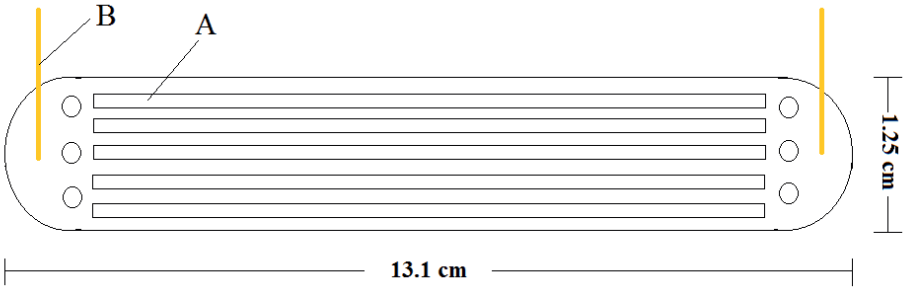

Figure 2: Gold wires welded to the bipolar plate. A) Flow field. B) Gold wire.

After assembling the fuel cell, it was mounted into the test station rig. The cables connected to the heating elements, thermocouples and also the cables measuring and controlling the voltage load, were all connected to the fuel cell, as well as gas inlets and outlets. The fuel and air was humidified by use of a Fuel Cell Technologies, inc humidifier, and no cooling was used inside the cell. The fuel cell was operated with the parameters presented in Table II, and a custom made Lab View program was used to operate the cell. A lower temperature was used to humidify the air entering the fuel cell on the cathode side of the fuel cell to compensate for the extra water produced on this side of the fuel cell. Preliminary results had shown that a lower humidification temperature on the cathode resulted in more stable operation of the fuel cell. The pneumatic pressure refers to the pressure of the pneumatic system, while the compaction pressure is the calculated pressure applied on the land area of the bipolar plate to the GDL. The Lab View program used had been designed especially for the measurements performed in this work, and it calculated the ICR from the current measured trough the cell and the potential measured between the bipolar plate and the GDL. The cell was set to operate under voltage control, and thus the current varied somewhat throughout the tests.

Table II: Parameters used to operate the PEM fuel cell.

Parameter	Value	Parameter	Value
Cell temperature [^{o}C]	50	Cell voltage [V]	0.7
Temperature humidifier anode [^{o}C]	50	Conversion air	0.4
Temperature humidifier cathode [^{o}C]	37	Conversion hydrogen	0.6
Gas pressure anode [bar]	0.3	Pneumatic pressure [bar]	3.3
Gas pressure cathode [bar]	0.45	Compaction pressure [N cm^{-2}]	205.79

Ex situ ICR measurements

The setup for the ex situ ICR measurements is shown in Figure 3. The setup was designed to simulate the inside structure of a PEM fuel cell, where the bipolar test plate is only in direct contact with the cell housing and the GDL. A gold coated bipolar plate was used as standard, and the contact resistance was measured between this plate, the backing and the bipolar test plate. Conduction wires were welded to both the gold coated bipolar plate and the bipolar test plate. A pneumatic cylinder (Camozzi QP2A080A010) was used to control the compaction pressure indicated by the arrows in Figure 3. A XDL 56-4 DC power supply (Xantex) was connected to the copper plates in order to pass current

through the entire setup, and the resulting voltage was measured with a Fluke 76 True RMS multimeter connected to the setup through the wires point-welded to the two bipolar plates (gold standard and test plate).

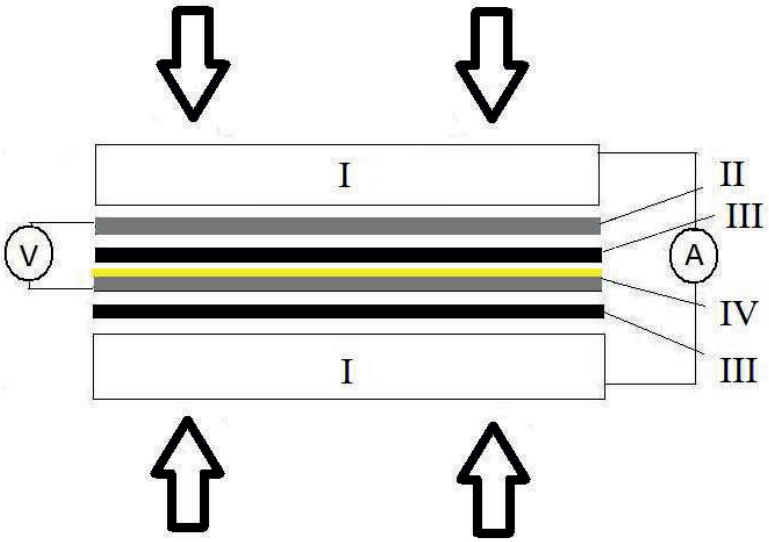

Figure 3: Setup for measuring of ICR ex situ. I) Copper plates. II) Bipolar test plate. III) GDL. IV) Gold coated stainless steel plate (standard).

Results and discussion

In situ ICR measurements

The results obtained from the in situ contact resistance measurements are presented in Figure 4 and 5. By comparing Figure 4 and 5 it can be seen that the ICR for gold was significantly lower compared to steel. Both figures include the contact resistance measured in the fuel cell from the startup of the cell, and the instability at the beginning is caused by the activation of the MEA, where the voltage was alternated between 0.3 V and 0.7 V. After the activation, the ICR seems to stabilize at around 50 mΩ cm^2 at the top of the fuel cell and at around 90 mΩ cm^2 at the bottom. The non- coated 316 L stainless steel bipolar plates had been etched in a hydrochloric acid solution before the ICR measurements, in order to remove the oxide layer on the steel surface. This could be a reason why the contact resistance measured both ex situ and in situ was relatively low. As expected , the ICR measured for the fuel cell containing gold coated stainless steel (Figure 5) is lower than the ICR measured for non-coated steel (Figure 4).

The ICR measurements were performed on the bipolar plate placed on the cathode side of the cell, because it is assumed that the environment on the cathode is more aggressive towards corrosion and degrading than the environment on the anode side. The

graphs in both Figures 4 and 5 show that the ICR is relatively stable after the activation of the membrane is done. This is to be expected for both stainless steel and gold, because the oxide layer on stainless steel forms rapidly and keeps the resistance stable, and the gold should produce a generally low and stable contact resistance over time. As described earlier, there were two points of measuring the ICR on each bipolar plate, and as the cell was tilted during operation, one measuring point became at the top and the other at the bottom of the cell. In both Figure 4 and Figure 5 one can see a difference between the measuring point at the top and the one at the bottom.

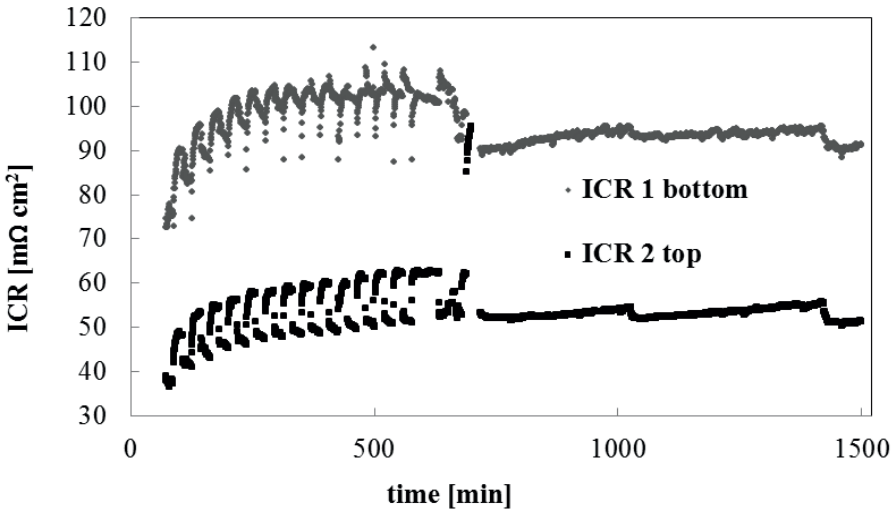

Figure 4: ICR measurements from the top and bottom of the fuel cell with non-coated 316L stainless steel bipolar plates. Compaction pressure 205.79 N cm^{-2})

The gas entering the fuel cell is humidified, and water is also produced inside the fuel cell. Because the cell is tilted, one expects more water at the bottom than at the top of the cell housing. This extra water at the bottom would cause both current and temperature at the bottom of the cell to be lower than at the top. The oxide layer formed on the stainless steel is dependent on several factors, and one of them is the electrolyte the steel is polarized in. If more water was gathered at the bottom of the fuel cell, the oxide layer might be thicker on this end of the bipolar plate. This would in turn result in a higher contact resistance measured at the bottom of the fuel cell compared to at the top. This variation is very clear from figure 4, where the ICR is generally almost twice as high at the bottom as opposed to the top of the fuel cell. In addition, the calculated ICR does not take into consideration that the current distribution might vary throughout the bipolar plate. We know that the water and gas amounts vary from top to bottom in the fuel cell, and it can be assumed that the current distribution also varies from top to bottom in the fuel cell. Some variations in ICR can thus be expected between the measuring points at the top and bottom of the fuel cell.

Figure 5 does not display the same difference in contact resistance between the top and bottom measurements as was seen in Figure 4. Furthermore, the ICR obtained from the bottom of the fuel cell fluctuates more than the ICR obtained from the top of the cell. This fluctuation can to some extent be explained by the instable currents produced by this cell, but it is hard to determine exactly why only one of the measuring points produced such instable contact resistances. Several factors inside the fuel cell could cause such instabilities. Gases and water are continuously moving around inside the cell, and as mentioned earlier, more water is found at the bottom than at the top of the fuel cell. There is also a peak in the ICR in the curve obtained from the measuring point at the bottom in Figure 5. This peak is a result of the unstable operation of the fuel cell during this particular test, and is thus not expected to be reproduced in other similar tests. It is hard to determine exactly what causes instabilities in the ICR when measuring in situ, and only trends and plateau values are considered and commented on.

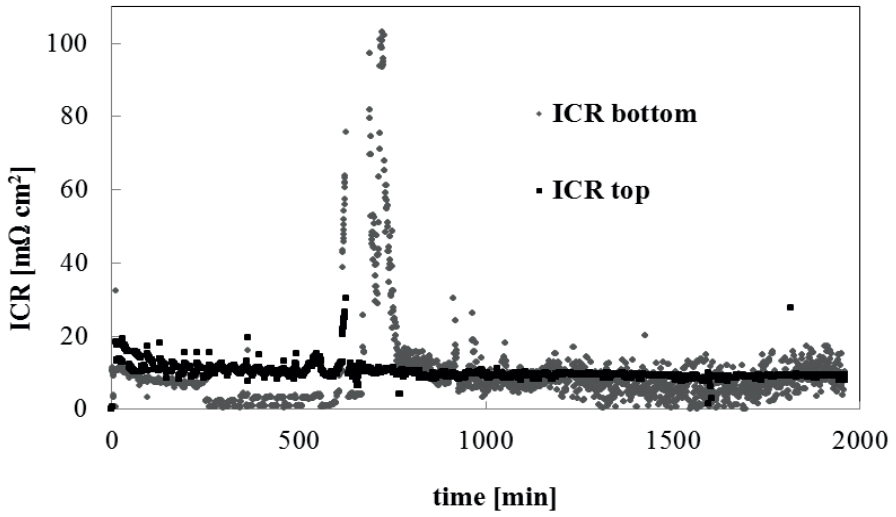

Figure 5: ICR measurements from the top and bottom of the fuel cell with gold coated 316L stainless steel bipolar plates. Compaction pressure 205.79 N cm^{-2})

Ex situ ICR measurements

Figure 6 displays the results obtained from the ex situ ICR measurements. Both the gold coated stainless steel plates and the non-coated stainless steel plates that had been through the in situ measurements (Figures 4 and 5) were put through the ex-situ ICR measurements. A new, unused stainless steel bipolar plate was also measured in the ex situ ICR setup before it was tested in the fuel cell. The results are displayed in Figure 6. The ex-situ ICR measurements performed on gold coated stainless steel before and after the in situ testing showed very similar ICR results. Even though the in situ measurements were only conducted on the bipolar plates placed on the cathode side of the fuel cell, the bipolar plates from the anode side of the cell was also included in the ex situ ICR measurements. As can be seen from figure 6, the ICR values for the uncoated stainless steel cathode plate are slightly higher than the corresponding values obtained for the

anode side plate at low compaction pressures. At higher pressures, however, the values from cathode and anode plates seem to coincide quite well. The variation at low pressures might arise because the ICR values are much higher in general at low compaction pressures, and thus the variation is higher as well. In addition, the uncertainty of the ICR measurements at high compaction pressures is higher than at low pressures due to possible friction between the moving and non-moving parts inside the ex situ ICR setup.

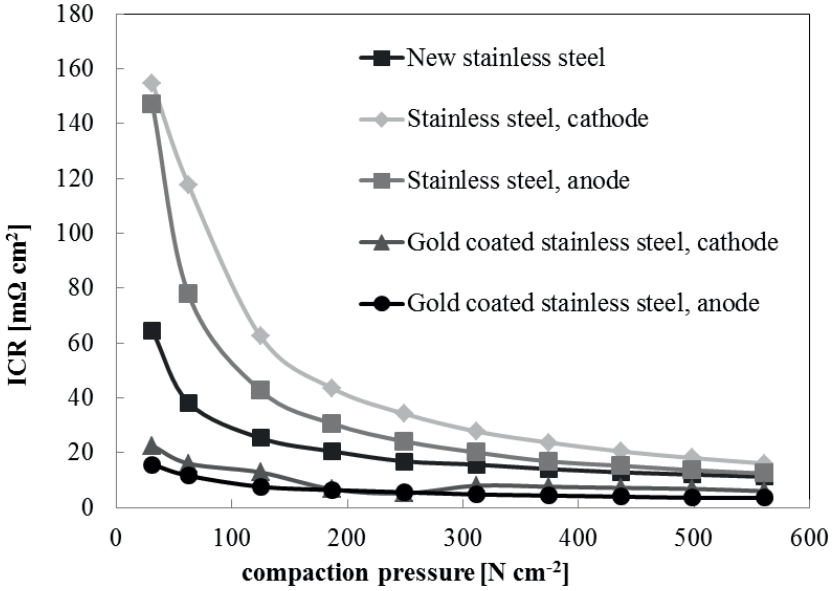

Figure 6: Ex situ ICR measurements performed after in situ operation of fuel cell.

Ex situ vs. in situ ICR measurements

Various methods for ex situ measuring of contact resistance between bipolar plates and the other components in a PEM fuel cell have been described in the literature (2, 4, 11). A small number of methods for in situ contact resistance measurements (11, 17) have also been described. The ex situ measurements are often easy to perform, but it is hard to establish similar conditions as the ones experienced by the bipolar plate when inside an operating fuel cell. As mentioned earlier, in situ measurements are conducted in a real operating PEM fuel cell, which makes the ICR measured more realistic than what is measured ex situ. As the ex situ measurements are performed in a dry setup without any gas flow inside, one cannot expect the results from the ex situ measurements to be the same as the ones obtained from the in situ measurements.

Table III: in situ and ex situ ICR results at a compaction pressure of 205.79 N cm^{-2}. The in situ values are measured after 1500 minutes of operation.

ICR	Bare Stainless Steel	Gold coated stainless steel
In situ, top [mΩ cm^2]	50	9.2
In situ, bottom [mΩ cm^2]	90	5.9
Ex situ, anode [mΩ cm^2]	30	6.2
Ex situ, cathode [mΩ cm^2]	40	6.2

When comparing the results obtained from the in situ measurements with the ex situ measurements (Figures 4-6) it is obvious that gold coated stainless steel shows lower ICR than non-coated stainless steel. If one compares the ICR measurements performed at the top of the fuel cell for both gold coated and non-coated stainless steel in Figures 4 and 5, the non-coated steel shows ICR values about 5-6 times as high as for the gold coated steel. If we compare the corresponding ICR values measured ex situ, at a compaction pressure of 205.79 N cm^{-2} (Figure 6), the non-coated steel show ICR values about 5-8 times higher compared to the gold coated. The ICR ratio between the gold coated and the non-coated steel is thus almost the same for the in situ and ex situ measurements.

The absolute values of the ICR measured in the ex situ and in situ setups are hard to compare directly because of the different conditions experienced by the bipolar plate in the two setups. The ex situ measurements were performed under ambient, and rather dry conditions, with no fuel or air pressure inside the setup. The in situ measurements are, on the other hand, performed in a rather challenging environment, due to the water and gases inside the fuel cell. In addition, the moving parts in the in situ setup were more prone to friction due to O-rings used to prevent leakage. This could also have caused instability in the in situ measurements. Even though the in situ and ex situ ICR values differ somewhat from one another, the variation is comparable. For non-coated stainless steel bipolar plates, the in situ ICR measured at the top of the cell house was around 50 mΩ cm^2, while the corresponding value (at the same compaction pressure) measured for the cathode plate ex situ was found to be close to 40 mΩ cm^2. In any case the contact resistance has to be lowered in order to meet the requirements out forth by the Department of Energy (Table I), which is an overall electrical resistance of less than 10 mΩ cm^2. This can be done by applying an electrical conductive, corrosion resistive and stable coating to a stainless steel surface without passivating oxide.

Conclusions

The contact resistance between the bipolar plate and the GDL inside a PEM fuel cell was measured successfully by use of an in situ setup. The ICR between the bipolar plate and GDL were found to depend on the location of the gold wires. This was most likely caused by variations in oxide layer thickness on the bipolar plate, but could also have been caused by the variation in current distribution throughout the bipolar plate.

The ex situ ICR measurements were conducted at various pressures, and the results showed higher instability in the measured ICR at low pressures than at high pressures. Due to the different conditions experience by the BPPs inside the ex situ setup compared to the in situ setup, the ICR measured in situ was not expected to be identical to the corresponding ex situ measurement (205.79 N cm^{-2}). However, the ICR values did not

differ much from one another if one compares the ex situ ICR values to the corresponding ICR values obtained from the measuring point at the top of the in situ setup. The ratio between the ICR measured for non-coated steel and the gold coated steel is very similar for both the ex situ and the in situ measurements.

Acknowledgments

Sør-Trøndelag University College (HIST) financed this work together with Norwegian University of Science and Technology (NTNU), SINTEF and Nordic innovation. Nordic innovation is greatly acknowledged for funding the NORCOAT project (09051). S.L. thanks HIST for the award of a PhD-scholarship.

References

1. A. Hermann, T. Chaudhuri and P. Spagnol, *Int. J. of Hydrogen Energy*, **30**, 1297 (2005).
2. H. L. Wang, M. A. Sweikart and J. A. Turner, *J. Power Sources*, **115**, 243 (2003).
3. R. A. Antunes, M. C. L. Oliveira, G. Ett and V. Ett, *Int. J. of Hydrogen Energy*, **35**, 3632 (2010).
4. H. Wang and J. A. Turner, *Fuel Cells*, **10**, 510 (2010).
5. U. S. D. o. energy, Hydrogen, Fuel Cells & Technologies Program. Multi-year Research, development and Demonstration Plan, in, D. o. energy Editor, p. 26, http://www1.eere.energy.gov/hydrogenandfuelcells/mypp/ (2005).
6. N. D. L. Heras, E. P. L. Roberts, R. Langton and D. R. Hodgson, *Energy Environment. Science*, **2**, 206 (2009).
7. H. Tawfik, Y. Hung and D. Mahajan, *J. Power Sources*, **163**, 755 (2007).
8. Y. Wang and D. O. Northwood, *Electrochim Acta*, **52**, 6793 (2007).
9. A. M. Lafront, E. Ghali and A. T. Morales, *Electrochim. Acta*, **52**, 5076 (2007).
10. Y. Yang, L.-j. Guo and H. Liu, *Int. J. of Hydrogen Energy*, **36**, 1654 (2011).
11. Y. B. Lee and D. S. Lim, *Curr. Appl. Phys.*, **10**, S18 (2010).
12. L. Wang, D. O. Northwood, X. Nie, J. Housden, E. Spain, A. Leyland and A. Matthews, *J. Power Sources*, **195**, 3814 (2010).
13. Y. Zhou, G. Lin, A. J. Shih and S. J. Hu, *J. Power Sources*, **163**, 777 (2007).
14. M. H. Akbari and B. Rismanchi, *Renewable Energy*, **33**, 1775 (2008).
15. X. Lai, D. a. Liu, L. Peng and J. Ni, *J. Power Sources*, **182**, 153 (2008).
16. R. C. Makkus, A. H. H. Janssen, F. A. de Bruijn and R. K. A. M. Mallant, *J. Sources*, **86**, 274 (2000).
17. J. Ihonen, F. Jaouen, G. Lindbergh and G. Sundholm, *Electrochim. Acta*, **46**, 2899 (2001).